The Role of Collagen VI in the Structure and Properties of the Knee Joint

by

Susan Elizabeth Christensen

Department of Biomedical Engineering
Duke University

Date:_____

Approved:

_____
Dr. Farshid Guilak, Supervisor

_____
Dr. Harold Erickson

_____
Dr. Lori Setton

_____
Dr. George Truskey

_____
Dr. Fan Yuan

Dissertation submitted
in partial fulfillment of the requirements
for the degree of Doctor of Philosophy
in the Department of Biomedical Engineering
in the Graduate School of Duke University

2009

ABSTRACT

The Role of Collagen VI in the Structure and Properties of the Knee Joint

by

Susan Elizabeth Christensen

Department of Biomedical Engineering
Duke University

Date:_____

Approved:

_____
Dr. Farshid Guilak, Supervisor

_____
Dr. Harold Erickson

_____
Dr. Lori Setton

_____
Dr. George Truskey

_____
Dr. Fan Yuan

An abstract of a dissertation submitted
in partial fulfillment of the requirements
for the degree of Doctor of Philosophy
in the Department of Biomedical Engineering
in the Graduate School of Duke University

2009

Abstract

Knee pain is a common complaint among older Americans, nearly half of whom have developed or will develop painful osteoarthritis. Osteoarthritis is primarily a disease of articular cartilage, the low-friction, shock-absorbing connective tissue that lines long bones at their articulating surfaces. Within these joint tissues and within arthritis, the protein collagen VI plays an uncertain role, although it has been implicated in several muscle and ligament disorders. Determination of the collagen VI role in bone and cartilage of the knee is the focus of this dissertation.

Within articular cartilage, collagen VI exclusively localizes to and delimits the pericellular matrix (PCM), which differs from the extracellular matrix (ECM) in composition and structure. To interact with the cell, a molecule must first pass through the PCM. Fluorescent dextran diffusivities were quantified in the cartilage PCM using a newly developed model of scanning microphotolysis (SCAMP), a line photobleaching technique. Diffusion was slower in the PCM than in the ECM, although not in early-stage arthritic tissue. These results support the hypothesis that diffusivity is lower in the PCM than in the ECM of healthy articular cartilage, presumably due to differences in proteoglycan content.

Arthritic degradation is partly mediated by interleukin-1 (IL-1), a catabolic cytokine that affects the mechanical properties of articular cartilage and preferentially

binds to cell-surface receptors in the surface zone. Since cells are the cartilage metabolic units, matrix degradation is hypothesized to influence molecular transport in the PCM before the ECM. Cartilage was cultured with or without IL-1, soaked in FITC-ovalbumin, and photobleached using SCAMP to measure diffusivity. Over 7 days of culture, IL-1 doubled the diffusivity in both zones (surface, middle) and matrices (PCM, ECM) of the cartilage. Diffusivity within the PCM was slightly lower than within the ECM. No increase in PCM diffusivity relative to ECM diffusivity was detected within either zone, suggesting that PCM-localized degradation either cannot be distinguished at these time points or cannot be detected by measures of ovalbumin diffusion.

To determine the effects of collagen VI absence on the morphometry and physical properties of the joint, knees of 2-, 9-, and 15-month-old *Col6a1*+/+ and *Col6a1*-/- mice were studied. Bone morphometry was evaluated using micro-computed tomography (microCT). Subchondral bone thickness, joint-capsule thickness, and cartilage degradation were assessed by histology. Cartilage elastic modulus, roughness, and coefficient of friction were measured by atomic force microscopy (AFM). Diffusion through the cartilage ECM was determined by SCAMP. Overall, collagen VI absence had profound effects on the morphometry of the proximal tibia and the overall histological structures of the mouse knee, yet minimal effects on the friction, roughness, elastic modulus, and diffusional properties of the articular cartilage. Musculoskeletal abnormalities at the knee do result from collagen VI absence.

Contents

List of Tables

List of Figures

Acknowledgments

Science doesn't always cooperate. Those days when progress seems least attainable are the very days when the support of advisors, colleagues, friends, and family makes the greatest difference. These are the people to whom I owe a debt of gratitude for their willingness to stand with me through both the victories and the setbacks.

My thanks go out to my advisor, Dr. Farshid Guilak, and to the other members of my committee: Dr. Harold Erickson, Dr. Lori Setton, Dr. George Truskey, and Dr. Fan Yuan. Their guidance and insights have helped shape the direction and interpretation of this research.

Second, I extend my gratitude to my many colleagues. How wonderful to have worked in a collaborative environment filled with keen minds trained in a wide range of disciplines! They have walked me through new techniques, brainstormed with me, answered my endless questions, shared protocols with me, encouraged me, educated me, and loaned me reagents that I forgot I would need. Several researchers collaborated with me on specific projects: Holly Leddy worked with me on the scanning microphotolysis model development and Jeffrey Coles worked with me on the atomic force microscope characterization of the mouse cartilage. Steven Johnson oversaw the mouse colonies. Their assistance has been critical to the success of my research.

Third, I thank the dozens of friends who have supported me during this endeavor. Some are at Duke, some are in Durham, and some are scattered across the country and beyond. Thank you for your hugs, your phone calls, your emails, your laughter!

Finally, I am grateful to my family. My parents have helped provide a healthy perspective every step of this journey. My local cousins have been marvelously supportive with brownies, hugs, outings, dinners, and lodging. My far-off husband has done an exceptional job in motivating me to push my research forward and helping to keep me sane.

This work has been a remarkable journey and I am indebted to all who have shared in it.

Chapter 1.

Background and Significance

1.1 Arthritis and the Knee

Arthritis is a joint disease that can impair the function, alter the composition, and erode the structures of articular cartilage. In the United States alone, more than 46 million people suffer from this degradative disease at a cost of more than $81 billion annually in medical expenses. Nearly half of all Americans will develop painful osteoarthritis in the knee (CDC 2008).

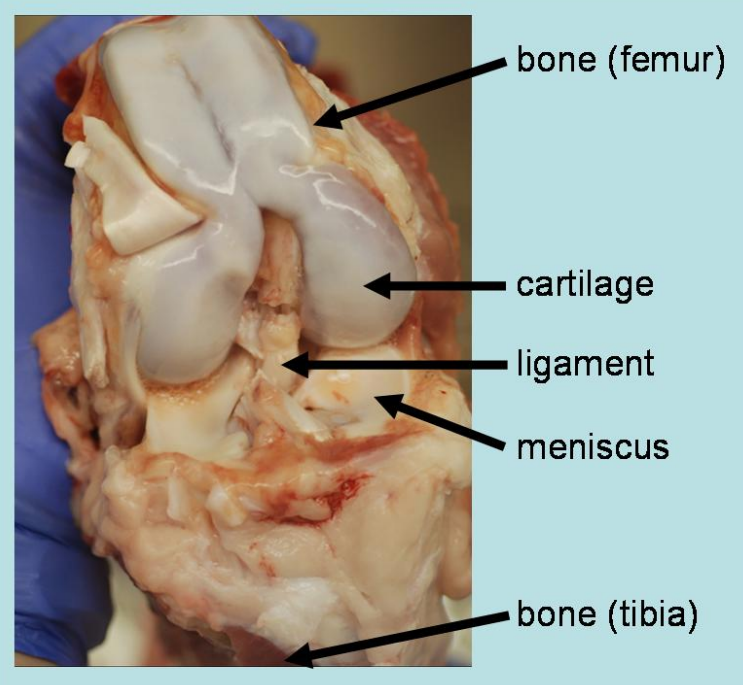

Figure 1.1: A dissected porcine knee joint showing cartilage, bone, ligament, and meniscus.

The causes of arthritis are difficult to pinpoint. Risk factors include old age, obesity, joint injuries, and genetic predisposition. Treatment for arthritis can involve

pain medication, weight loss, activity modification, physical therapy, and cortisone injections (Cole and Harner 1999). These treatments primarily address symptoms of arthritis but neither heal the cartilage nor reverse the course of the disease. For severely advanced arthritis, total knee arthroplasty (joint replacement) is the best available treatment; however, this treatment is expensive, invasive, and limited in its durability and replaceability. Consequently, the quests for a better understanding of arthritis and a cure for the disease are driving factors in research.

1.2 Bone

Bone is a calcified, rigid structure with biomechanical and biochemical roles. The skeleton protects vital organs, provides a supporting frame, helps transfer forces, stores mineral reserves, and produces blood cells within its marrow. Mobility is achieved when the remaining musculoskeletal components attach to the stiff framework bones provide; muscle and tendon serve as actuators, ligaments as stabilizers, and cartilage as a bearing (Fritton 2006). In the leg, the femur and tibia articulate at the knee, with the fibula providing additional support alongside the tibia.

Bone matrix is comprised of organic and inorganic components. The organic constituents, dominated by collagen I, also include glycosaminoglycans and various growth factors. The inorganic portion of bone is predominately hydroxyapatite ($Ca_{10}(PO_4)_6(OH)_2$). Hydroxyapatite is detectable by x-ray and therefore by computerized

tomography (CT), a quantitative, non-destructive tool that can be used to evaluate or assess bone's three-dimensional architecture, mineral content, and density.

Bone is categorized as trabecular (also "cancellous" or "spongy") or cortical (also "compact"). Trabecular bone is porous, characterized by small plate-like and rod-like connecting elements (trabeculae) arranged as a three-dimensional lattice. Trabecular bone is high in surface area and low in volume fraction (0-50%). Trabecular bone is found in inner regions of bones, such as in the femoral neck. Cortical bone, by contrast, has a relative bone volume greater than 95% and a much lower surface area relative to its volume (Recker 1983). Cortical bone forms the outer shell of most bones. In the diaphysis of long bones such as the femur, the tubular geometry of cortical bone enables it to resist both axial loading and bending or torsional loads.

Bone adapts both its tissue architecture and its material in response to its mechanical loading environment. Reduced loading leads to bone loss (Li *et al.* 1990; Vico *et al.* 1991; Matsumoto *et al.* 1998; Rantakokko *et al.* 1999; Sakata *et al.* 1999; Laib *et al.* 2000; Amblard *et al.* 2003; Damrongrungruang *et al.* 2004), whereas increased loading can lead to increased bone mass (Woo *et al.* 1981; Biewener and Bertram 1994; Fritton *et al.* 2005).

Skeletal maturation is marked by predictable changes in bone properties. Animals reach peak bone density at skeletal maturity; mice of most strains reach this milestone by about four months (Beamer *et al.* 1996). At this milestone, the growth

plates in long bones close (mice are an exception) and the animal has achieved its full stature.

1.3 Articular Cartilage

Articular cartilage is a thin, deformable, connective tissue that lines the ends of long bones at diarthrodial joints. Healthy articular cartilage serves as an extremely low-friction surface for articulation, provides joint congruity, and distributes loads which routinely reach approximately three times body weight (Guilak *et al.* 1997). As such, the role of cartilage is primarily mechanical in function; this tissue can withstand decades of use and millions of loading cycles without apparent degradation, although joint trauma, overuse, or aging can lead to arthritis (Buckwalter and Mankin 1997).

Adult articular cartilage is aneural, alymphatic, and avascular (Guilak *et al.* 2000). Cartilage is modeled as a triphasic material with fluid, solid, and ionic phases (Lai *et al.* 1991). Water accounts for 65%-80% (wet weight) of the cartilage (Maroudas 1979; Lai *et al.* 1991). Cations and anions comprise the ionic phase (Lai *et al.* 1991). The solid phase consists predominately of proteoglycans (5-10% by wet weight) and cross-linked collagen, mostly type II (15%-20% by wet weight) but also small amounts of other collagens, including types VI, IX, X, and XI (Maroudas 1979; Heinegard and Oldberg 1989; Poole 1997). Although cartilage cells are responsible for producing and

maintaining this cartilage matrix, they usually comprise less than 10% of the tissue volume (Stockwell 1979; Guilak and Mow 2000).

The collagen fibrils assemble to form fibers that effectively stratify the matrix architecture of the cartilage into three distinct zones (Figure 1.2). In the surface zone, typically 10% to 20% of the total cartilage thickness (Mow *et al.* 1989), small-diameter collagen fibrils (25-50 nm in diameter) pack densely and align highly parallel to the articulating surface (Muir *et al.* 1970; Hwang *et al.* 1992). In the middle zone, typically 40% to 60% of the total cartilage thickness (Mow *et al.* 1989), slightly larger collagen bundles (60-140 nm in diameter) begin to form arcade-like structures amidst some randomly-oriented fibers (Hwang *et al.* 1992). The deep zone, typically about 30% of the total cartilage thickness (Mow *et al.* 1989), closest to the subchondral bone, hosts the largest collagen fiber bundles (up to 160 nm in diameter), which orient perpendicular to the underlying bone (Weiss *et al.* 1968; Hwang *et al.* 1992). Overall, the collagen forms a network that restrains the swelling of the hydrated, negatively-charged proteoglycans (Lai *et al.* 1991).

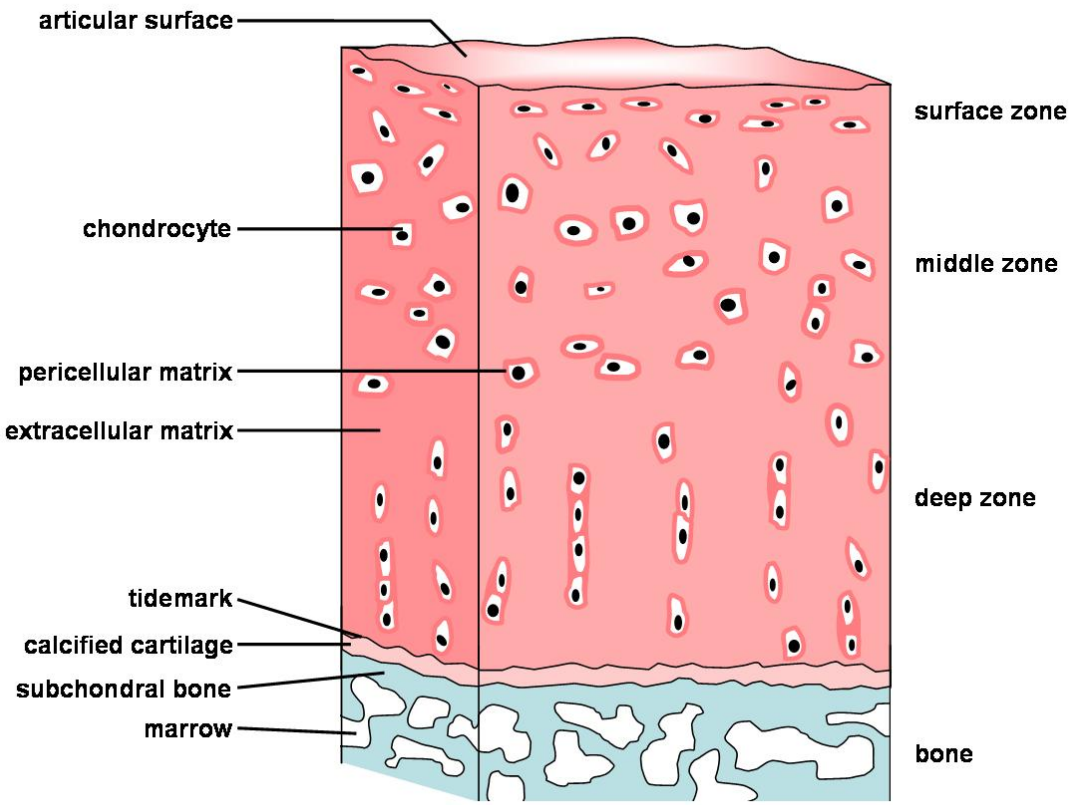

Figure 1.2: Articular cartilage structure.

The negatively-charged proteoglycan molecules form aggregates that are interspersed throughout the collagen ultrastructure. Aggregan, the most common proteoglycan aggregate, consists of glycosaminoglycan chains — predominately chondroitin sulfate and keratin sulfate — attached to a hyaluronic acid backbone by link proteins (Mow and Ratcliffe 1997). The surface zone of cartilage is characterized by a low proteoglycan count, the middle zone by a high level of proteoglycans, and the deep zone by an intermediate proteoglycan count (Poole 1997). The negative charge of these

molecules enables the cartilage matrix to swell, taking in additional water as it attempts to maintain physicochemical equilibrium (Urban *et al.* 1979; Maroudas *et al.* 1985). The collagen network restrains that swelling and, in consequence, the tissue is pressurized (Krishnan *et al.* 2004).

The fluid phase of the matrix consists of water that is closely associated with the collagen matrix and water that is free to move through the matrix during cartilage loading (Maroudas 1979; Torzilli *et al.* 1982). The interstitial water facilitates solute transport into, through, and out of the cartilage (Linn and Sokoloff 1965; Mow *et al.* 1984), which predominately occurs via diffusion (Maroudas 1979).

The cells of cartilage, termed chondrocytes, produce and maintain the cartilage matrix. In humans, chondrocytes comprise only 1.7% of cartilage by volume (Hunziker *et al.* 2002); typically, chondrocytes represent less than 10% of the cartilage (Stockwell 1979; Guilak and Mow 2000) although this cellular fraction is markedly greater in smaller mammals. For example, mouse cartilage has a cell density more than 20 times as great as that of human cartilage (Stockwell 1971). Cells of the surface zone present as flattened discs, cells of the middle zone as spheroids, and cells of the deep zone as spheroids in columns (Poole 1997) (Figure 1.2).

1.4 The Pericellular Matrix of the Chondrocyte

Chondrocytes are directly surrounded by a pericellular matrix (PCM). This region is compositionally and structurally distinct from the extracellular matrix (ECM). The PCM is characterized by high proteoglycan content and by other PCM constituents including collagen types II, IX, and XI, fibronectin, aggrecan, and decorin (Poole *et al.* 1988; Poole *et al.* 1990; Poole *et al.* 1991; Poole *et al.* 1992; Poole *et al.* 1996; Poole 1997). Most notably, however, the PCM is the only place in cartilage that collagen VI is found (Poole *et al.* 1988). The collagen VI in the PCM is thought to interact directly with the cell surface (Poole 1997). Together, the PCM and the cell form a unit termed the chondron (Poole 1992).

The role of the PCM is yet unclear. The PCM is mechanically distinct from the ECM by its lower Young's modulus (Alexopoulos *et al.* 2003; Alexopoulos *et al.* 2005a; Alexopoulos *et al.* 2005c), which indicates the possibility of a biomechanical role for the PCM. At the same time, signaling proteins and matrix molecules traversing the PCM can be retained and modified on their way to or from the cell (Sandy *et al.* 1989; Ruoslahti and Yamaguchi 1991), implying a biochemical role for this matrix. Furthermore, the PCM creates a distance between the cell and the ECM, which limits the interactions between cell surface receptors and proteins in the ECM that might influence metabolism and gene expression (Boudreau *et al.* 1995; Loeser 1997; Bornstein 2002; Petreaca and Martins-Green 2008). In consequence, the PCM is thought to modulate the

biomechanical, biochemical, and biophysical environments of the cells (Guilak *et al.* 2006).

1.5 Collagen VI

Collagen VI, one of several collagens found in the knee joint, is present both in cartilage and in bone. In articular cartilage, collagen VI is localized to the pericellular matrix (Poole 1997) along with other basement membrane proteins, namely laminin, nidogen, and perlecan (Kvist *et al.* 2008). In bone, collagen VI is found in developing bone, particularly the young growth plate (Alexopoulos *et al.* 2009), and in remodeling bone (Keene *et al.* 1991). Collagen VI has also been identified in numerous other tissues including muscle (von der Mark *et al.* 1984), ligament (Bray *et al.* 1993), meniscus (Chevrier 2009), tendon (Bruns *et al.* 1986), and others (Keene *et al.* 1988; Dziadek *et al.* 1996).

Collagen VI is heterotrimeric, formed of three distinct polypeptides: a1(VI), 140 kDa encoded by *col6a1*; a2(VI), 140 kDa encoded by *col6a2*; and a3(VI), ~260-300 kDa encoded by c*ol6a3* (Lampe 2008). Each polypeptide has a central, short, triple-helical domain between two terminal, globular, von Willebrand factor (vWF) type A domains (Chu *et al.* 1990). The three different chains bundle together into a three-chain monomer, which subsequently assembles into antiparallel dimers and then tetramers, each time stabilized by disulfide bonds. Recent research has identified three other collagen VI

variants, c*ol6a4*, c*ol6a5*, and c*ol6a6*, which encode polypeptides that may substitute in place of COL6A3 in the heterotrimeric fibrils (Fitzgerald *et al.* 2008; Gara *et al.* 2008).

Once in tetrameric form, the collagen VI is secreted into the extracellular matrix where end-to-end association yields assembly into 100-nm-long monofibrils with the characteristic beaded structure (Engvall *et al.* 1986; Colombatti and Bonaldo 1987; Colombatti *et al.* 1987; Colombatti *et al.* 1995). In the presence of biglycan in vitro, collagen VI further assembles into hexagonal-like networks where monofibrils aggregate into small bundles with outer ends connecting at the vertex, in 60-degree angles (Wiberg *et al.* 2002). In skin tissue, however, collagen VI monofibrils do not present in so geometric a fashion; rather, the monofibrils connect in short (~200-300 nm) linear segments, with some branching (Keene *et al.* 1998). Collagen VI fibrils are degraded by serine proteinases commonly associated with inflammation (Kielty *et al.* 1993; Poole 1997).

Although the exact function of collagen VI is yet unknown, this protein has been shown to play a bridging role in connective tissues, where it forms a flexible network interlinking ECM components and joining those with cell membrane proteins. Collagen VI interacts with cells via integrin receptors, including β_1 integrins (particularly $\alpha_3\beta_1$) and an integral membrane proteoglycan, NG2 (Doane *et al.* 1992; Salter *et al.* 1992; Pfaff *et al.* 1993; Woods *et al.* 1994; Burg *et al.* 1996; Doane *et al.* 1998; Howell and Doane 1998). Collagen VI also binds decorin (Bidanset *et al.* 1992), biglycan (Wiberg *et al.* 2001),

hyaluronan (McDevitt *et al.* 1991; Specks *et al.* 1992), keratin sulfate glycosaminoglycan (Takahashi *et al.* 1993), heparin (Specks *et al.* 1992), collagen I (Bonaldo *et al.* 1990), collagen II (Bidanset *et al.* 1992), and collagen IV (Kuo *et al.* 1997).

The details on location and interactions of collagen VI have suggested specific roles for this protein in certain tissues. Evidence suggests that the role of collagen VI in the cartilage, where it is exclusively localized to the pericellular matrix, may be two-fold: to anchor the chondrocyte to the PCM (Keene *et al.* 1988; Marcelino and McDevitt 1995; Buckwalter and Mankin 1997) and to interconnect a variety of matrix proteins (McDevitt *et al.* 1991; Bidanset *et al.* 1992; Specks *et al.* 1992; Takahashi *et al.* 1993; Wiberg *et al.* 2001). In bone, where collagen VI has been found in the growth plate (Alexopoulos *et al.* 2009), in remodeling bone (Keene *et al.* 1991), and in the vascularized marrow (Klein *et al.* 1995), the role of collagen VI is still unclear. Of note, long bone formation includes endochondral ossification, the process by which cartilage is matured, invaded, mineralized, and thereby made into bone (Ballock and O'Keefe 2003). Thus, any role of collagen VI in cartilage has the potential to directly influence bone during skeletal development.

Mutations in the genes encoding collagen VI have been linked to muscular disorders, particularly Bethlem myopathy and Ullrich congenital muscular dystrophy (Bertini and Pepe 2002; Lampe and Bushby 2005; Lampe *et al.* 2008), and to ligamentous disorders, namely ossification of the ligamentum flavum, ossification of the posterior

longitudinal ligament of the spine, and diffuse idiopathic skeletal hyperostosis (Tanaka *et al.* 2003; Tsukahara *et al.* 2005). Mutations in collagen VI genes have also been linked to mitochondrial dysfunction (Irwin *et al.* 2003) and to abnormal expression of proteoglycans and adhesion molecules in some tissues (Petrini *et al.* 2005; Higashi *et al.* 2006). Recently, a susceptibility locus for atopic dermatitis was identified in *col6a5* (Söderhäll *et al.* 2007) and the DVWA susceptibility locus for knee osteoarthritis identified as part of *col6a4* (Miyamoto *et al.* 2008; Wagener *et al.* 2009).

In general, increased amounts of collagen VI are associated with stiffness and fibrosis, whereas decreased amounts of collagen VI are associated with laxity and hypotonia. Bethlem myopathy and Ullrich congenital muscular dystrophy, with symptoms of muscle weakness and hyperlaxity, are both generally associated with decreased levels of collagen VI (Lamande *et al.* 1999; Pepe *et al.* 1999; Pan *et al.* 2003), although some of the mutations identified in these diseases do not appear to affect the quantity of collagen VI secreted (Lamande *et al.* 1998a; Zhang *et al.* 2002). In case studies, deletion of a *col6a3* allele yielded joint laxity and hypotonia (Lin *et al.* 1992; Rauch *et al.* 1996), whereas triplication of *col6a3* yielded joint stiffness and epiphyseal dysplasia (Rauch *et al.* 1996). Collagen VI has also been detected in increased quantities in fibrosis of many tissues: skin, as in scar tissue and wound healing (Betz *et al.* 1993; Oono *et al.* 1993); lung (Specks *et al.* 1995); liver, leading to cirrhosis (Griffiths *et al.* 1992);

kidney (Groma 1998); myocardium (Mollnau *et al.* 1995); and even the joint, in arthrofibrosis (Zeichen *et al.* 1999).

To study the effects of collagen VI by its absence, Bonaldo and colleagues generated a *Col6a1*-knockout mouse model on a CD1 background by targeted gene disruption (Bonaldo *et al.* 1998). Although genes *Col6a2* and *Col6a3* were not affected, no triple-helical protein was present in the cartilage matrix; COL6A2 and COL6A3 may have been degraded within the cells of the knockout mice (Bonaldo *et al.* 1998; Lamande *et al.* 1998b).

The joints of *Col6a1*$^{-/-}$ mice have been minimally studied. Skeletal staining of 1-month-old wild-type and knockout mice with alcian blue and alizarin red, to dye cartilage and bone, respectively, revealed that knockout mice are smaller and exhibit a delayed extremity ossification process (Alexopoulos *et al.* 2009). Dual energy X-ray absorptiometry studies revealed a lower bone mineral density in knockout mice at ages 3 and 6 months, as compared to wild-type mice; this difference was no longer present by 11 months of age (Alexopoulos *et al.* 2009). Micropipette aspiration experiments revealed a lower Young's modulus for the PCM of knockout versus wild-type hip chondrons (Alexopoulos *et al.* 2009). Microindentation tests failed to reveal any significant differences between knockout and wild-type mice in terms of the mechanical properties of cartilage of the femoral head (Alexopoulos *et al.* 2009). Semi-quantitative grading of hip joint histology revealed that *Col6a1*$^{-/-}$ mice undergo accelerated

development of hip arthritis (Alexopoulos *et al.* 2009), but this was not seen in 11-month-old femoral condyle cartilage comparisons (Flahiff *et al.* unpublished data). Cartilage thickness of the medial femoral condyle of 11-month-old knockout mice was markedly greater than that of wild-type mice: 57.4 ± 8.9 μm versus 37.8 ± 3.4 μm, respectively (Flahiff *et al.* unpublished data). The surface zone fraction of the cartilage, measured via polarized light microscopy, was smaller in 11-month-old knockout mice (Flahiff *et al.* unpublished data). Overall, these studies present valuable but limited data on the bone and cartilage properties of *Col6a1*$^{-/-}$ mice.

1.6 Joint Degradation

The degenerative changes typically seen with arthritis can be grouped into three overlapping stages. In the first stage, the cartilage matrix is disrupted or altered; in the second, the chondrocytes respond metabolically to that tissue damage; and in the third, the chondrocytes reduce synthesis and tissue is progressively lost (Buckwalter and Mankin 1997).

A number of grading scales have been established for evaluating the severity of arthritis. One scale for visually assessing cartilage is known as the Collins grading scale: Grade 0, cartilage appears smooth and healthy; Grade 1, cartilage shows signs of superficial flaking; Grade 2, cartilage shows indications of more extensive degradation, although not to the bone; Grade 3, cartilage has totally eroded in at least one pressure

area; Grade 4, cartilage is completely lost over large areas with eburnation of bone (Collins and McElligott 1960). Another scale is the semi-quantitative Mankin grading scale (Mankin *et al.* 1971), used to assess cartilage degradation from histological images by incorporating scores from multiple categories: cartilage structure, which addresses surface irregularities and clefts; cell population, which addresses cloning or hypocellularity; safranin-O staining, which addresses normal or reduced levels of proteoglycan staining; and tidemark integrity. Higher Mankin scores indicate further cartilage degeneration. Modified versions of this grading scheme, which sometimes include a category to evaluate subchondral bone thickness, have been used by a number of researchers (e.g., (van der Sluijs *et al.* 1992; Costouros *et al.* 2004; Tadashi *et al.* 2006; Furman *et al.* 2007); see also Appendix B).

To model osteoarthritic joint degradation in the laboratory, several animal models have been developed. The two most common strategies are injecting collagenase (van der Kraan *et al.* 1990) and inducing joint laxity, as by a meniscectomy (Moskowitz *et al.* 1973) or resection of the anterior cruciate ligament (ACL) (Hulth *et al.* 1970). Researchers continue to develop new models of osteoarthritis (Ameye and Young 2006).

1.7 Interleukin-1

Inflammatory cytokines play an important role in joint degradation. Of the many cytokines which act catabolically upon cartilage, interleukin-1 (IL-1) has one of the most potent effects (Goldring 2000).

Interleukin-1 is a 17 kDa protein that suppresses collagen and proteoglycan synthesis while stimulating the synthesis and activity of matrix metalloproteinases (Neidel and Zeidler 1993; Gouze *et al*. 2001; Jacques *et al*. 2006). In advanced arthritis, where IL-1 is more prevalent (Saha *et al.* 1999), IL-1 is able to sustain both inflammation and cartilage erosion (van den Berg *et al*. 1999). Surface-zone chondrocytes have been shown to be more susceptible to IL-1 than chondrocytes from deeper layers (Hauselmann *et al*. 1996). Activated IL-1 signaling pathways have been found at highest concentrations in the surface zone of both normal and osteoarthritic cartilage (Fan *et al*. 2007). At the same time, IL-1 tends to localize to cells of the surface zone (Saha *et al.* 1999). Thus, the effects of IL-1 may first manifest near the surface of articular cartilage.

1.8 Cartilage Surface Properties

Maintenance of healthy surface properties may be critical for proper articular cartilage function given that one important role of this tissue is to provide a low-friction surface for joint articulation. A variety of measures have been used to characterize these

surface properties. Recently, atomic force microscopy (AFM) has enabled assessment of elastic modulus, roughness, and friction at the micro- to nano-scale.

Elastic modulus can be measured by indenting the cartilage and recording the force relationship to indentation depth. When the Poisson's ratio of cartilage is known, extraction of the modulus values (Darling *et al.* 2007; Coles *et al.* 2008; Darling *et al.* 2008) can be accomplished with a Hertz contact model for a rigid sphere indenting an elastic solid half-space (Harding and Sneddon 1945):

$$F = \frac{4ER^{1/2}}{3(1-\nu^{1/2})}\delta^{3/2} \qquad \text{(Eq. 1.1)}$$

where F is the applied force, E is the elastic modulus, R is the radius of the indenter, ν is Poisson's ratio, and δ is the indentation. With this tiny indenter, the interstitial fluid load support decreases to equilibrium in a small fraction of a second, since the characteristic time constant scales with the contact area (Park *et al.* 2004). The linear elastic model used here is a simple model of cartilage; more complex models (e.g., biphasic (Mow *et al.* 1980), triphasic (Lai *et al.* 1991), or viscoelastic (Hayes and Mockros 1971)) are better able to predict cartilage behavior. When the articular surface elastic modulus is measured on the nano-scale, surface inhomogeneities in the form of surface-zone cells may influence the data and, if indented, yield a lower value than the extracellular matrix test sites.

Nano-scale roughness can be measured by scanning across the cartilage using a low, constant, normal force and recording the topography (Coles *et al.* 2008). Root mean square (RMS) roughness is calculated as:

$$R_q = \left[\frac{1}{N} \sum_{i=1}^{N} z_i^2 \right]^{1/2} \quad \text{(Eq. 1.2)}$$

where N is the total number of points sampled and z_i is the height deviation from the mean plane. A first-order flattening procedure is necessary to eliminate orientation effects (i.e., tilt of the surface).

Friction can be quantified by tracking the lateral deflection while scanning across the cartilage surface using a sequence of known normal forces. The load on the system can be expressed as a sum of the external load and the adhesive load:

$$F = \mu(L_0 + L) = F_0 + \mu L \quad \text{(Eq. 1.3)}$$

according to Derjaguin's modification of Amontons' Law (Derjaguin 1934), where F is the friction force, μ is the coefficient of friction, L is the normal load, and "$_0$" indicates a condition of zero applied load. Thus, the coefficient of friction is the slope in the graph of friction force versus the applied normal load (Coles *et al.* 2008). *In vivo*, cartilage undergoes interstitial fluid pressurization when loaded, which contributes markedly to its frictional properties. However, studies using the AFM measure only boundary friction, nonetheless accommodating four possible friction mechanisms: interfacial shear

(found to be dominant in one mouse study), internal friction, plowing friction, and friction due to collisions with asperities (Coles *et al.* 2008).

1.9 Diffusion Through Cartilage

1.9.1 Diffusional Properties of Articular Cartilage

Because cartilage is avascular, molecular transport is a critical issue for the health of the tissue. Oxygen, nutrients, waste products, signaling molecules, matrix macromolecules, and more must all pass through the tissue by diffusion or convection. Convection plays a role while the joint is in motion, since molecules can be expected to flow with water under the effect of the hydraulic pressure gradient (Maroudas 1979). Even so, this motion is likely to be a dominant transport mechanism only for large molecules which diffuse slowly (Maroudas 1975). Overall, diffusion appears to serve as the major transport mechanism within the tissue for most molecules.

The rate of molecular diffusion through cartilage is affected by numerous factors (Leddy 2007). First of all, solutes diffuse more slowly through cartilage than through free solution (Maroudas 1970). This decrease in diffusion coefficient can be attributed to the hydrodynamic drag on the solid portions of the extracellular matrix, which reduce the effective area available to the diffusing molecules and simultaneously increase in the tortuosity of the path (Maroudas 1979). Second, diffusion coefficients through cartilage increase with temperature (Torzilli 1993). Third, diffusion coefficients through cartilage

vary inversely with molecular size (Torzilli *et al.* 1987). For example, for dextran molecules of various sizes, the diffusion coefficients in porcine cartilage were found to be 75 $\mu m^2 s^{-1}$ for 3kDa dextran, 56 $\mu m^2 s^{-1}$ for 40kDa dextran, 32 $\mu m^2 s^{-1}$ for 70kDa dextran, and only 6 $\mu m^2 s^{-1}$ for 500kDa dextran (Leddy and Guilak 2003). Fourth, the charge of a molecule influences its diffusion through cartilage. Negatively charged chloride ions (Cl^-) diffuse more rapidly than positively charged sodium ions (Na^+), likely due to reduced interactions with negatively charged proteoglycans (Maroudas 1975). Fifth, diffusion coefficients through cartilage vary with the cartilage zone (Leddy and Guilak 2003); this relationship is not straightforward and may be partly attributable to the different structure and composition of the zones.

Evidence suggests that the structure and composition of the matrix do play an important role in determining diffusion rates within articular cartilage. For example, enzymatic removal of 71% of proteoglycans increases the diffusion coefficient of 70kDa dextran without affecting that of inulin (5000 Da) or glucose (180 Da) (Torzilli *et al.* 1997); meanwhile, removal of 93% of proteoglycans raises the diffusion rates of 70kDa dextrans and inulin without affecting that of glucose. Interestingly, an increase in fixed charge density, which is another measure of proteoglycan content, has been shown to decrease the diffusion coefficients of 10kDa and 40kDa dextrans without affecting that of urea (60 Da) or glucose (180 Da) (Maroudas 1970). The results from these two studies together

suggest a complex influence of proteoglycans and charge density upon diffusion coefficients of different molecules.

For the much smaller molecule water, magnetic resonance diffusion tensor imaging studies have shown that diffusion increases with cartilage degradation resulting from osteoarthritis (David-Vaudey *et al.* 2004; Watrin-Pinzano *et al.* 2005; Regatte *et al.* 2006). However, *in vitro* studies with collagenase-based models of degradation have inconsistently influenced measures of water diffusion through cartilage (Henkelman *et al.* 2002; Regatte *et al.* 2002; Menezes *et al.* 2004).

Local structures can also influence the diffusion properties of a region. A single study has researched diffusion within the pericellular matrix (Lee *et al.* 1993), although not of a chondrocyte. Gold-tagged lipids were tethered to the membranes of isolated keratocytes. The diffusion of the free end of these lipids was quantified. As the isolated keratocytes synthesized a new pericellular matrix in culture, the measured diffusivity of the lipid ends decreased by about half. This study provides evidence that a pericellular structure reduces diffusion coefficients in the region directly surrounding a cell.

1.9.2 Techniques for Measuring Diffusion

Diffusion is currently measured by a variety of means and on a range of scales. On a tissue level, radiolabel tracer tracking (Torzilli *et al.* 1987; Torzilli 1993) and fluorescence desorption (Quinn *et al.* 2000) are useful techniques for determining diffusion coefficients that are spatially-averaged for a full piece of tissue. Magnetic

resonance imaging can be used to measure diffusivity of small molecules and ions, even *in vivo* (Fischer *et al.* 1995). Fluorescence correlation spectroscopy can be used to measure diffusion coefficients in a picoliter detection volume, to-date either in a cell or in a solution (Trier *et al.* 1999; Wachsmuth *et al.* 2003).

Fluorescence photobleaching techniques are the most widely used strategies for measuring diffusion coefficients. Photobleaching photochemically destroys a fluorophore by overloading the fluorescent group with photons. When a laser illuminates and thereby photobleaches fluorescent molecules, it creates a visible disruption that is traceable over time. The traceable disruption, together with an appropriate model of the diffusion process, yields a meaningful diffusion coefficient. Such models rely on the diffusion equation:

$$\frac{\partial C(\vec{x},t)}{\partial t} = D\frac{\partial^2}{\partial \vec{x}^2}C(\vec{x},t) \qquad \text{(Eq. 1.4)}$$

where C is the concentration of the fluorescent (or photobleached) molecule, $\vec{x}$ is space (usually considered in only two dimensions: x and y), t is time, and D is the diffusion coefficient. Initial conditions appropriate for the model must typically be measured or estimated.

One common photobleaching experiment, fluorescence recovery after photobleaching (FRAP), involves bleaching a small region and watching the fluorescence gradually return to that location, as non-impaired fluorescent molecules diffuse in from outside the photobleached region. For this simple setup, a variety of

methods have been developed to analyze the experimental data, fit the results with the diffusion equation, and thereby extract a diffusion coefficient (for a review, see (Leddy 2007)).

Another strategy for experimental setup involves studying the pattern of fluorescence decay rather than recovery. This approach has given rise to continuous microphotolysis (Peters *et al.* 1981), scanning microphotolysis (Wedekind *et al.* 1994; Kubitscheck *et al.* 1998), continuous fluorescence photobleaching (Wachsmuth *et al.* 2003), and fluorescence imaging of continuous point photobleaching (Leddy *et al.* 2006).

All of these techniques except scanning microphotolysis (SCAMP) (Kubitscheck *et al.* 1998) assume a planar geometry in their model and diffusion calculation. This setup is appropriate for many experiments, but photobleaching at a high magnification requires a model that takes into account the three-dimensional geometry of bleaching through a high-numerical-aperture objective. As developed, the scanning microphotolysis model provides excellent fits to experiments with diffusivities less than 2 $\mu m^2 s^{-1}$ (Kubitscheck *et al.* 1998). However, many diffusion coefficients that have been measured in cartilage are larger than this model accommodates.

To measure diffusion within a very small volume of tissue, the SCAMP technique bears promise. A faster scan time would be necessary in order for the model to accommodate the higher coefficient of diffusion (greater than 2 $\mu m^2 s^{-1}$) typically measured in the cartilage matrix. If successful, the modified SCAMP technique would

enable measurement of diffusion through the thin pericellular matrix of articular cartilage or through the scant regions of extracellular matrix in mouse cartilage.

1.10 Specific Aims and Hypotheses

The goal of this study was to determine the role of collagen VI in the structure and properties of the knee joint. In cartilage, the presence of collagen VI defines the pericellular matrix (PCM) around each chondrocyte. A modified version of scanning microphotolysis (SCAMP) was developed and validated for the purpose of measuring diffusion within that PCM. Subsequently, diffusion was measured in the PCM of cartilage that had been cultured with interleukin-1 (IL-1). Finally, the knees of *Col6a1*-knockout mice were evaluated: cartilage surface properties were measured by atomic force microscopy, cartilage diffusivity was measured by SCAMP, joint histology was evaluated by modified Mankin scoring, and joint morphometry was assessed by micro-computed tomography. The following Specific Aims and hypotheses were proposed:

Specific Aim 1: *Measure molecular diffusion within the pericellular matrix of articular cartilage.* I developed a technique to measure diffusion rates within the thin pericellular region and to use said technique to compare diffusion rates in the pericellular matrix versus the adjacent extracellular matrix, for two sizes of fluorescently-labeled dextrans. Both healthy cartilage and early-stage arthritic cartilage were studied. I hypothesized that diffusion rates would be lower in the pericellular matrix than in the extracellular

matrix, lower for larger molecules, and higher in early-stage arthritic cartilage than in normal cartilage.

Specific Aim 2: *Evaluate diffusivity through the pericellular matrix of interleukin-1-treated articular cartilage.* I evaluated the diffusivity of a fluorescein-labeled globular protein, ovalbumin, within articular cartilage cultured with the catabolic cytokine interleukin-1 (IL-1). Matrix effects, zonal effects, and time effects were considered. I hypothesized that the diffusion rate of ovalbumin would: (a) be higher in the extracellular matrix than in the pericellular matrix, (b) be higher in the middle zone than in the surface zone, and (c) increase sooner in the pericellular matrix.

Specific Aim 3: *Characterize physical properties of the knee joints of Col6a1-knockout mice.* I evaluated and compared physical properties of C*ol6a1*$^{-/-}$ mouse knee joints for a range of ages (2, 9, and 15 months old) and in contrast to the wild-type (CD1) mouse. This study examined joint morphometry via micro-computed tomography, joint degradation via histology, cartilage surface properties via atomic force microscopy (AFM), and cartilage diffusion properties via scanning microphotolysis (SCAMP). I hypothesized that the collagen VI absence would delay skeletal maturation at the knee yet accelerate cartilage degradation.

The results of these studies provide new insights about the influence of collagen VI in the knee and the role of the pericellular matrix in cartilage. In cartilage, the first

studies determine the role of the collagen-VI-defined pericellular matrix as a diffusion gateway for the chondrocyte and the influence of interleukin on matrix degradation. More widely, the last of these studies exposes the larger role of collagen VI by determining how the knee joint differs in its absence. Hopefully, this information will lead to the development of new strategies for monitoring, slowing, or reversing the progression of arthritis at the knee.

Chapter 2.

Measuring Diffusion in the Cartilage Pericellular Matrix

Original article co-authored with HA Leddy and F Guilak. Text and figures reprinted with permission of ASME: "Microscale Diffusion Properties of the Cartilage Pericellular Matrix Measured Using 3D Scanning Microphotolysis." Journal of Biomechanical Engineering 130(6): 061002, 2008.

2.1 Introduction

Articular cartilage is the connective tissue that lines surfaces of bones in synovial joints. Cartilage disease, primarily in the form of osteoarthritis, is a major problem that affects 21.6% of adults in the United States (Hootman *et al.* 2006). Cartilage is an avascular and alymphatic tissue, suggesting that the primary mode of transport for nutrients, oxygen, waste products, signaling molecules, and matrix macromolecules is by diffusion or convection. Thus, over the course of aging or disease, alterations in tissue properties may influence chondrocyte metabolism by altering the transport of nutrients, signaling molecules or metabolites. The extracellular matrix (ECM) of articular cartilage is primarily water, making up 60–85% of the tissue's wet weight. The remaining solid matrix is composed of a crosslinked network of type II collagen (15–22% by wet weight), proteoglycan (4–7% by wet weight), and lesser amounts of other collagen types (e.g., VI and IX) and noncollagenous proteins (Heinegard and Oldberg 1989). The aggregating proteoglycan, or aggrecan, in cartilage is composed of a hyaluronic acid backbone to which numerous chondroitin and keratan sulfate chains are attached by a link protein. The constituents of articular cartilage are organized in a stratified structure that contributes to the unique mechanical behavior of the ECM (Mow *et al.* 1992).

Understanding the factors that influence diffusive transport is crucial to determining not only the normal physiological functions of articular cartilage but also how those functions are altered by a disease. In general, it has been shown that larger

molecules diffuse more slowly than smaller ones through the cartilage tissue (Maroudas 1976; Torzilli *et al.* 1987; Quinn *et al.* 2000; Leddy and Guilak 2003). In particular, the local structure and composition of the cartilage matrix appear to have significant effects on the rate of diffusion in the tissue. For example, removal of proteoglycans by enzymatic degradation (Torzilli *et al.* 1997) or removal of the entire surface zone (Torzilli 1993) increases the bulk tissue diffusion coefficient of 70 kDa dextran. In the surface zone, the diffusion coefficient of 70 kDa dextran is also lower than in the middle and deep zones (Leddy and Guilak 2003) and is anisotropic (Leddy *et al.* 2006), potentially due to differences in the composition and orientation of collagen fibers in this zone. Furthermore, proteoglycan concentration has been shown to be inversely correlated with diffusivity (Evans and Quinn 2005). Studies of macromolecular diffusion in engineered cartilage show that the accumulation of matrix components, coupled with cell-induced tissue contraction, can significantly decrease tissue diffusivity (Leddy *et al.* 2004).

The structure and composition of cartilage vary significantly with proximity to the cells, termed "chondrocytes," which are responsible for maintaining the tissue. The region immediately surrounding the cell, the pericellular matrix (PCM), is characterized by high proteoglycan content, the exclusive presence of type VI collagen in cartilage, and the presence of other molecules such as types II, IX, and XI collagen, fibronectin, aggrecan, and decorin (Poole *et al.* 1988; Poole *et al.* 1990; Poole *et al.* 1991; Poole *et al.*

1992; Poole *et al.* 1996; Poole 1997). In addition to these structural and compositional differences, the PCM exhibits a lower Young's modulus than the surrounding ECM (Alexopoulos *et al.* 2003; Alexopoulos *et al.* 2005b; Alexopoulos *et al.* 2005c). Because of such differences in properties, the presence of the PCM has significant effects on the mechanical environment of the chondrocyte (Buschmann *et al.* 1995; Guilak and Mow 2000; Alexopoulos *et al.* 2005b; Haider *et al.* 2006; Choi *et al.* 2007), and it has been hypothesized that the PCM serves as a transducer, or "filter," of mechanical signals in cartilage (Poole *et al.* 1988; Guilak *et al.* 2006).

To date, there have been few reports on the diffusivity or transport properties of the native PCM. One study has examined diffusion in a reconstituted PCM in vitro (Lee *et al.* 1993), showing that the presence of a PCM slows the diffusion of gold-labeled lipids extending 30–40 nm out from the cell membrane. In other studies, micropipette aspiration has been used to measure the biphasic properties of mechanically extracted chondrons, showing a significant increase in the hydraulic permeability of the PCM with osteoarthritis (Alexopoulos *et al.* 2005c).

The native PCM provides unique challenges for diffusion measurements. Because the PCM is typically quite thin (~3 μm thick in porcine chondrons (Youn *et al.* 2006)), the techniques historically used to measure diffusion in cartilage (i.e., radiolabel tracer tracking or fluorescence desorption (Maroudas 1970; Torzilli 1993; Quinn *et al.* 2000)) cannot be scaled easily to perform such measurements within the PCM.

Photobleaching techniques such as fluorescence recovery after photobleaching (FRAP) have been widely used at this size scale, but were developed to measure diffusion in two-dimensional (2D) systems such as cell membranes (Axelrod *et al.* 1976; Tsay and Jacobson 1991). While this technique has recently been extended using 2D numerical simulations to account for tissue inhomogeneity (Sniekers and van Donkelaar 2005), photobleaching in the PCM requires the use of a high numerical aperture (NA) lens, which contributes to substantial out-of-plane bleaching that significantly affects the fluorescence intensity measured in the imaging plane and requires a three-dimensional (3D) analysis.

Consequently, the goal of this study was to develop a modified version of the scanning microphotolysis (SCAMP) technique (Kubitscheck *et al.* 1998) to overcome the challenges of measuring diffusion within the PCM. SCAMP uses a high laser power both to image and to photobleach a line segment, taking advantage of the fast *x*-direction scanning rate (~20 μm/μs) of the laser scanning confocal microscope (Kubitscheck *et al.* 1998). The output of this procedure is a single *x*-line that decreases in intensity over time (Fig. 2.1). The change in fluorescence intensity is a function of two variables: the rate of photobleaching and the rate of diffusion of the fluorescent molecule of interest. Faster-moving molecules traverse the laser's path more rapidly and so are subjected to the laser for a briefer duration, thereby producing a slower intensity decrease; on the other hand, slower-moving molecules remain in the laser's path and so are more likely to be

photobleached, yielding a more rapid intensity decrease (Fig. 2.2). Because the SCAMP procedure measures only the change in intensity during the bleaching period and not the fluorescence recovery period, the experiments can be performed very rapidly(<50 ms) as compared with typical FRAP experiments (minutes), and bleaching is confined spatially to a relatively small region (<37 μm^3 for this study's configuration). To determine the diffusion coefficient and a bleaching rate constant, the intensity-versus-time data are fitted to a 3D theoretical diffusion-reaction model that accounts for the out-of-plane bleaching effects (Kubitscheck *et al.* 1998) (Fig. 2.3).

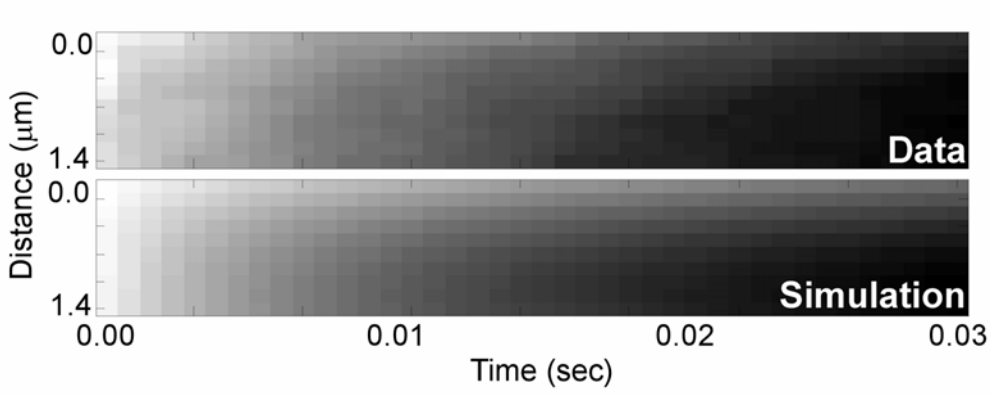

Figure 2.1: The intensity of the photobleached line decreases over the course of a SCAMP experiment. Throughout this time frame, the intensities are similar for an experimental data set (top) and its corresponding theoretical simulation (bottom).

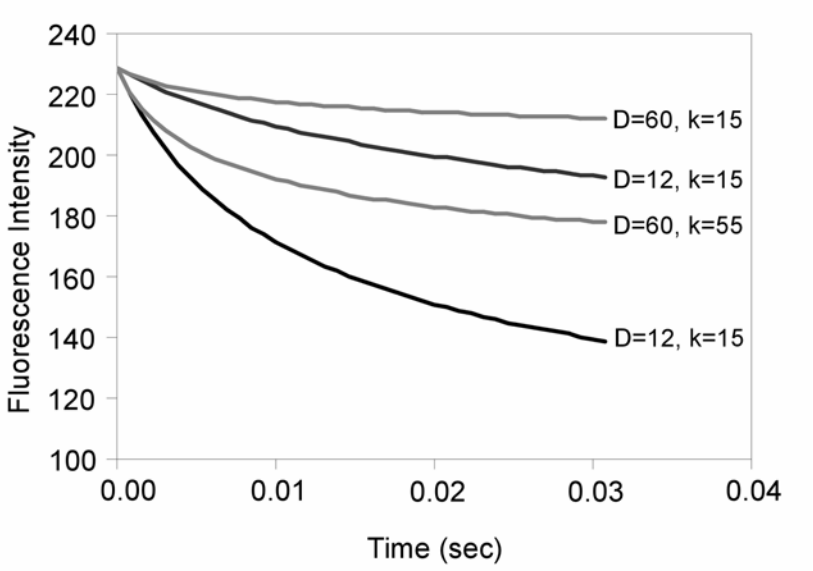

Figure 2.2: The average fluorescence intensity across a SCAMP line is plotted for a range of diffusion coefficients, D (μm²/s) and bleaching rate constants, k (s^{-1}). Higher diffusion coefficients and lower bleaching rate constants lead to slower bleaching.

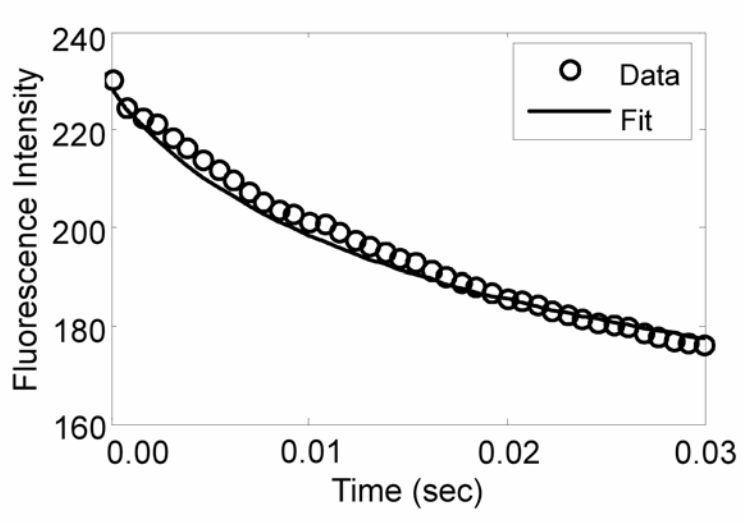

Figure 2.3: The average line intensity decreases over time due to photobleaching in SCAMP experiments. The simulation provides excellent fits to the data (R^2=0.98).

With the technique developed in this study, a single diffraction-limited line could be rapidly bleached and simultaneously imaged. From these images, the microscale diffusivity was measured within both the PCM and adjacent ECM of porcine cartilage for two different dextran sizes. Due to the higher PCM proteoglycan content, the PCM diffusivity was hypothesized to be lower than that of the ECM. Similarly, the diffusivity of the larger dextran was expected to be lower than that of the smaller dextran.

2.2 Methods

2.2.1 Numerical Modeling of the SCAMP Procedure

The SCAMP method was originally developed by Kubitscheck et al. (Kubitscheck *et al.* 1998), who implemented an analytical solution that involved specific assumptions regarding the physical process of the experiment. This model provided excellent fits to SCAMP experiments for diffusivities less than 2 $\mu m^2/s$. In applying this method to measure the diffusivity of larger molecules within the cartilage PCM, however, a number of these assumptions were not valid in our experimental configuration, and a new numerical model was developed to incorporate specific experimental parameters involved in the present testing system.

2.2.2 Measuring Larger Diffusion Coefficients

The basic SCAMP analysis assumes that the *x*-line is bleached instantaneously, which is a reasonable assumption only if the molecules at one end of the line have not yet diffused away by the time that the other end is scanned. This constraint determines the maximum diffusion coefficient that can be measured using SCAMP. In the original description of the method, Kubitscheck et al. (Kubitscheck *et al.* 1998) estimated that the characteristic diffusion time, $\tau = l^2/6D$ (where l is the length of the line being scanned and D is the diffusion coefficient), should be at least ten times the line-scan time in order to maintain this assumption. In the previous configuration (Kubitscheck *et al.* 1998), the upper limit of D was 2 $\mu m^2/s$. By scanning a very short line (1.44 μm) using a faster bidirectional microscope, this limit was extended in the present study to 5120 $\mu m^2/s$.

2.2.3 Accounting for Time Spent Not Bleaching

The confocal microscope used in this study (LSM 510, Zeiss Inc., Thornwood, NY) does not scan the laser continuously back and forth across the proscribed 12-pixel line, but rather moves over a longer region than the 12-pixel line (with the laser off) and takes a finite amount of time to reverse direction. Whenever the laser is off, the fluorescence distribution recovers. This is a significant portion of time; ~300 ms are spent with the laser off for each millisecond with the laser on. An enhancement to the numerical model incorporates this illumination pattern by alternating long and short time steps. During the short time step, bleaching occurs and the process is modeled as

diffusion with a consumption term where C is the concentration of fluorphore over space ($\vec{x}$) and time (t), D is the diffusion coefficient, and k is the space-dependent bleaching rate constant,

$$\frac{\partial C(\vec{x},t)}{\partial t} = D\frac{\partial^2}{\partial \vec{x}^2}C(\vec{x},t) - k(x)C(\vec{x},t) \qquad \text{(Eq. 2.1)}$$

However, during the long time step, the molecules only diffuse,

$$\frac{\partial C(\vec{x},t)}{\partial t} = D\frac{\partial^2}{\partial \vec{x}^2}C(\vec{x},t) \qquad \text{(Eq. 2.2)}$$

Equations (2.1) and (2.2), which govern the SCAMP process, were solved by the Douglas–Gunn alternating-direction implicit (ADI) method of discretization (Douglas and Gunn 1964). The resulting equations (Eqs. A1-A6) are provided in Appendix A.

2.2.4 Accounting for Data Asymmetry

Experimental data showed a consistent asymmetry across the x-line that was not predicted by the original SCAMP model, which uses theoretical illumination profiles for the simulation (Fig. 2.1). The observed variability in intensity was caused by the asymmetric nature of our microscope's point-spread function. Thus, to allow for this type of real-world variation in the optical symmetry of the microscope and to improve the accuracy of our simulation, instead of using theoretical descriptions, we incorporated the microscope's optical asymmetries into the model. We empirically derived the point-spread function (detection profile) and the bleach matrix (excitation profile).

The point-spread function was determined by collecting *z*-stack images of subresolution fluorescent microspheres (Fig. 2.4) (Shaw and Rawlins 1991). The bleach matrix was measured by photobleaching an immobilized fluorophore, fluorescein isothiocyanate (FITC)-dextrans, in a dehydrated agarose gel. This photobleached region was imaged by *z*-stack and then 3D deconvolved from the point-spread function using the XCOSM software with the expectation maximization algorithm (Conchello *et al.* 1994; Conchello 1995; Conchello 1998) to extract the bleach (excitation) matrix (Fig. 2.5).

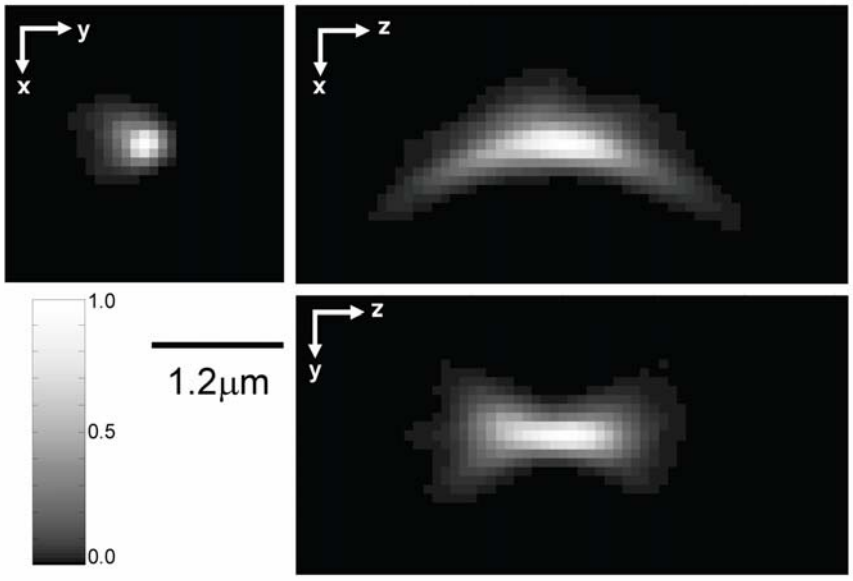

Figure 2.4: The point-spread function was measured by assembling *z*-stack images of subresolution fluorescent microspheres. *x*-*y* is the imaging plane. The clear asymmetry varies greatly from the theoretical point-spread function, which would show rotational symmetry along the *z*-axis. An intensity of 1.0 represents a voxel maximally detectable by the microscope; an intensity of 0.0 represents a voxel minimally detectable by the microscope.

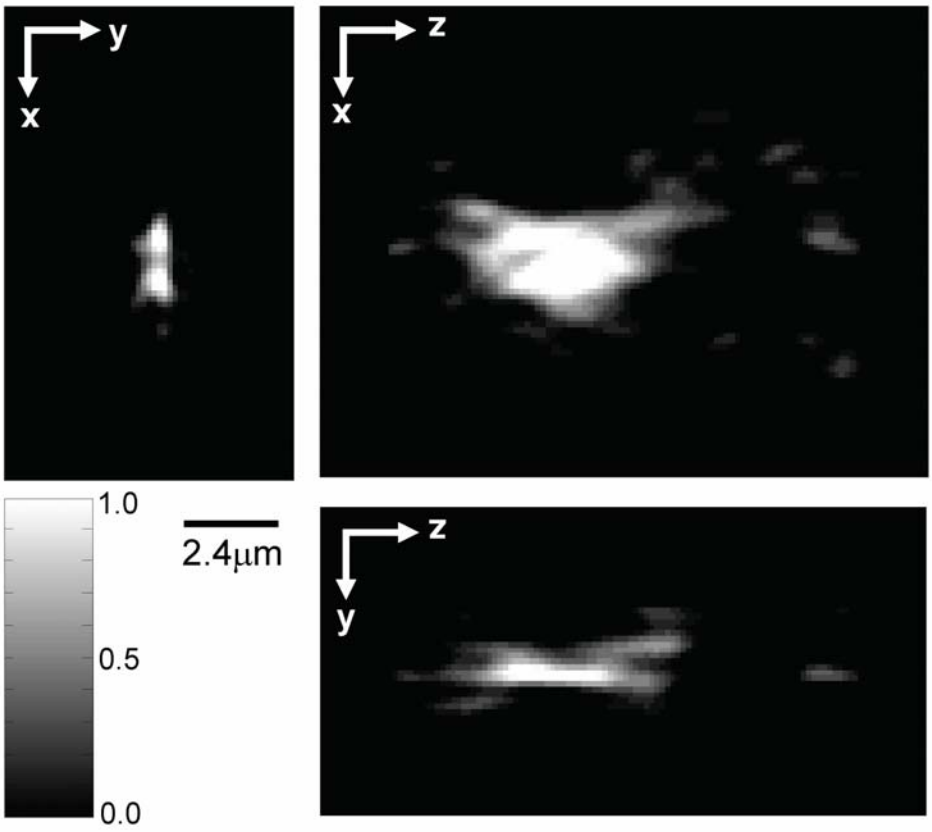

Figure 2.5: The bleach (excitation) matrix was determined by photobleaching along a 12-pixel line in an agarose gel, which contained immobilized fluorophore, and then by imaging the matrix at very low laser power. *x*-*y* is the imaging plane; *x* is the linescan direction. A higher intensity corresponds to a greater degree of bleaching that occurs at a given point in space.

2.2.5 Incorporating Pre-Bleach Assumption for First Time Point

Although the laser nominally bleaches and images simultaneously, the fact that the characteristic asymmetric intensity variation was already present in the first line of

each data set indicated that the collected intensity data were already bleached before the first image was recorded. Thus, the background fluorophore level was estimated from the measured first line of data, and a perfectly linear correlation was interpolated from simulated data sets of known background intensity.

2.2.6 Determining Simulation Parameters

The 3D simulation space was 83x53x114 pixels (x, y, z) based on the proportions of the bleach matrix. This simulation space was selected to be large enough to avoid any edge effects; this was verified by increasing the space size and observing no numerical changes in the simulations. Spatial steps were set to equal the pixel size on the data derived from the microscope. The time steps were set to mimic actual timing; subdividing time steps further did not change the simulations.

The duration of the experiment balanced a number of conflicting factors. Theoretically, a better fit is achieved for longer experiments. However, since diffusion causes the photobleached volume to increase with time, shorter experiments are required to keep the bleach region within the confines of the PCM. In addition, computation time increases when simulating and fitting longer data sets. For simulated data sets with typical noise levels added, a fit of 40 time points was found to balance appropriately the goals of keeping the computation time reasonable, the bleach region within the PCM, and the fitting error low (Fig. 2.6a).

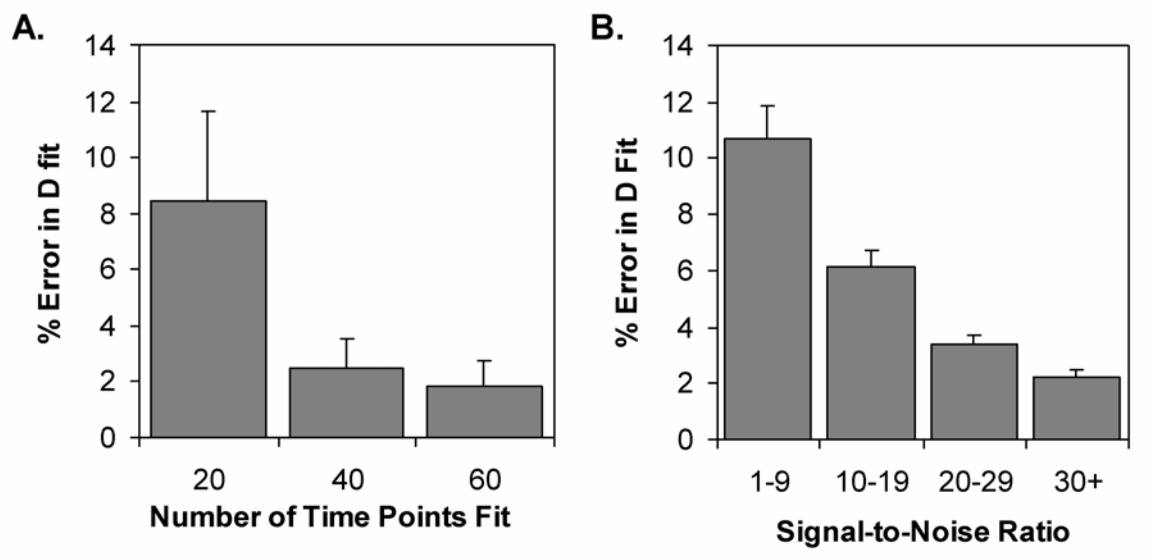

Figure 2.6: (a) The percentage error in the estimate of *D* decreases as more time points are fitted (*n*=11/bar; mean+SEM). (b) The percentage error in the estimate of *D* decreases as the signal-to-noise ratio increases (*n*>100/bar; mean+SEM). The data sets being fitted were simulations of known *D*, covering the range of expected values, to which random noise with a standard deviation of 1, 2, or 3 was added.

To speed up the computation, simulations were generated for a series of *D* and *k* values and saved to a lookup table. This created a searchable library of possible *D* and *k* combinations to which data could be quickly compared while simultaneously sidestepping the earlier strategy of recreating the simulations to fit each new data set. The implementation of the lookup table reduced from hours to seconds the time required to fit the data.

Data quality was tested by adding different noise levels to data sets created from simulations of known *D* and *k*. The new best-fit *D* and *k* values were determined for each

noisy data set by comparison to the clean lookup simulations. The signal-to-noise ratio was calculated to describe each data set. The signal was defined as the change in intensity from the start to the end of the experiment; the noise was the standard deviation of the difference between the best-fit simulation and the data. The error in fit increases significantly with increasing noise, but a signal-to-noise ratio of at least 10 limits the average errors in the fits to less than 6% (Fig. 2.6b). Therefore, only experimental data with a signal-to-noise ratio of 10 or greater were used.

2.2.7 Fitting Experiment Within the PCM

To determine whether a SCAMP experiment would fit within the confines of the PCM, the maximum excursions of the bleached regions were measured at the end of simulated experiments. Since molecules at the periphery do not strongly affect the measured intensity, to consider even the faint bleaching far from the proscribed bleach line yields a generous estimate of the bleach region. The size of the rectangular prism that enclosed the bleach volume was 3.3x1.9x5.7 μm^3 (x, y, z) (Fig. 2.7), which fits within the typical porcine PCM (Youn *et al.* 2006).

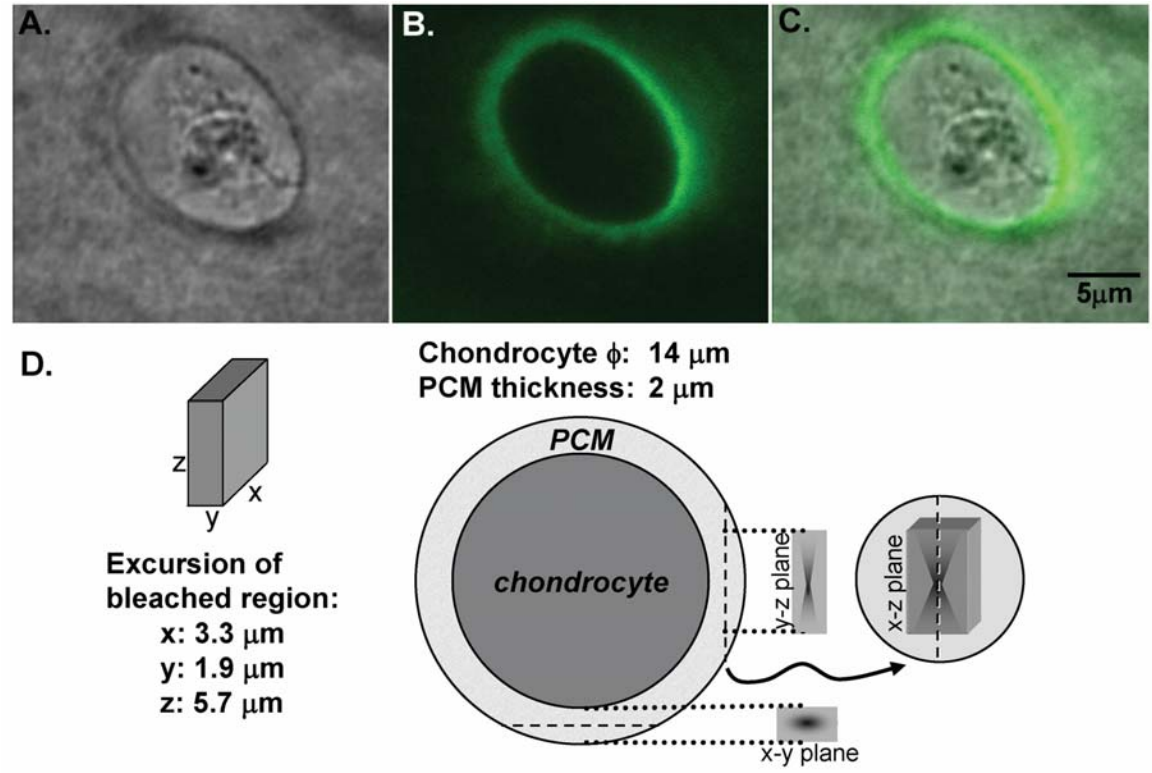

Figure 2.7: The relative size of the SCAMP photobleaching region and the PCM. (a) A DIC image, (b) a fluorescence image stained for collagen VI, and (c) an overlay of the two show a porcine chondrocyte with the surrounding PCM defined by the presence of collagen VI (staining as described in Youn *et al.* (2006)). A porcine chondrocyte is typically 14 μm in diameter and surrounded by a 2-μm-thick PCM. (d) When positioned appropriately, a rectangular region containing the maximal excursion of a bleached region (3.3x1.9x5.7 μm^3) fits within this PCM.

2.3 Experimental Procedure

Tissue was obtained from the femoral condyles of skeletally mature female pigs. A full-thickness slice of cartilage was removed from the femoral condyle of joints that showed no signs of degeneration and then was incubated overnight in a concentrated

solution of FITC-tagged 70 kDa (25 mg/ml) or 500 kDa (10 mg/ml) dextran (Molecular Probes/Invitrogen, Eugene, OR). For testing of arthritic cartilage, joints were graded macroscopically for osteoarthritis using the Collins scale, as described by Muehleman et al. (Muehleman *et al.* 1997). Cartilage was taken from early-stage arthritic joints showing minimal fibrillation and fissuring (Collins grade 1 or 2) and was incubated in a concentrated solution of 70 kDa dextran (25 mg/ml).

The cartilage tissue sample was placed in a coverslip chamber with the full-thickness cross-section against the coverslip. The tissue was then covered with phosphate buffered saline (PBS) and immobilized with a custom-built holder. Using the 100x, 1.3 NA oil immersion lens at 6*x* zoom on a confocal laser scanning microscope (LSM 510, Zeiss), a 1.44 μm wide line (12 pixels) at a depth of 6 μm into the tissue was bleached (excitation wavelengths: 458 nm and 488 nm) forward and backward for a total of 40 passes. As the laser bleached, the emission intensity was also collected (long-pass filter, LP505) and stored as the image for that pass. At each site, five to seven experiments were performed; their intensity values were averaged and median filtered to minimize noise.

The ability of the model to detect changes in the bleaching rate constant, k, was tested by a series of measurements made at increasing depth into the tissue. Since tissue reflects and absorbs some of the laser light, the laser intensity decreases as it penetrates further into the tissue. As the laser intensity decreases, so should the bleaching rate

constant. Depth data were log-transformed to maintain normality and satisfy linear regression assumptions.

SCAMP experiments were performed in pairs: for each SCAMP measurement in the PCM, a paired experiment was carried out in the adjacent ECM in the same sample. The PCM experimental sites were chosen on the surface- or deep-zone sides of middle-zone cells since these PCM areas tended to be thickest. All PCM sites were within 2 μm of the edge of the cell; all ECM sites were at least 5 μm from the edge of the cell. The diffusion coefficient was determined for each test site by fitting the experimental data to a precalculated entry in the lookup table by minimizing the sum of the squares of error. A signal-to-noise ratio was then calculated as the maximum change in intensity over time divided by the standard deviation of the noise that remained once the best-fit simulation was subtracted out; data sets were used only if their signal-to-noise ratio was greater than 10. All data processing, fits, and simulations were performed in MATLAB (The Mathworks, Natick, MA). Statistics were computed with STATISTICA (Statsoft, Tulsa, OK). A repeated-measures analysis of variance (ANOVA) with paired PCM and ECM measurements was used to determine the effects of the matrix and the molecule size. A paired *t*-test was used to determine the effect of matrix type in arthritic cartilage.

2.4 Results

Overall, the SCAMP model provided excellent fits to the experimental data, with a mean correlation of R^2=0.92 (e.g., Figs. 2.1 and 2.3). The depth series confirmed that the bleaching rate constant decreases significantly with increasing natural log of depth (Fig. 2.8). Importantly, however, the diffusion coefficients measured through this depth series did not vary significantly, indicating that the model is able to discriminate between changes in D and k.

The diffusion coefficients of both 70 kDa and 500 kDa dextrans were determined in the PCM and ECM of porcine tissue samples. The mean (± standard error) diffusion coefficient of 70 kDa dextran in the middle zone of healthy porcine cartilage was 23±2 $\mu m^2/s$ in the ECM and 19±2 $\mu m^2/s$ in the PCM. For 500 kDa dextran, the diffusivity of the ECM was 17±2 $\mu m^2/s$, and that of the PCM was 14±2 $\mu m^2/s$ (Fig. 2.9). The repeated-measures ANOVA showed no significant size-by-matrix interaction (p=0.43), but a significant size effect (p=0.02) and matrix effect (p=0.00008). The diffusion coefficient for 500 kDa dextran was significantly lower than that of 70 kDa dextran (Fig. 2.9). For both dextran sizes, the diffusivity of the PCM was significantly lower than that of the ECM (Fig. 2.9). In contrast to the healthy cartilage, the diffusivity of 70 kDa dextran in the ECM of the early-stage arthritic samples was not significantly different from that in the PCM (ECM:24±2 $\mu m^2/s$, PCM:24±2 $\mu m^2/s$, paired t-test, and p=0.6).

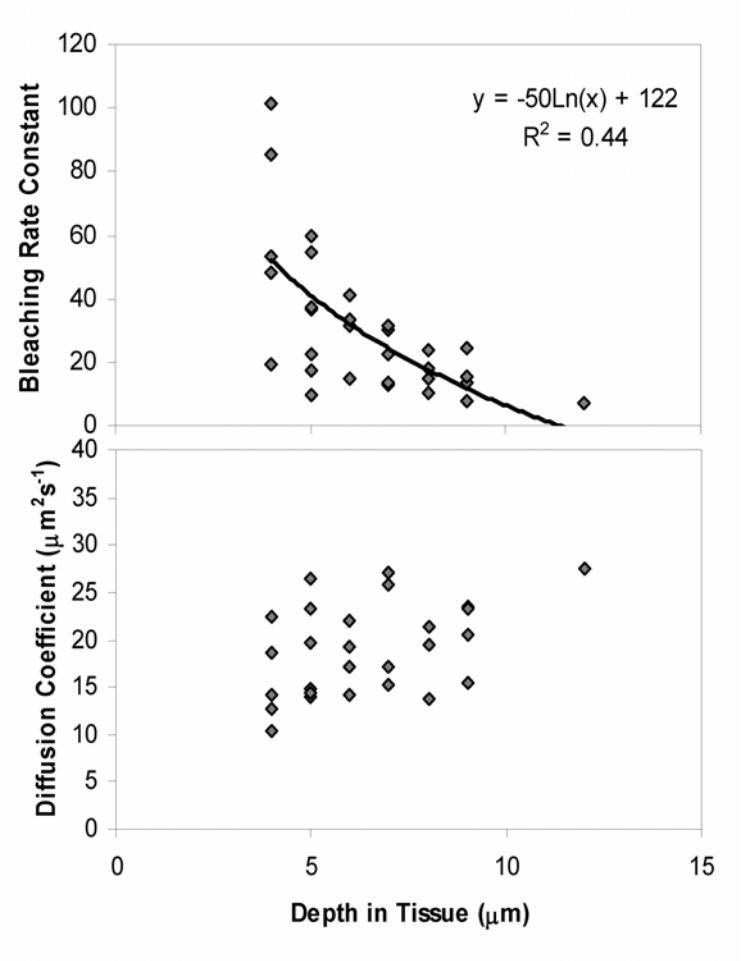

Figure 2.8: The bleaching rate constant, k (s^{-1}), decreases significantly with increasing depth into the tissue (top, linear regression p=0.00005), while the diffusion coefficient, D ($\mu m^2/s$), does not change significantly (bottom, linear regression p=0.1). The line and equation (top) show the significant fit of the bleaching rate constant versus ln(depth) (R^2=0.44).

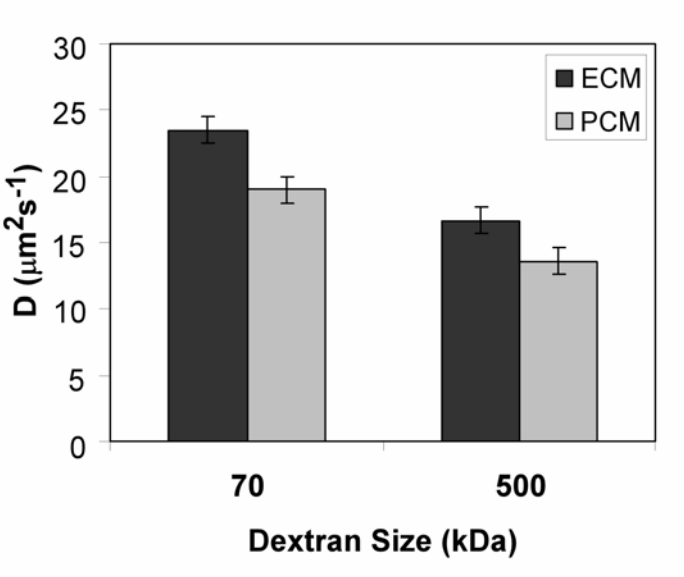

Figure 2.9: Diffusion coefficients for the ECM (dark bars) and PCM (light bars) of porcine cartilage for 70 kDa and 500 kDa dextrans (mean±SEM). There was a significant effect of both dextran size and matrix with no significant interactive effect (ANOVA, $p<0.00001$). Diffusion coefficients were significantly lower in the PCM than in the adjacent ECM ($p=0.0001$) and were significantly lower with the 500 kDa dextran than with the 70 kDa dextran ($p=0.02$). $N\geq3$ pigs per bar; $n\geq15$ sites per bar.

2.5 Discussion

Our modifications to the original SCAMP technique (Kubitscheck *et al.* 1998) allow for increased applicability of the method. By implementing the asymmetrical time step, the revised SCAMP method accounts for time spent not bleaching, an issue on commercial microscopes. This also allows for measurement of larger diffusion coefficients. Our revised technique also incorporates any real-world asymmetries in the point-spread function of the microscope by utilizing the measured point-spread function

rather than an idealized theoretical one. Finally, our technique also addresses the ambiguity in the first bleached line and extrapolates back to an appropriate initial unbleached condition. It is possible that the SCAMP technique could be further modified to measure diffusional anisotropy (see, e.g., Refs. (Kinsey *et al.* 1999; Gennerich and Schild 2002; Leddy *et al.* 2006)). For example, if the scanned line in SCAMP is sufficiently long and narrow, the measured diffusivity will be dominated by the effects of diffusion across the thickness of the line (i.e., one pixel in our case), thus creating a largely one-dimensional *D* measurement.

Our findings show that the SCAMP technique, in combination with an appropriate theoretical analysis, can be used to measure site-specific diffusivity in a relatively small volume of tissue. The mean diffusion coefficients measured in the ECM, 23 $\mu m^2/s$ for 70 kDa dextran and 17 $\mu m^2/s$ for 500 kDa dextran, are in good agreement with values measured previously using other techniques (31 and 7 $\mu m^2/s$ for 70 and 500 kDa, respectively, using fluorescence recovery after photobleaching; 40 $\mu m^2/s$ for 70 kDa using radiotracer tracking (Torzilli *et al.* 1997; Leddy and Guilak 2003)). Using the SCAMP method to probe the small volume of the PCM, we have shown in porcine articular cartilage that diffusivity of the PCM is slower for a larger molecule, is lower than that of the adjacent ECM, and, in the case of early-stage arthritis, has become indistinguishable from that of the ECM.

Only one previous study has measured diffusion in the PCM by quantifying the motion of diffusion of gold-tagged lipids tethered to the membranes of isolated keratocytes that were synthesizing a new PCM in culture (Lee *et al.* 1993). This study showed that the presence of a PCM can decrease diffusivity by about half as compared with cells with no newly formed encompassing matrix. Our study, however, is the first to measure the diffusion of a freely mobile molecule in the native chondrocyte PCM in situ. Similar to the study of Lee et al. (Lee *et al.* 1993), our values for diffusivity in the PCM are less than what would be expected with no matrix present (i.e., free solution) (Luby-Phelps *et al.* 1986).

The difference in diffusivity between PCM and ECM in healthy cartilage is likely attributable to the differences in the structure and composition of the PCM, which contains finer collagen fibers and a higher concentration of proteoglycans relative to the ECM (Poole 1997). A previous study in the ECM has shown that diffusivity is inversely correlated with proteoglycan concentration (Evans and Quinn 2005). The PCM is also characterized by a network of collagen VI, which is not present in the ECM of the cartilage under normal circumstances. SCAMP measurements showed a high degree of variability within both the PCM and ECM, which is potentially attributable to inhomogeneities that may be present in the small regions over which the measurement is taken. A similar variability has been observed previously in tests of the biomechanical

properties of the PCM (Alexopoulos *et al.* 2003; Alexopoulos *et al.* 2005b; Alexopoulos *et al.* 2005c).

Although normal cartilage showed a significant difference in diffusivity between the PCM and ECM, this difference was no longer present in early-stage osteoarthritic samples. This appears to be due to increased diffusivity in the PCM of osteoarthritic tissue. However, the lack of changes in diffusivity in the osteoarthritic ECM with the 70 kDa dextran does not preclude different diffusivity properties since molecules of other sizes may have the sensitivity to detect differences (Han and Herzfeld 1993; Lubkin and Wan 2006). Nonetheless, the increased diffusivity of the PCM with osteoarthritis is consistent with the previous report of increased hydraulic permeability in the PCM of human end-stage osteoarthritic cartilage (Alexopoulos *et al.* 2003). An increase in PCM diffusivity in early osteoarthritis suggests that initial tissue degradation is likely mediated by the chondrocyte's release of enzymes that first affect the pericellular region. These findings are also in general agreement with previous reports of swelling and enlargement of the PCM in osteoarthritic cartilage (Lee *et al.* 2000). Taken together, these studies suggest that an early step in the development of osteoarthritis may be the chondrocyte-mediated degradation of the PCM (Poole 1997; Söder *et al.* 2002), wherein the chondrocyte releases enzymes that first affect the pericellular region. An increase in PCM diffusivity may alter the modification or retention of growth factors or

chondrocyte-released matrix macromolecules or perhaps influence the transport rate of growth factors or cytokines to the chondrocyte.

Ultimately, the PCM may regulate both the biomechanical and biochemical environments of the cell (Poole *et al.* 1988; Poole *et al.* 1990; Poole *et al.* 1991; Poole *et al.* 1992). To interact with the chondrocyte surface or be released from the chondrocyte into the ECM, molecules must pass through the pericellular environment, which completely encompasses the cell. Although the data presented here show a significantly lower diffusivity in the PCM as compared with the ECM, these differences in diffusion coefficients are relatively small and unlikely to limit the bulk transport of nutrients or signaling molecules, particularly in the presence of significant convective transport (O'Hara *et al.* 1990; Mauck *et al.* 2003; Evans and Quinn 2006a; Evans and Quinn 2006b). As soluble mediators traverse the PCM, they can be modified or retained (Ruoslahti and Yamaguchi 1991), and the longer time spent in the healthy PCM may be crucial to achieve these alterations. An assembly of the mature aggrecan-hyaluronan complex, required to form the ECM, occurs as the aggrecan and hyaluronan molecules move across the PCM after being secreted from the chondrocyte (Sandy *et al.* 1989). In addition, enzymes and pro-enzymes that degrade cartilage matrix (metalloproteinases and aggrecanases) must also pass through the PCM before affecting the ECM. Therefore, the rate of molecular diffusion through the PCM may control the proper synthesis, assembly, and function of matrix macromolecules; subsequently, alterations in PCM

structure or properties, as may occur with aging or disease (Alexopoulos *et al.* 2003), may have secondary effects on the cartilage ECM. Further quantitative understanding of the diffusional properties of the PCM could help elucidate the regulatory role of this tissue region in controlling molecular transport to and from the chondrocyte.

Chapter 3.

Influence of Matrix and Zone on Diffusion Through Interleukin-1α-Treated Cartilage

3.1 Introduction

Articular cartilage is a thin, deformable, connective tissue that lines the ends of long bones at diarthrodial joints. Healthy articular cartilage serves as an extremely low-friction surface for articulation, provides joint congruity, and distributes loads which routinely reach approximately three times body weight (Guilak *et al.* 1997). Arthritis, the most prevalent disease affecting this tissue, can impair the function, alter the composition, and erode the structures of articular cartilage. In the United States alone, more than 46 million people suffer from this degradative disease (CDC 2008). Study of the changes that occur with cartilage degradation will provide critical insights into practical treatment of this disease.

Adult articular cartilage is aneural, alymphatic, and avascular (Guilak *et al.* 2000). Water accounts for 65% to 80% (wet weight) of the cartilage (Maroudas 1979; Lai *et al.* 1991). Cations and anions comprise the ionic phase (Lai *et al.* 1991). The solid phase consists predominately of proteoglycans (5-10% by wet weight) and cross-linked collagen, mostly type II (15%-20% by wet weight) but also small amounts of other collagens, including types VI, IX, X, and XI (Maroudas 1979; Heinegard and Oldberg 1989; Poole 1997). Overall, the collagen forms a network that restrains the swelling of the hydrated, negatively-charged proteoglycans that are interspersed throughout the collagen ultrastructure; the end result is pressurized tissue (Lai *et al.* 1991; Krishnan *et al.* 2004). Although cartilage cells, termed chondrocytes, are responsible for producing and

maintaining this cartilage matrix, they usually comprise less than 10% of the tissue volume (Stockwell 1979; Guilak and Mow 2000).

The distribution of cartilage components varies with depth to produce three tissue zones: the surface, the middle, and the deep. In the surface zone, typically 10% to 20% of the total cartilage thickness (Mow *et al.* 1989), small-diameter collagen fibrils (25-50 nm in diameter) pack densely and align highly parallel to the articulating surface (Muir *et al.* 1970; Hwang *et al.* 1992), the proteoglycan count is low (Poole 1997), and the cells present as flattened discs (Poole 1997). In the middle zone, typically 40% to 60% of the total cartilage thickness (Mow *et al.* 1989), slightly larger collagen bundles (60-140 nm in diameter) begin to form arcade-like structures amidst some randomly-oriented fibers (Hwang *et al.* 1992); proteoglycans are present in high levels and cells are spheroids (Poole 1997). Closest to the subchondral bone and comprising about 30% of the total cartilage thickness (Mow *et al.* 1989), the deep zone hosts the largest collagen fiber bundles (up to 160 nm in diameter), which orient perpendicular to the underlying bone (Weiss *et al.* 1968; Hwang *et al.* 1992); there, cells present as spheroids in columns (Poole 1997).

The cartilage matrix is also affected by the proximity to or distance from the chondrocytes, which are surrounded by a pericellular matrix (PCM). This region is compositionally and structurally distinct from the extracellular matrix (ECM). The PCM is characterized by high proteoglycan content and by other PCM constituents including

collagen II, IX, and XI, fibronectin, aggrecan, and decorin (Poole *et al.* 1988; Poole *et al.* 1990; Poole *et al.* 1991; Poole *et al.* 1992; Poole *et al.* 1996; Poole 1997). Most notably, however, the PCM is the only place in cartilage that collagen VI is found (Poole *et al.* 1988). The PCM is also mechanically distinct from the ECM by its lower Young's modulus (Alexopoulos *et al.* 2003; Alexopoulos *et al.* 2005a; Alexopoulos *et al.* 2005c). In consequence, the PCM is thought to act as a mechanical transducer in cartilage and to modulate the biochemical environment of the cells (Guilak *et al.* 2006).

Because adult cartilage is avascular, molecular transport is a critical issue for the health of the tissue. Oxygen, nutrients, waste products, signaling molecules, matrix macromolecules, and more must all pass through the tissue by diffusion or convection. Overall, diffusion appears to serve as the major transport mechanism within the tissue for most molecules. Measures of diffusion can also serve as a probe of the underlying tissue structure.

The rate of molecular diffusion through normal cartilage is affected by numerous factors, including molecule size, molecule charge, tissue zone, and tissue matrix. Generally, larger molecules diffuse more slowly through cartilage (Maroudas 1976; Torzilli *et al.* 1987; Leddy and Guilak 2003). Negatively charged molecules (Cl^-) diffuse faster through cartilage than positively charged molecules (Na^+), likely due to reduced interactions with negatively charged proteoglycans (Maroudas 1975). Molecular diffusion rates vary between the surface and middle/deep zones, but this relationship is

complex and depends at least on the size of the diffusing molecule (Leddy and Guilak 2003). The cartilage matrix also influences molecular diffusion; dextrans diffuse faster through the ECM than through the PCM (Leddy/Christensen *et al.* 2008).

A few studies have examined diffusion in diseased or modified cartilage. In early-stage arthritic cartilage, matrix-based diffusion differences are no longer detectable (Leddy/Christensen *et al.* 2008), indicating that early arthritic breakdown may first occur nearest the cell. Modifying cartilage by enzymatically removing proteoglycans raises the diffusion rates of many — but not all — of the molecules studied (Torzilli *et al.* 1997), indicating an availability of diffusion pathways characterized by fewer molecular obstacles.

Since the degradative process of arthritis is known to involve cytokines, study of diffusion through cartilage that has been cultured in the presence of a catabolic cytokine could reveal disease-related changes in diffusional properties of the tissue. These changes could vary with zone, with matrix, and over time.

Of the many cytokines which act catabolically upon cartilage, interleukin-1 (IL-1) has one of the most potent effects (Goldring 2000). Interleukin-1 suppresses collagen and proteoglycan synthesis while stimulating the synthesis and activity of matrix metalloproteinases that promote proteoglycan breakdown (Neidel and Zeidler 1993; Gouze *et al.* 2001; Jacques *et al.* 2006). Interleukin-1 culture reduces the mechanical properties of cartilage, although this mechanical degradation takes weeks; IL-1

treatment has not influenced the cartilage tensile strength or failure strain after 7 days in culture (Temple *et al.* 2006), nor the Young's modulus and dynamic modulus after 14 days in culture (Lima *et al.* 2008). In advanced arthritis, IL-1 is able to sustain both inflammation and cartilage erosion (van den Berg *et al.* 1999). Furthermore, surface-zone chondrocytes have been shown to be more susceptible to IL-1 than chondrocytes from deeper layers (Hauselmann *et al.* 1996), although IL-1 does not markedly reduce cell viability in any zone (Fermor *unpublished data*). Activated IL-1 signaling pathways have been found at highest concentrations in the surface zone of both normal and osteoarthritic cartilage (Fan *et al.* 2007). These cartilage responses to IL-1 make this cytokine particularly appealing for modeling tissue degradation.

To study diffusion through IL-1-treated cartilage, fluorescently-labeled ovalbumin was selected. Since this 45kDa protein is globular, it resembles native proteins more closely than do the commonly studied linear dextran molecules. Consequently, the diffusional behavior of cytokines and biologically relevant molecules is more closely modeled. The fluorescent tag allows the use of a photobleaching technique for measuring diffusion; for these experiments, scanning microphotolysis (SCAMP) is most appropriate because it can be used to measure diffusion in extremely small volumes, such as within the 2μm-thick PCM (Youn *et al.* 2006; Leddy/Christensen *et al.* 2008).

Overall, this study examined the IL-1 treatment effects on zonal and matrix diffusivity in articular porcine cartilage. Diffusion of FITC-ovalbumin was measured after 0, 1, 3, or 7 days of culture. Because the cartilage zones interact differently with IL-1 and have demonstrated different diffusivities in healthy tissue, the surface zone was expected to show an earlier and more drastic increase in diffusivity as compared to the middle zone. Furthermore, the PCM and ECM were expected to respond differently to IL-1 treatment, with the PCM affected first because it is adjacent to the metabolic unit, the chondrocyte. To better understand the results of this diffusion study, tissue histology samples were also stained to reveal the proteoglycan distribution and intensity throughout the cultured explants.

3.2 Materials and Methods

3.2.1 Tissue Culture

3.2.1.1 Tissue Preparation for Culture

Knee joints of two- to three-year-old female pigs were obtained from a local abattoir. From the lateral femoral condyles of joints showing no signs of degradation, fresh, full-thickness cartilage explants were excised with a 6mm-diameter biopsy punch and quartered with a razor blade, all while using sterile technique. Each cartilage wedge was placed into a single well of a 96-well plate with 200 μl of culture medium.

3.2.1.2 Culture Conditions

The culture medium consisted of DMEM (Invitrogen), 10% heat-inactivated fetal bovine serum (HyClone), 0.1 mM non-essential amino acids (Invitrogen), 100 U/ml antibiotics (penicillin/streptomycin, Invitrogen), 10 mM HEPES buffer solution (Invitrogen), and 37.5 μg/ml L-ascorbic acid 2-phosphate (Sigma-Aldrich). Medium was changed every 2 days. Cartilage samples were incubated at 37°C in a 5% CO_2, humidified incubator for 0, 1, 3, or 7 days.

3.2.1.3 IL-1α Treatment

Tissue samples were site-matched for standard culture treatment or supplemental IL-1α treatment. For IL-1α -treated samples, recombinant porcine IL-1α (RnDsystems, lot # BNJ0208081) was added to the culture well to a concentration of 10 ng/ml with each medium change.

3.2.2 Diffusion Measurements

3.2.2.1 Tissue Preparation for SCAMP

Upon removal from culture, the cartilage samples were rinsed briefly in PBS. A razor blade was used to slice thin (<0.5 mm), full-thickness cartilage samples from the tissue wedge. Two to three such slices were soaked in a 25 mg/ml solution of FITC-labeled ovalbumin (Molecular Probes) at least 30 minutes to allow the fluorescent molecules to reach an equilibrium distribution within the cartilage. The remainder of the cartilage wedge was wrapped in PBS-soaked gauze and frozen at -20°C for histology.

3.2.2.2 SCAMP Setup

For microscopy, a FITC-ovalbumin-soaked slice of cartilage was placed in a humidified coverslip chamber with the full-thickness cross-section against the coverslip. The cartilage was covered with several microliters of PBS and immobilized within a holder specially designed to reduce evaporation.

3.2.2.3 SCAMP Settings

Microscopy settings were the same as used previously (Leddy/Christensen *et al.* 2008). The 100x, 1.3-NA oil immersion lens was used in combination with the 6x optical zoom on a confocal laser scanning microscope (LSM 510, Zeiss). Six-μm deep within the tissue, a 12-pixel line (1.44 μm) was bleached 40 times with an argon laser (excitation wavelengths: 458 and 488 nm). The emission intensity was collected during bleaching and saved as the image for that experiment.

3.2.2.4 SCAMP Measurements

At each site, multiple experiments were performed and their intensity values averaged to minimize noise. Sites were paired; for each PCM site approximately 1 μm from a cell's edge, a neighboring ECM site at least 5 μm from the cell's edge was also evaluated. Experimental sites were selected within the surface and middle zones. SCAMP experiments for this range of diffusion values do fit within the confines of a middle-zone porcine PCM (average thickness: 3 μm) and a surface-zone porcine PCM

(average thickness: 2 μm) (Youn *et al.* 2006). Experiments were oriented parallel to the tissue surface.

3.2.2.5 Data Processing

The diffusion coefficient of the FITC-tagged ovalbumin was calculated for each site by best-fit to simulated data according to unconstrained nonlinear optimization. A signal-to-noise ratio of 10 was the minimum value required for data quality standards (Leddy/Christensen *et al.* 2008). All data processing and fits were accomplished in Matlab (The Mathworks, Natick, MA). Statistics were run in Statistica (Statsoft, Tulsa, OK). The effects of the matrix, the zone, the culture time, and the IL-1α treatment were determined by a repeated-measures analysis of variance (ANOVA) on the calculated diffusion coefficients; ECM and PCM measurements were paired.

3.2.3 Histology

A frozen cartilage sample from each time point (Day 0, 1, 3, and 7) and for each treatment group (with or without IL-1α) was thawed. The tissue was processed for staining according to standard procedures. Tissue was fixed in 10% buffered neutral formalin (VWR), dehydrated with increasing concentrations of ethanol, cleared with xylenes (Mallinckrodt Chemicals), infiltrated with paraffin (Paraplast® tissue embedding medium, Fisher), and embedded for slicing. Full-thickness cartilage slices were cut 8-μm thick with a microtome (Reichert-Jung), collected on slides (Superfrost®/Plus, Fisher), and dried overnight on a slide warmer at 45°C. Slides were

stained with Harris' hematoxylin, safranin-O, and fast green. Coverslips were adhered with Permount (Fisher Scientific); they were dried overnight. Images of the stained sections were taken on a light microscope (Zeiss).

3.3 Results

The FITC-ovalbumin coefficient of diffusion was measured in pig cartilage: in the PCM and ECM; in the surface and middle zones; after 0, 1, 3, and 7 days of culture; and after IL-1α treatment or lack thereof (Figure 3.1).

Overall, the FITC-ovalbumin coefficient of diffusion was influenced by all of the factors examined: matrix ($p < 0.0004$), zone ($p < 10^{-6}$), time ($p < 10^{-6}$), and treatment ($p < 10^{-6}$). Differences between PCM and ECM diffusivities were slight but statistically significant ($p < 0.0004$); the ECM diffusivity averaged 2 $\mu m^2/s$ higher than that of the PCM. Treatment by IL-1α influenced both the middle and surface zones about equally, increasing their diffusivity over time. Without IL-1α treatment, the middle zone retained its original, low diffusivity over the entire course of the experiment. However, without IL-1α treatment, diffusivity increased in the surface zone through the third day before leveling off; surface zone diffusivity with or without IL-1α treatment was about the same at Day 1 and again at Day 3.

Additionally, the repeated-measures ANOVA revealed significant interactive effects on diffusion: day-by-treatment ($p < 10^{-6}$), treatment-by-zone ($p < 10^{-6}$), and day-

by-treatment-by-zone ($p < 0.00003$). No significant day-by-zone interactive effect was evident ($p = 0.6$). The matrix type (PCM v. ECM) had only one significant interactive effect: matrix-by-day ($p < 0.03$).

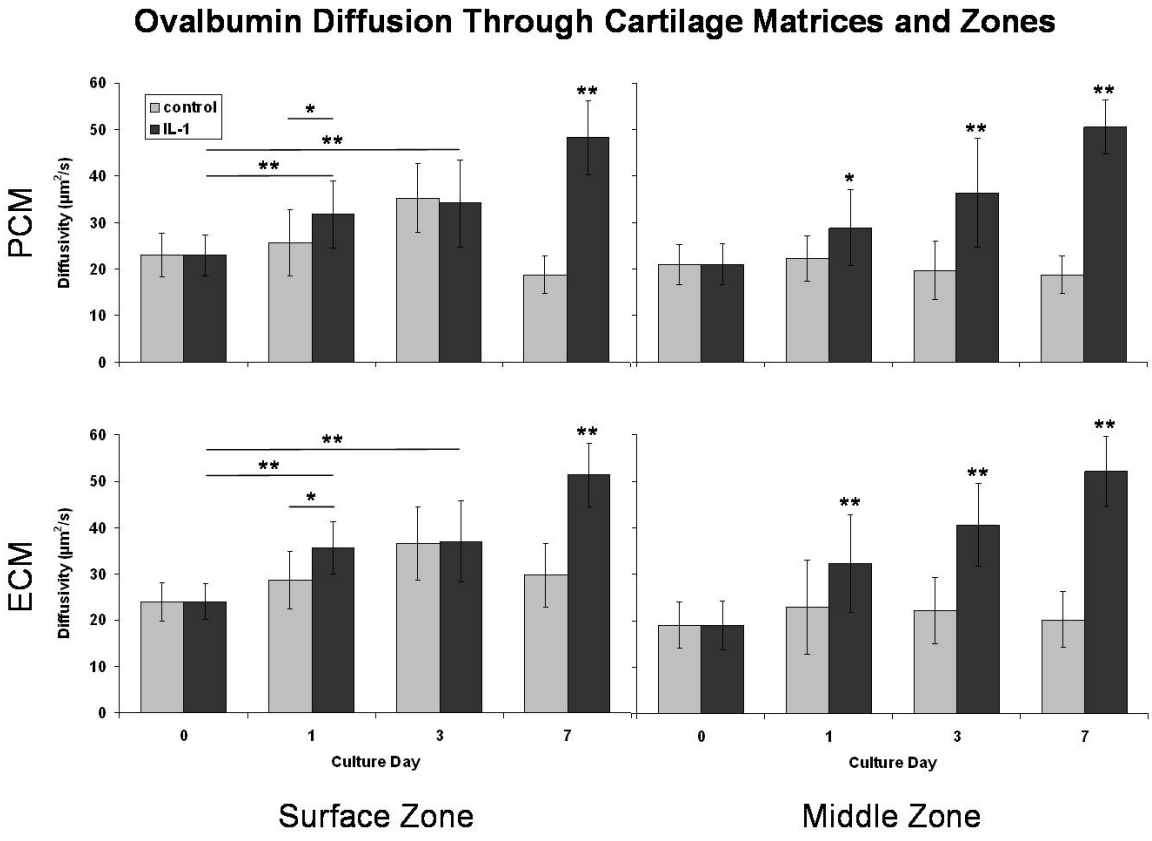

Figure 3.1: Diffusion of ovalbumin increases with IL-1 culture. Diffusivity in the PCM is consistently about 2 μm²/s lower than the ECM. With IL-1 treatment, surface zone and middle zone average values are similar. Under control culture conditions, middle zone diffusivity remains constant while the surface zone diffusivity increases to Day 3. From the repeated-measures ANOVA (PCM and ECM paired) followed by Fisher's LSD post-hoc, graphs show IL-1 bars compared to each other and to their control. *p<0.05; **p<0.01. For each bar, n=15-20 sites from N=3-5 pigs. Bars are mean ± standard deviation.

Although the histology images (Figure 3.2) showed no changes in cell distribution (hematoxylin: black stain of nuclei) or in collagen (fast green: blue stain of collagen), culture time and IL-1α treatment both influenced the proteoglycan distribution (safranin-O: red stain of proteoglycans). Proteoglycan staining decreased marginally over time in the control explants. In the IL-1α-treated samples, this process was hugely accelerated. Proteoglycan loss occurred most rapidly the surface zone, followed by the deep zone (an exposed face), and finally the middle zone. IL-1α-treated explants show near-total proteoglycan loss within 7 days.

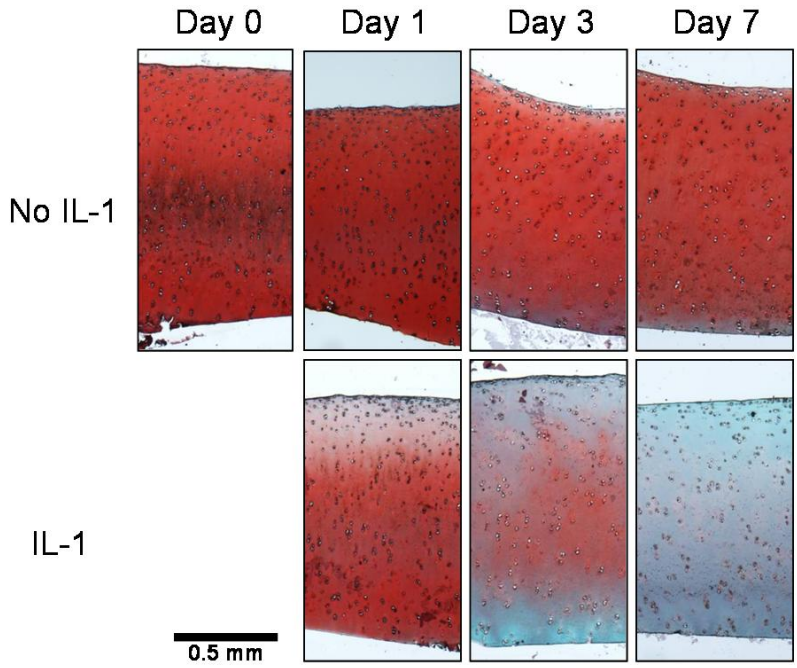

Figure 3.2: Histological sections of cultured explants are stained with safranin-O (red, proteoglycans), fast green (blue, collagen), and hematoxylin (black, nuclei). IL-1 treatment spurs dramatic proteoglycan loss first from the surface zone by Day 1, then from the deep zone by Day 3, and lastly from the middle zone by Day 7. The control explants show faint loss of proteoglycans, primarily at the outer explant faces (surface zone and exposed deep zone). Collagen staining is masked by the strong proteoglycan staining in most images. Scale bar is 0.5 mm.

3.4 Discussion

Interleukin-1α treatment of articular cartilage increases the diffusion of ovalbumin irrespective of zone and matrix. Although ovalbumin is not found in native cartilage, this 45kDa protein serves as an affordable model for globular proteins, including cytokines such as transforming growth factor-β (TGF-β) and interleukins, that habitually move through cartilage tissue.

Before culture, at Day 0, ovalbumin diffused at near-identical rates (about 20 $\mu m^2/s$) through the surface and middle zones. This was surprising in view of zonal diffusivity studies carried out using dextrans molecules, where both the 40kDa and 70kDa dextrans diffused more than three times faster in the middle/deep zone relative to the surface zone (Leddy and Guilak 2003). However, the 45kDa ovalbumin protein is globular rather than linear in conformation, and molecule shape affects the diffusion properties based on interactions with the structures through which the molecule passes. Overall, then, the initial lack of diffusivity differences between the surface and middle zone is attributed to this molecular shape difference.

Relative to the ECM, the PCM had a lower diffusivity throughout the study. This pattern is consistent with an earlier SCAMP study (Leddy/Christensen *et al.* 2008), which showed slower diffusion of 70kDa and 500kDa dextrans through the PCM versus ECM of healthy pig cartilage. Although cellular metabolic activity in the presence of IL-1α was expected to yield earlier degradation of the PCM relative to the ECM, particularly in the surface zone, the diffusion measurements did not provide support for this hypothesis. (Evidence would have taken the form of an increase in diffusion rates within the PCM at an earlier time point than in the ECM.)

If such PCM-first degradation does exist in IL-1α-mediated degradation, as suggested by studies of arthritis showing increased diffusivity in the PCM (Leddy/Christensen *et al.* 2008), decreased stiffness of the PCM (Alexopoulos *et al.* 2003),

swelling and enlargement of the PCM (Poole 1997), altered organization of collagen VI in the PCM (Söder *et al.* 2002), and loss of PCM fibrillar architecture (Poole 1997), this study may have missed detecting it because of any of the following reasons, or combination thereof: (1) ovalbumin may be too large or too small a diffusing molecule to be affected by the degradation patterns; (2) the time points examined may not have captured the difference; and (3) the high dosage of IL-1α may have overwhelmed the cells, causing an unnaturally high release of degradative enzymes (MMPs) whose effects promptly extended beyond the confines of the PCM.

IL-1α had a similar effect on the surface zone and the middle zone. Given the higher net metabolic activity of the densely cellular surface zone and the increased prevalence of activated IL-1α signaling receptors in surface-zone cells (Fan *et al.* 2007), the surface zone was expected to produce more degradative enzymes, which would hypothetically correlate with proteoglycan breakdown and increased diffusivity in that zone relative to the middle zone. Interestingly, diffusivity was never significantly different between zones in the IL-1α-treated explants. However, the control group of explants cultured without IL-1α showed increased diffusivity in the surface zone through the third day, but no increase in the middle zone. This is attributed to the moderate amount of proteoglycan leaching that typically occurs during the first few days of cartilage explant culture, with greater proteoglycan loss from the surface zone, perhaps due to the increased metabolic activity in the surface zone relative to the middle

zone. Lower proteoglycan content has been previously correlated with increased rates of diffusion through cartilage (Maroudas 1970; Torzilli *et al.* 1997).

Because of the pain and expense of arthritis, the gradual process of cartilage degradation warrants careful study. As demonstrated in this set of experiments, diffusion of molecules through cartilage varies during the degradative process. This not only reflects structural changes within the cartilage but also potentially changes the biochemical signals received by the chondrocytes, skews the balance between catabolic and anabolic tissue processes, and drives a feedback loop to accelerate degradation. Further determining how native, diffusing proteins are influenced by gradual cartilage degradation will be an important step in improving scientific understanding of arthritis and choosing potential therapeutic targets within cartilage.

Chapter 4.

Physical Properties of the *Col6a1*-knockout Mouse Knee

4.1 Introduction

Collagen VI, one of several collagens found in the knee, is a heterotrimeric protein present both in bone and in articular cartilage. In bone, collagen VI has been identified both in remodeling bone (Keene *et al.* 1991) and in developing bone, particularly the young growth plate (Alexopoulos *et al.* 2009). In articular cartilage, collagen VI is localized to the pericellular matrix (PCM) (Poole *et al.* 1988; Poole 1997) alongside various basement membrane proteins (Kvist *et al.* 2008). Collagen VI has also been found in other tissues of the knee, including the electron-dense seams of ligaments (Bray *et al.* 1993) and the cellular, pericellular, and main-body regions of the menisci (Chevrier 2009).

Collagen VI is heterotrimeric, formed of three distinct proteins: a1(VI), encoded by *col6a1*; a2(VI), encoded by *col6a2*; and a3(VI), encoded by *col6a3* (Lampe *et al.* 2008). Collagen VI has been shown to play a bridging role in connective tissues, where it forms a flexible network interlinking collagen types I, II, IV, proteoglycans, hyaluronan, and cells (Keene *et al.* 1988; Bonaldo *et al.* 1990; Specks *et al.* 1992; Kuo *et al.* 1997; Zeichen *et al.* 1999). Recent research has identified three other collagen VI variants, *col6a4*, *col6a5*, and *col6a6*, which encode proteins that may substitute in place of COL6A3 in the heterotrimeric fibrils (Fitzgerald *et al.* 2008; Gara *et al.* 2008).

Human collagen VI genetic abnormalities have been linked to muscular disorders, specifically Bethlem myopathy and Ullrich congenital muscular dystrophy

(Bertini and Pepe 2002; Lampe and Bushby 2005; Lampe *et al.* 2008), and to ligamentous disorders, namely ossification of the ligamentum flavum, ossification of the posterior longitudinal ligament of the spine, and diffuse idiopathic skeletal hyperostosis (Tanaka *et al.* 2003; Tsukahara *et al.* 2005; Kong *et al.* 2007). Mutations in collagen VI genes have also been linked to mitochondrial dysfunction (Irwin *et al.* 2003), to abnormal expression of proteoglycans and adhesion molecules in some tissues (Petrini *et al.* 2005; Higashi *et al.* 2006), and to a skin disorder, atopic dermatitis (Gara *et al.* 2008). Recently, a susceptibility locus for atopic dermatitis was identified in *col6a5* (Söderhäll *et al.* 2007) and the *DVWA* (double von Willebrand factor A domains) susceptibility locus for knee osteoarthritis identified as part of *col6a4* (Miyamoto *et al.* 2008; Wagener *et al.* 2009).

The role of collagen VI in the knee is poorly understood. In articular cartilage, where collagen VI in conjunction with decorin, fibronectin, and hyaluronan helps anchor the chondrocyte to the PCM (Keene *et al.* 1988; Marcelino and McDevitt 1995; Chang *et al.* 1997), collagen VI may be critical to proper transduction of biochemical and biomechanical signals to the cell. In bone, collagen VI may play a role in bone formation at the growth plate (Alexopoulos *et al.* 2009) and may regulate collagen I expression in the early phase of IL-4-induced mineralization (Harumiya *et al.* 2002). In leg muscles, collagen VI is critical to normal function; abnormal levels of collagen VI lead to laxity or contractures and thereby change the mechanical forces at the joint. Failure of collagen

VI to perform these roles in cartilage, bone, and muscle may alter joint development or tissue homeostasis in the knee.

Collagen VI knockout mice have been developed by Bonaldo and colleagues using targeted gene disruption of *Col6a1* (Bonaldo *et al.* 1998), who initially studied the skeletal muscles of these mice (Bonaldo *et al.* 1998; Irwin *et al.* 2003). More recently, the hip cartilage and some skeletal characteristics of these knockout mice have been carefully studied (Alexopoulos *et al.* 2009). Skeletal staining of 1-month-old wild-type and knockout mice with alcian blue and alizarin red, to dye cartilage and bone, respectively, revealed that knockout mice are smaller and exhibit a delayed extremity ossification process. Dual energy X-ray absorptiometry studies revealed a lower bone mineral density in knockout mice at ages 3 and 6 months, as compared to wild-type mice; this difference was no longer present by 11 months of age. Micropipette aspiration experiments revealed a lower Young's modulus for the PCM of knockout versus wild-type hip chondrons, yet microindentation tests showed no differences in the cartilage extracellular matrix Young's modulus at the femoral head. Semi-quantitative grading of hip joint histology revealed that *Col6a1*$^{-/-}$ mice undergo accelerated development of hip arthritis (Alexopoulos *et al.* 2009). Overall, that study presents valuable data on the skeletal development and hip cartilage properties of *Col6a1*$^{-/-}$ mice, but leaves open the question of how collagen VI influences physical properties at the knee.

We have hypothesized that absence of collagen VI affects the development and aging of the knee joint and examined this hypothesis using several distinct analytical tools. We have examined knee joints of collagen VI knockouts by assessing the morphometry of the tibia at the knee, evaluating histological sections of the knee, testing the elastic modulus, roughness, and coefficient of friction along the surface of the tibial plateau, and probing the cartilage structure by measuring diffusion of a fluorescent molecule through the tissue of *Col6a1*-knockout mice.

4.2 Materials and Methods

4.2.1 Tissue Preparation

Twenty-five *Col6a1*$^{+/+}$ and *24 Col6a1*$^{-/-}$ mice on a CD1 genetic background (as used in (Alexopoulos *et al.* 2009)) were raised under the approval of the Duke University Institutional Care and Use Committee. Most were bred from heterozygous parents, but control mice were purchased from Charles River Laboratories for all CD1 2-month-old mice and three CD1 male 15-month-old mice. At the target age of 2, 9, or 15 months old, 8 or 9 mice per group (4 males and 4 or 5 females) were sacrificed and promptly frozen at −20°C. An autopsy saw was used to isolate the frozen left and right legs from the remainder of the carcass. The legs were thawed for dissection directly before fixation (right limb: microCT and histology studies) or before microscopy (left limb: AFM and diffusion studies).

4.2.2 Microcomputed Tomography (MicroCT)

Right knee joints were fixed in 10% buffered neutral formalin (VWR) for 24 to 72 hours. Knees were scanned by a microCT system (microCT 40, Scanco Medical AG, Bassersdorf, Switzerland). Application of an appropriate global thresholding value, 364, distinguished calcified tissues from soft tissues. Scans from a hydroxyapatite (HA) calibration phantom were used to calculate bone density values (mg HA/cm^3) from collected linear attenuation values for the samples. The morphometry of the calcified tissues was evaluated in the proximal tibial plateau down to the growth plate and in the 25 slices of the metaphyseal region immediately distal to the fibular attachment. Several tibial plateau measures were calculated from the raw microCT data values: for the cortical and trabecular bone together, the total volume (TV, mm^3), bone volume (BV, mm^3), relative bone volume (BV/TV), and bone tissue density (Mean2, mg HA/cm^3); and for the trabecular bone alone, the total volume (mm^3), bone volume (mm^3), relative bone volume, bone tissue density (mg HA/cm^3), structure model index (SMI, a quantification of the shape of the trabeculae) (Hildebrand and Ruegsigger 1997; Smit *et al.* 2003), connectivity density (ConnDens, 1/mm^3), trabecular number (Tb.N, 1/mm), trabecular thickness (Tb.Th, mm), and trabecular separation (Tb.Sp, mm). In the metaphyseal region of the tibia, similar measures were evaluated for the cortical and trabecular bone together: bone volume (BV, mm^3) and bone tissue density (Mean2, mg HA/cm^3), which could be multiplied to calculate the mineral content. The length of the tibial plateau was

also crudely measured by counting the number of 16-μm slices from the growth plate to the proximal end of the calcified region of the bone; the lengths of two subsets of this region, the trabecular and non-trabecular (subchondral bone) portions, were also measured.

Abbreviations for MicroCT Measures

TV	total volume (mm^3)
BV	bone volume (mm^3)
BV/TV	relative bone volume
Mean2	bone tissue density (mg HA/cm^3)
ConnDens	connectivity density, normed by TV (1/mm^3)
SMI	structure model index
Tb.N	trabecular number (1/mm)
Tb.Th	trabecular thickness (mm)
Tb.Sp	trabecular separation (mm)

4.2.3 Histology

4.2.3.1 Sample Preparation

Right knee joints were fixed in 10% buffered neutral formalin (VWR) for 3 days, during which time they were scanned by microCT. Knees were subsequently soaked in Cal-Ex® Decalcifier (Fisher Scientific) for 3 days. Dehydration was performed at room temperature: 30% EtOH for 20 minutes, 50% EtOH for 20 minutes, 75% EtOH for 20 minutes, 90% EtOH for 20 minutes, and finally 100% EtOH for 40 minutes. Samples were infiltrated at room temperature: 100% EtOH and xylenes (Mallinckrodt Chemicals) (50:50) for 20 minutes, xylenes for 60 minutes, and xylenes again for 60 minutes. Samples were embedded in paraffin using a 60°C oven: xylenes and paraffin (50:50) for

60 minutes, paraffin for 90 minutes, and paraffin for at least 8 hours. Samples were transferred to cassettes and then sectioned by microtome into 7μm coronal slices. For each mouse, the slide bearing sections with the smallest wedge of medial and lateral meniscus was chosen for staining. These samples were deparaffinized, hydrated, and stained with hematoxylin, Fast Green, and safranin-O. Staining was protected by Permount (Fisher Scientific) with a coverslip.

4.2.3.2 Direct Measurements

The subchondral thickness was measured from across the full width of the loaded regions of the femoral condyle and tibial plateau in histologically stained sections. These subchondral thickness measures did not include calcified cartilage. For each of the medial and lateral condyles and plateaus, ten lines were drawn from the internal edge of the calcified cartilage to the nearest bone marrow. Lines were equally spaced along the subchondral bone and perpendicular to the cartilage surface. These lengths were averaged to determine the mean subchondral thickness for the joint. Additionally, the thickness of the joint capsule was measured on the medial side of the joint alongside the meniscus. This joint capsule, which primarily included the medial collateral ligament (MCL), was measured with five lines drawn perpendicular to the joint space adjacent to the meniscus. Line lengths were averaged.

4.2.3.3 Modified Mankin Scoring

Three blinded graders evaluated histological samples to assess arthritic progression according to a modified Mankin scoring rubric previously established (Furman *et al.* 2007). No grades were given for chondrocyte cloning. The grading rubric is included in Appendix B. Four sites were scored: the lateral femoral condyle, lateral tibial plateau, medial femoral condyle, and medial tibial plateau. A score ranging from 0 to 28 was possible; higher scores indicated further degeneration of the cartilage.

4.2.4 Atomic Force Microscopy (AFM)

4.2.4.1 Sample Preparation

The left mouse tibia was thawed, carefully dissected, and cut at mid-shaft with a razor blade to shorten its length. Hot-melt glue (Arrow Fastener Co., Saddle Brook, NJ) was used to secure the diaphysis of the tibia vertically within a small polystyrene Petri dish lid (Falcon), leaving the tibial plateau near-horizontal within the lid. Phosphate-buffered saline (PBS, Gibco, Carlsbad, CA) at room temperature was added to cover the tibial plateau. The lid was secured to a glass microscope slide and oriented such that the anterior-posterior direction on the lateral tibial plateau was perpendicular to the AFM cantilever.

4.2.4.2 Tip Preparation

AFM cantilever tips were constructed by gluing (Norland optical adhesive #81, Norland Products Inc., Cranbury, NJ) 10μm-diameter borosilicate microspheres (Duke

Scientific Corporation, Palo Alto, CA) near the free end of a triangular silicon nitride AFM cantilever (Veeco, Santa Barbara, CA) with a nominal spring constant of 0.58 N/m (Coles *et al.* 2008). Tips were coated with gold, ozone-cleaned, and functionalized with a monolayer of tri-ethylene glycol-terminated alkane thiol ($SH\text{-}(CH_2)_{11}\text{-}EG_3$, Sigma Aldrich, St. Louis, MO) to inhibit tip fouling during the test procedure.

4.2.4.3 Friction Measurements

Friction was measured on lateral tibial plateaus of mice aged 2 months and 15 months according to the boundary friction measurement technique recently described by Coles *et al*. (Coles *et al.* 2008). A MFP-3D atomic force microscope (Asylum Research, Santa Barbara, CA) was used. Normal force spring constants were found using the MFP-3D software provided by Asylum Research (Walters *et al.* 1996) and lateral calibration constants were calculated by the wedge method (Ogletree *et al.* 1996; Han *et al.* 2007). For three different 50x50μm cartilage areas, the probe was raster-scanned at 40 μm/s for 16 scan lines and 512 points captured per scan line. Each area was scanned at applied normal loads of 20 nN, 40 nN, 60 nN, 80 nN, and 100 nN (Coles *et al.* 2008). The friction force was graphed versus the applied normal load, after which the slope was taken as the coefficient of friction.

4.2.4.4 Roughness Measurements

Roughness was calculated from an AFM image (128 scan lines by 128 points) of one of the friction sites on each tibia. The 50x50μm field was scanned with a 20nN

applied normal load and a 100 μm/s scan speed. To avoid any plateau tilt effects on these data, a first-order flattening procedure was applied and the root mean square (RMS) roughness recorded.

4.2.4.5 Elastic Modulus Measurements

AFM indentation was used to determine the elastic modulus of the cartilage surface via elastic tests previously described (Darling *et al.* 2006; Darling *et al.* 2007; Coles *et al.* 2008; Darling *et al.* 2008). At each of the three 50x50μm tibial plateau fields where friction was measured, 1μm/s indentation testing was performed at 16 sites using a 4x4 layout. The sampling rate was 1 kHz and a force trigger of 100 nN was used. The elastic modulus was calculated from the force vs. indentation data using a Hertz contact model for a hard sphere against an infinite plane in which the Poisson's ratio for the murine cartilage was assumed to be 0.20 (Cao *et al.* 2006) (similar to the 0.23 value determined by (Chiravarambath *et al.* 2009)). Dr. Eric Darling generously provided his Matlab script for these calculations.

4.2.5 Scanning Microphotolysis (SCAMP)

4.2.5.1 Sample Preparation

The left mouse femur was carefully dissected and soaked overnight in 70kDa dextrans (25 mg/mL) at 4°C. A razor blade was used to slice sagittally through the lateral and medial condyles. The femur was placed in a coverslip chamber with a sliced condyle face positioned flush against the coverslip to allow a full-thickness view of the

cartilage via the inverted microscope (Figure 4.1). Extra PBS was applied to keep the femur hydrated during experimentation. All SCAMP experiments were executed in the extracellular matrix of the articular cartilage middle zone of any of the sliced, exposed faces. Within that condyle cartilage, sites subject to frequent loading were preferentially chosen.

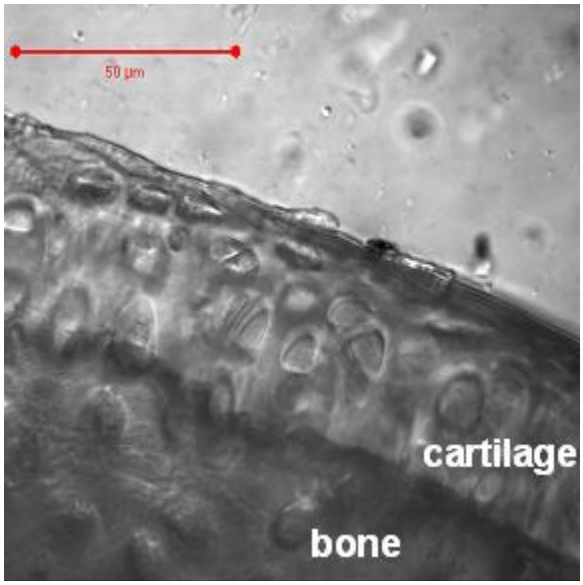

Figure 4.1: This sagittal cross-section of a fresh wild-type mouse femoral condyle shows murine articular cartilage to be approximately 50 µm thick and highly cellular. Diffusion measurements were made outside of the chondrocytes, in the small regions of extracellular matrix (ECM). (DIC image, scale bar = 50 µm.)

4.2.5.2 Scanning Procedure

As previously described (Leddy/Christensen *et al.* 2008), a 100x, 1.3-NA oil immersion lens at 6x zoom on a confocal laser scanning microscope (LSM 510, Zeiss)

was used to bleach a line 1.44μm wide (12 pixels) at a depth of 6 μm into the tissue. Bleaching was performed forward and backward for a total of 40 passes at two simultaneous excitation wavelengths, 458 and 488 nm. During bleaching, the emission intensity was also collected (long-pass filter, LP505) and stored as the image for that pass. At each site, five experiments were performed; their intensity values were averaged and median-filtered to minimize noise.

4.2.5.3 SCAMP Analysis

For each test site, the experimental data was compared to simulated datasets using the unconstrained nonlinear optimization function *fminsearch*; the resulting best fit established an appropriate value for the diffusion coefficient (*D*), which is the parameter of interest, and the space-dependent bleaching rate constant (*k*), which is a function of laser bleaching power and so varies with depth into the cartilage. All data processing, fits, and simulations were performed in Matlab (The Mathworks, Natick, MA).

4.2.6 Genotyping

The mice were all genotyped post-mortem to confirm they were *Col6a1*$^{-/-}$ or *Col6a1*$^{+/+}$. In brief, the DNA in a 2mm tail-snip from each sacrificed mouse was extracted with DirectPCR Lysis Reagent (Viagent Biotech, Inc.) and protein kinase K (Sigma). By polymerase chain reaction, two portions of the *Col6a1* gene were amplified from each of these DNA samples. The 22mer forward primer was 5'-TGC CCT GTG GAT CTA TTC TTC G-3' for both reactions. For the first amplification region, the 20mer reverse primer

was 5'TCG TGG CCA GCC ACG ATA GC-3', which corresponds to a portion of the *Neo* gene found in the mutated *Col6a1*; for the second region, the 21mer reverse primer was 5'CTG TCT CTC AGG TTG TCA ATG-3', which corresponds to the portion of the *Col6a1* gene that is excised by the targeted gene disruption procedure. DNA amplification products were analyzed via gel electrophoresis. Presence of a 609bp band in the first reaction indicated a knockout allele. Presence of a 128bp band in the second reaction indicated a wild-type allele.

4.2.7 Immunohistochemistry

Immunohistochemistry was performed to confirm the absence of COL6A1 in the cartilage of the knockout mice and to confirm the presence of COL6A1 in the PCM of the wild-type mice. Immunostaining was performed on remaining paraffin-embedded sections that had been prepared for histological analysis. An IgG rabbit polyclonal anti-collagen VI antibody was used to bind a peptide near the amino terminus of the murine α1(VI) chain (sc-20649, Santa Cruz Biotechnology, CA). An Alexa Fluor® 488-conjugated secondary antibody, goat anti-rabbit IgG (Invitrogen/Molecular Probes, Carlsbad, CA) was used for primary antibody detection (Choi *et al.* 2007; Alexopoulos *et al.* 2009). Samples were further incubated with ethidium homodimer-1 (Molecular Probes, Carlsbad, CA) to stain nucleic acids red. Samples were imaged using a 100x, 1.3-NA oil-immersion objective with differential interference contrast (DIC), an argon laser (excitation 488 nm), and a helium laser (excitation 633 nm). A long-pass filter (650 nm)

and a band-pass filter (505-550 nm) collected emissions from the ethidium homodimer-1 and the secondary antibody, respectively.

4.2.8 Statistical Analyses

In Statistica (StatSoft, Tulsa, OK), each dataset was evaluated with the Shapiro-Wilks test for normal distribution; based on those outcomes, the non-normal elastic modulus data were log-transformed for statistical analysis. Next, multifactorial analysis of variance (ANOVA) was performed to assess significant (α=0.05) main effects and interactive effects of genotype, sex, and age. Fisher's LSD post-hoc test was used to compare individual results where the ANOVA established a significant effect.

4.3 Results

As in previous studies with this strain of knockout mouse, the *Col6a1*-knockout mice did not present with any obvious abnormalities or show any increase in mortality. Genotyping confirmed the *Col6a1*$^{+/+}$ or *Col6a1*$^{-/-}$ status of each mouse. Immunohistochemistry staining confirmed collagen VI protein present in only the PCM of wild-type cartilage and absent from knockout cartilage (Figure 4.2); in the wild-type tibia, the growth plate also stained richly (*data not shown*). From the youngest age, additional ossification at or around the knockout joint was common, as seen in the microCT reconstructions (Figures 4.3A and 4.3B).

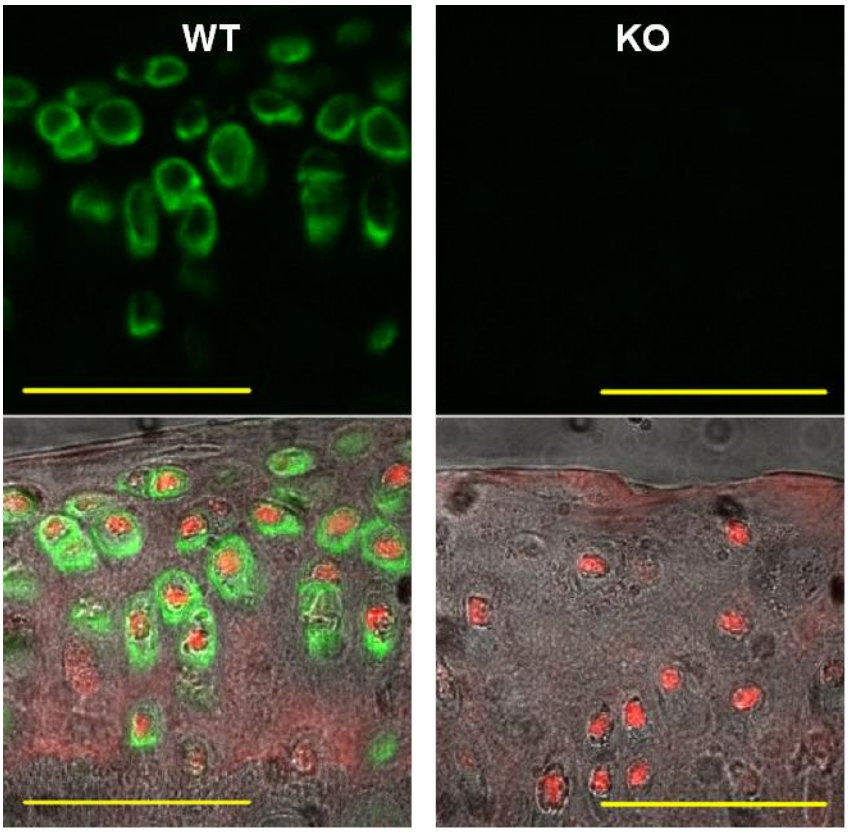

Figure 4.2: Immunostaining in the mouse tibial plateau cartilage. Top row: Collagen VI antibody binds only the wild-type PCM (left). Bottom row: Corresponding DIC images overlaid with collagen VI staining (green) and nuclear staining (red). The knockout cartilage (right) shows no sign of collagen VI. Scale bars = 50 μm.

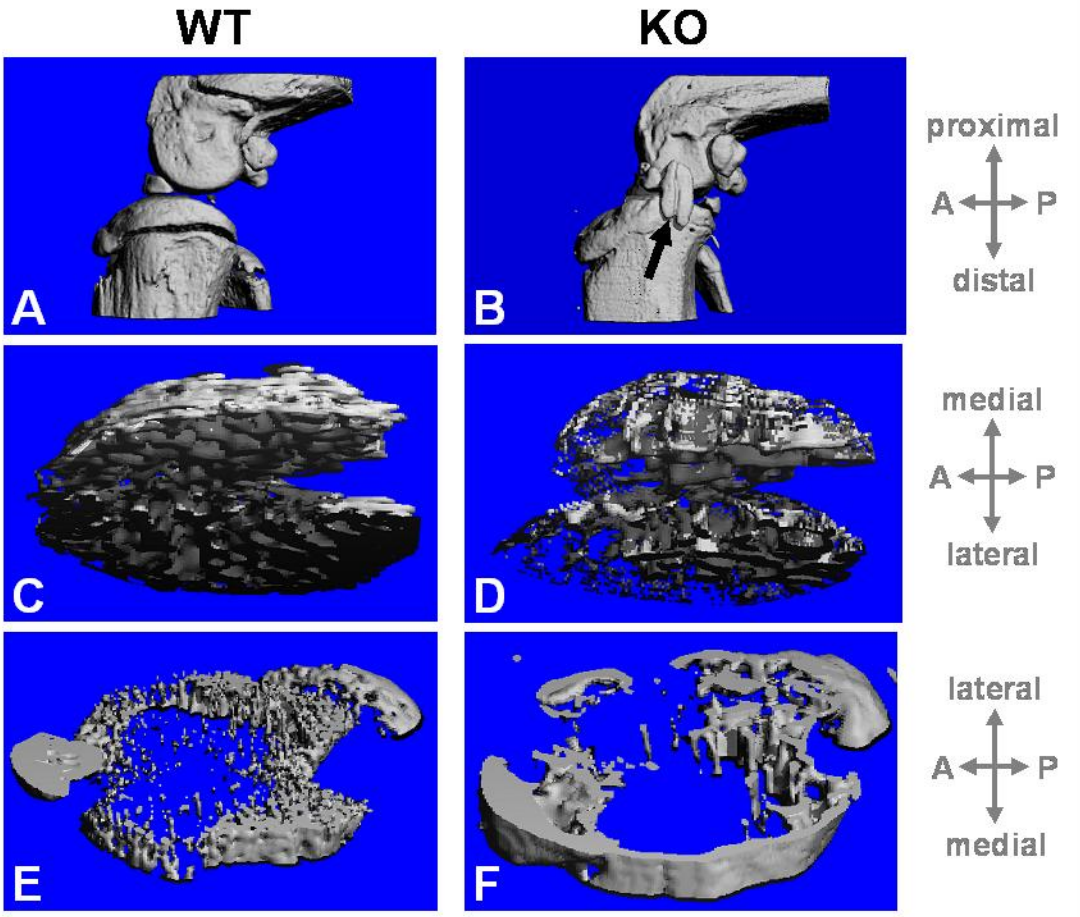

Figure 4.3: MicroCT images of 2-month-old mouse knees show the calcified structures of the right knees of a male wild-type (left images: A, C, E) and knockout mouse (right images: B, D, F). Top images, A and B, present a medial view of the knee; note the ossified medial collateral ligament in the knockout joint (arrow, B). Second row, C and D, presents a distal view of the tibial trabecular bone, where the knockout trabeculae are rod-like while the wild-type trabeculae are plate-like. Bottom images, E and F, present a proximal view of the tibial metaphyseal region, where the wild-type bone is immature in comparison to the knockout bone.

4.3.1 Tibial Epiphysis: Trabecular Bone

In the trabecular regions of the tibial epiphysis, the total volume, bone volume, relative bone volume, bone tissue density, connectivity density, SMI, trabecular number, trabecular separation, and trabecular thickness were all measured by microCT (Table 4.1). All parameters showed significant effects of genotype (except for bone tissue density) and of age (except for total volume). Briefly, knockout values were lower for bone volume, relative bone volume, connectivity density, trabecular number, and trabecular thickness; knockout values were higher for SMI and trabecular separation.

More specifically, the knockout SMI reflected rod-like structures (SMI closer to 3) from the youngest age, whereas the wild-type SMI indicated plate-like structures (SMI closer to 0) that became more rod-like over time (Figure 4.4A). The knockout bone volume remained small and constant, unlike the wild-type bone volume, which dropped precipitously with age (Figure 4.4B). The knockout connectivity density dropped sharply with age, whereas the wild-type connectivity density remained consistently high (Figure 4.4C). Knockout total volume values increased with age to surpass the wild-type values. With skeletal maturity (~4 months old (Beamer *et al.* 1996)), knockout bone tissue density increased only 4% while wild-type bone tissue density increased 19% (Figure 4.4D). MicroCT images comparing 2-month-old wild-type and knockout mouse trabecular bone are presented in Figures 4.3C and 4.3D.

Table 4.1: MicroCT results

	Wild-type			Knockout			ANOVA: Significant Effects		
	2-month-old	9-month-old	15-month-old	2-month-old	9-month-old	15-month-old	Age	Genotype	Age-by-Genotype
Epiphysis (trabecular only)									
TV (mm^3)	0.70 ± 0.15	0.52 ± 0.10	0.54 ± 0.39	0.60 ± 0.21	0.70 ± 0.16	0.87 ± 0.11		*	*
BV (mm^3)	0.40 ± 0.07	0.27 ± 0.06	0.18 ± 0.08	0.15 ± 0.02	0.16 ± 0.03	0.15 ± 0.03	**	**	**
BV/TV	0.55 ± 0.07	0.51 ± 0.08	0.38 ± 0.14	0.27 ± 0.11	0.24 ± 0.09	0.18 ± 0.05	**	**	
Mean2 (mg HA/cm^3)	995 ± 41	1187 ± 26	1154 ± 57	1094 ± 42	1142 ± 27	1137 ± 32	**		*
ConnDens (1/mm^3)	424 ± 51	403 ± 60	471 ± 69	411 ± 134	322 ± 107	211 ± 83	*	**	**
SMI	-0.01 ± 0.31	0.44 ± 0.42	1.25 ± 0.64	1.75 ± 0.45	1.86 ± 0.52	2.30 ± 0.43	**	**	
Tb.N (1/mm)	10.7 ± 0.5	9.3 ± 1.6	8.7 ± 3.4	7.6 ± 1.4	7.5 ± 2.5	5.8 ± 0.6	*	**	
Tb.Th (mm)	0.065 ± 0.006	0.069 ± 0.005	0.056 ± 0.010	0.047 ± 0.004	0.050 ± 0.009	0.047 ± 0.007	**	**	
Tb.Sp (mm)	0.091 ± 0.008	0.114 ± 0.011	0.142 ± 0.041	0.150 ± 0.027	0.157 ± 0.033	0.189 ± 0.019	**	**	
Epiphysis (trabecular + cortical)									
TV (mm^3)	1.22 ± 0.18	1.30 ± 0.13	1.63 ± 0.69	1.14 ± 0.33	1.27 ± 0.19	1.55 ± 0.17	**		
BV (mm^3)	0.80 ± 0.14	1.00 ± 0.11	1.17 ± 0.35	0.62 ± 0.15	0.67 ± 0.04	0.76 ± 0.08	**	**	
BV/TV	0.66 ± 0.09	0.76 ± 0.05	0.75 ± 0.09	0.56 ± 0.07	0.54 ± 0.07	0.49 ± 0.04		**	*
Mean2 (mg HA/cm^3)	996 ± 46	1203 ± 38	1192 ± 43	1052 ± 38	1102 ± 21	1090 ± 13	**	**	**
Length (µm)	438 ± 26	481 ± 25	518 ± 116	464 ± 72	466 ± 74	541 ± 63	**		
Epiphysis (subchondral only)									
Length (µm)	98 ± 33	168 ± 25	198 ± 49	131 ± 34	117 ± 44	135 ± 45	**	*	**
Metaphysis (trabecular + cortical)									
BV (mm^3)	0.35 ± 0.19	0.97 ± 0.20	0.98 ± 0.19	0.72 ± 0.27	0.66 ± 0.26	0.67 ± 0.14	**		**
Mean2 (mg HA/cm^3)	888 ± 29	1190 ± 41	1176 ± 33	1042 ± 81	1111 ± 18	1135 ± 19	**		**
Mineral content (µg HA)	0.31 ± 0.18	1.15 ± 0.22	1.15 ± 0.23	0.76 ± 0.31	0.73 ± 0.28	0.76 ± 0.15	**		**

mean ± SD
n=8 samples per group
(n=9 for wild-type 15mo)

Shading identifies the lowest three values per parameter.

* p<0.05
** p<0.01

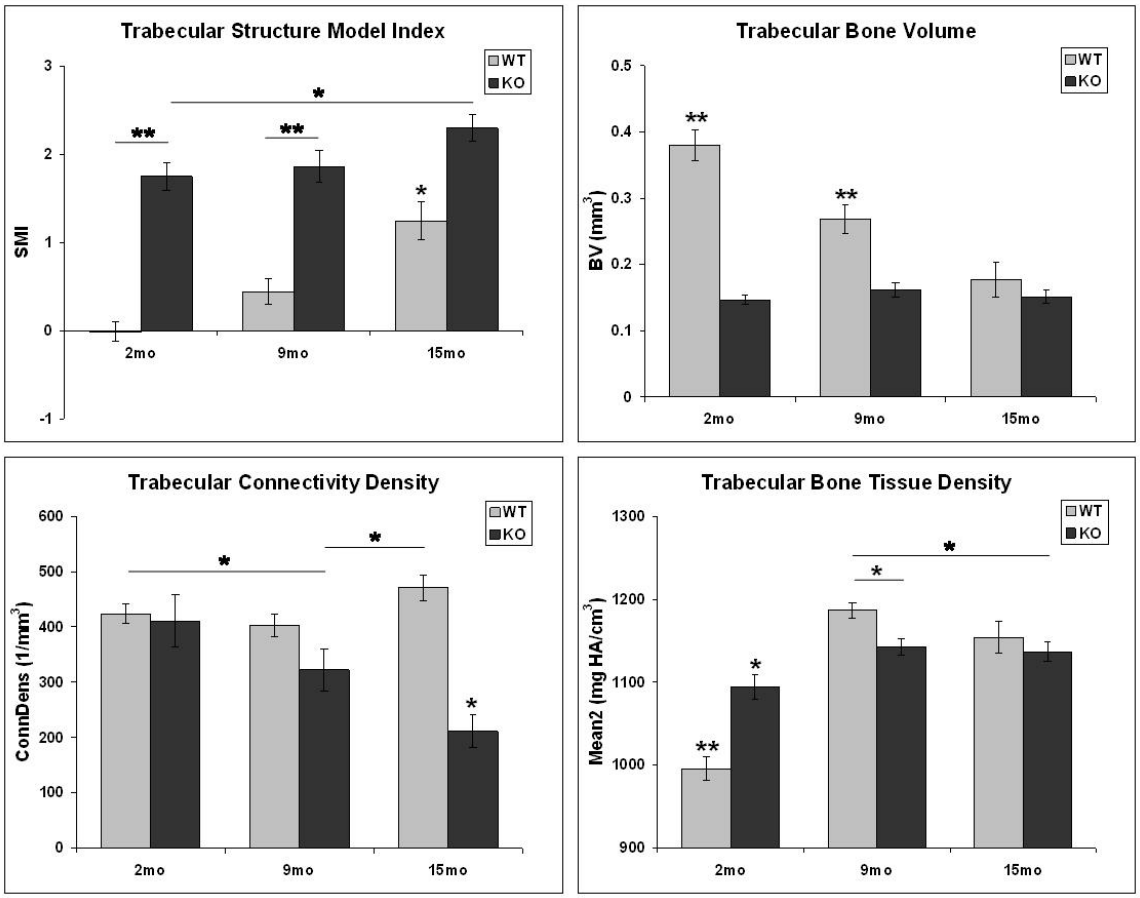

Figure 4.4: MicroCT measures reflect a variety of trabecular bone characteristics. In the tibial epiphysis of knockout mice, the structure model index (SMI, A) shows evidence of rod-like trabeculae from the earliest age, in contrast to the initially plate-like trabeculae of the wild-type mice. The trabecular bone volume (BV, B) is low from an early age and contributes to a higher bone tissue density (Mean2, D) in the 2-month-olds. With increasing age, the knockout connectivity density (ConnDens, C) drops unexpectedly. Bars are mean±SEM. *p<0.05; **p<0.01.

Sex was evaluated as a contributing factor in all analyses of the experimental design but was non-significant except for two measures in the tibial epiphysis trabecular bone: bone volume, where males had somewhat higher values than females; and bone

tissue density, where females generally had higher values than males. Aside from this note, the influence of sex is not further addressed.

4.3.2 Tibial Epiphysis: Cortical and Trabecular Bone

When both bone types of the tibial epiphysis were measured by microCT for total volume, bone volume, relative bone volume, bone tissue density, and length, several trends and differences emerged. Parameters showed statistically significant effects of genotype (except total volume and length) and of age (except relative bone volume) (Table 4.1). Length and total volume showed increases with age that were similar for both genotypes. Bone volume increased steadily with age at a faster rate for the wild-types than for the knockouts, and the highest knockout bone volume was lower than the lowest wild-type bone volume. Skeletal maturity appears to have influenced the remaining two parameters, but the knockout bone tissue density increased only 5% versus 21% for the wild-type bone tissue density, and the knockout relative bone volume remained unchanged (-3%) while the wild-type relative bone volume increased (16%).

4.3.3 Tibial Metaphysis: Cortical and Trabecular Bone

In the tibial metaphysis (Figures 4.3E and 4.3F), only bone volume and bone tissue density were quantified by microCT. Both showed a statistically significant main effect of age (but not of genotype) and a significant interactive effect of age-by-genotype (Table 4.1). Knockout bone volume did not change over time, but wild-type bone

volume jumped dramatically from a low 2-month value to a high 9-month value. Like the metaphyseal bone volume and as with density measures in the epiphysis, metaphyseal density was influenced by skeletal maturity; wild-type bone tissue density jumped 34% while the knockout bone tissue density increased by a slight 7%. The mineral content of this bone region was calculated from the bone volume and bone tissue density values to reveal a striking contrast: the knockout mice do not gain any mineral content as they age, whereas the mineral content almost quadruples with skeletal maturation in wild-type mice (Figure 4.5).

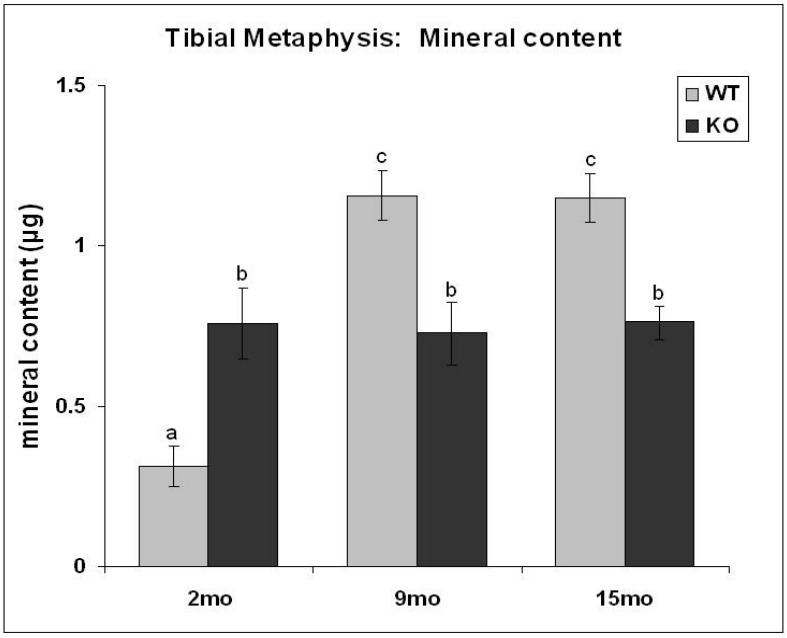

Figure 4.5: Mineral content of the knockout tibial metaphysis does not change. In the 25 microCT slices (0.4 mm) of the tibial metaphysis directly distal to the fibular attachment, wild-type mice quadrupled their mineral content from 2-months-old to 9-months-old. In contrast, the knockout mice already had an intermediate level of mineral content by 2 months of age; this mineral content never changed. Bars are mean±SEM; those sharing the same letter are not statistically different. Bars with different letters: $p<0.01$.

4.3.4 Joint Capsule Thickness

From the histology images, the joint capsule thickness (primarily the medial collateral ligament, MCL) was measured adjacent to the medial meniscus and was affected by genotype (ANOVA, $p<0.02$) (Table 4.2). In the knockout mice, the joint capsule was consistently thick at all ages, whereas the wild-type mice had initially thin joint capsules that thickened with age (Figure 4.6A). Interestingly, most of the 9-month

wild-type mice had a joint capsule thickness comparable to that of the 2-month wild-type mice (~70 μm), yet the 9-month wild-type average was raised substantially by two very thick values (~500 μm) in particularly degraded joints. Additionally, many of the joint capsules stained heavily for proteoglycan content (Figures 4.7 and 4.8) and a few had visible ossification.

Table 4.2: Results of histology and cartilage measures

	Wild-type			Knockout			n	ANOVA: Significant Effects		
	2-month-old	9-month-old	15-month-old	2-month-old	9-month-old	15-month-old	(per group)	Age	Genotype	Age-by-Genotype
Histology										
Modified Mankin Scores, max = 28	4.5 ± 2.2	7.5 ± 7.0	11.9 ± 8.8	4.6 ± 4.7	4.5 ± 3.1	7.1 ± 6.6	8-9	**	**	
Medial Joint Capsule Thickness (μm)	73 ± 9	166 ± 212	219 ± 114	246 ± 55	223 ± 91	256 ± 118	8-9		*	
Subchondral Thickness (μm)	29 ± 18	90 ± 17	126 ± 58	33 ± 5	39 ± 8	37 ± 23	8-9	**	**	**
Atomic Force Microscopy										
Elastic Modulus (kPa)†	58	62	39	46	52	32	22-27			
Roughness, RMS (nm)	347 ± 200	343 ± 232	582 ± 390	489 ± 267	353 ± 192	657 ± 116	6-8	*		
Coefficient of Friction	0.23 ± 0.12	not measured	0.17 ± 0.08	0.24 ± 0.20	not measured	0.19 ± 0.15	7-8			
Diffusion										
D ($\mu m^2/s$)	11 ± 7	13 ± 6	12 ± 7	17 ± 11	13 ± 8	13 ± 5	35-54		*	*

mean ± SD
* p<0.05
** p<0.01
† Data was log-transformed for statistical analysis. Here, those log-transformed averages were transformed back to kPa.
Shading identifies the lowest three values per parameter.

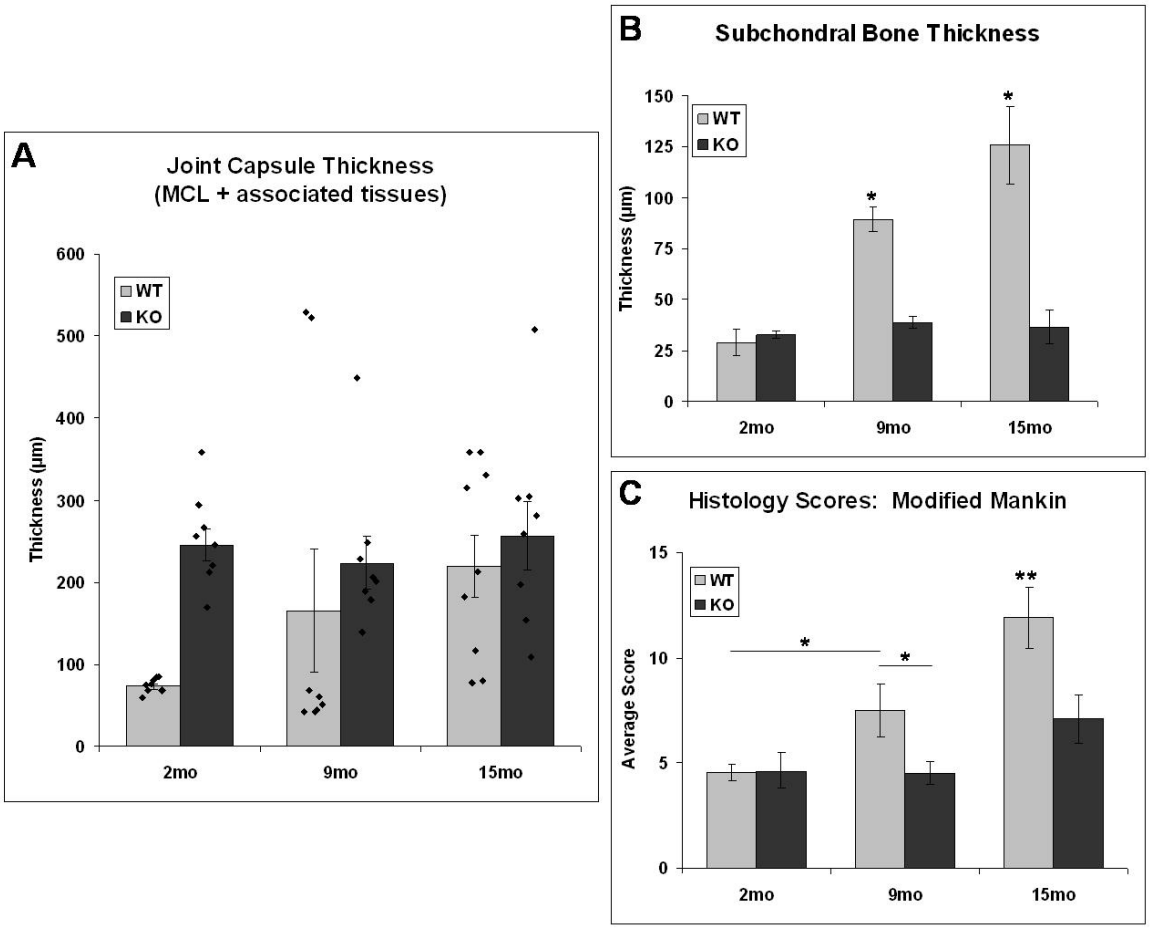

Figure 4.6: Histology reveals key effects of genotype on the joint capsule, bone, and cartilage. Joint capsule thickness on the medial side (A) was high in knockout mice from the youngest age but almost universally low in wild-type mice until the oldest age (note how two 9-month-old data strongly influence that wild-type average). Subchondral bone thickness (B), in contrast, shows that knockout bone fails to thicken with age, unlike the wild-type bone. Cartilage degradation (C) in knockout mice shows a small increase only in the oldest mice, whereas wild-type cartilage already shows signs of increasing degradation by 9 months. All of these graphs show restrained changes in knockout joint parameters relative to strongly changing wild-type parameters. Bars are mean±SEM. *p<0.05, **p<0.01. In A, ◊ symbols represent individual data points whose average yields the underlying bar. Wild-type 2-month-old data in A are significantly different (*) from all other bars except the 9-month-old wild-type.

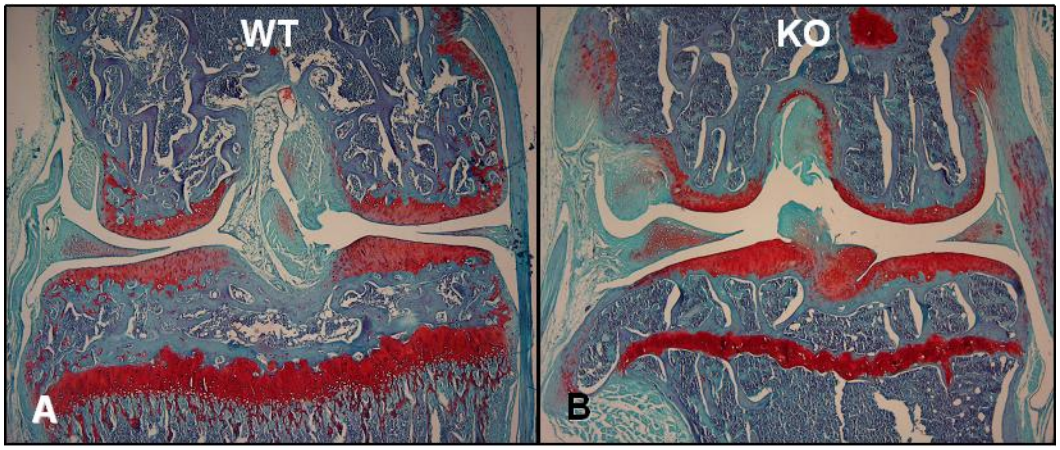

Figure 4.7: Histology images reveal differences between 2-month-old wild-type and knockout knees. Seven-um-thick tissue slices were stained with fast green (blue, collagen), safranin-O (red, proteoglycans), and Harris' hematoxylin (black, nuclei). These coronal slices show the femur above and tibia below; the left side is lateral while the right side is medial. The knockout knee (B) includes a thick and proteoglycan-rich medial collateral ligament, atypical pannus formation on the lateral femur, larger trabeculae in both bones, and more confined growth-plate staining relative to the wild-type knee (A).

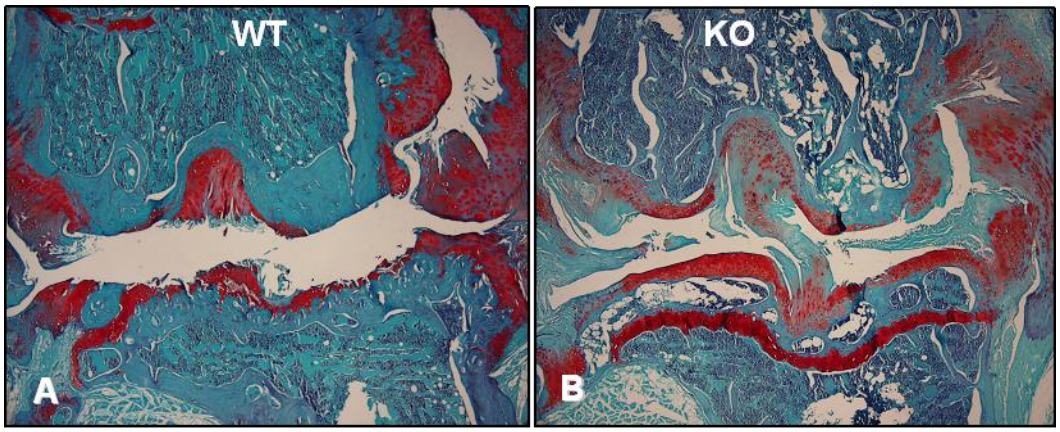

Figure 4.8: The worst joint degradation was seen in 15-month-old mouse knees. Of all the joints, this 15-month-old wild-type female (A) received the highest overall modified Mankin score, 24. (Joint score is an average of the scores for the lateral femoral condyle, lateral tibial plateau, medial femoral condyle, and medial tibial plateau.) This extreme case includes degradation into the tibial growth plate on both sides, as well as considerable thickening of the femoral subchondral bone and the medial joint capsule. In contrast, the highest modified Mankin score given to a knockout mouse was 14, a score also earned by a 15-month-old female (B). This joint shows extensive cartilage degradation at the medial femoral condyle and some cartilage loss to the medial tibial plateau, but the lateral side is still intact and the subchondral bone still quite thin.

4.3.5 Subchondral Bone Thickness

From histology images, the mean subchondral bone thickness per joint was calculated by averaging the subchondral thickness at four sites: the lateral femoral condyle, the lateral tibial plateau, the medial femoral condyle, and the medial tibial plateau. The subchondral bone remained thin for the knockout mice at all ages, but thickened markedly over time for the wild-type mice ($p<0.02$ for each comparison)

(Figures 4.6B, 4.7, and 4.8). ANOVA confirmed the significance ($p<0.0002$) of age, genotype, and age-by-genotype effects (Table 4.2).

The microCT measures of subchondral bone thickness reinforced these histology findings but were numerically higher (Table 4.1), presumably because the microCT measures averaged only subchondral bone of the tibia. Additionally, some portion of calcified cartilage may be captured by the microCT thickness measures.

4.3.6 Cartilage Degradation

Using a modified Mankin grading rubric (Appendix B), three blinded graders evaluated the histology images to assess the level of cartilage degradation in the lateral femoral condyle, lateral tibial plateau, medial femoral condyle, and medial tibial plateau of each joint. Since the grading rubric was designed to assess cartilage degeneration, it did not fully account for the extreme bone degradation seen in a few joints, where degradation extended to or through the tibial growth plate (Figure 4.8). Knockout mice showed delayed or reduced cartilage degradation with age relative to the wild-type mice (Figure 4.6C). The lateral side had fewer indications of degradation relative to the medial side (paired t-test, *data not shown*).

The ANOVA revealed significant effects of age ($p<0.000003$), genotype ($p<0.002$), and side (medial or lateral, $p<0.00003$), but not bone (femur or tibia, $p=0.13$). Genotype-by-age ($p<0.05$) and age-by-side ($p<0.02$) were significant interactive effects (Table 4.2).

4.3.7 Friction

Cartilage friction was measured on the tibial plateaus of the 2-month and 15-month mice. The cartilage surface of one 15-month knockout mouse was too rough to measure with this AFM setup. The coefficient of friction was marginally higher in the 2-month mice, although this difference did not reach statistical significance ($p=0.1$) (Table 4.2).

4.3.8 Roughness

RMS roughness was measured on tibial plateaus of all mice except one 15-month knockout mouse which was too rough to scan with this AFM setup. Age significantly influenced the roughness RMS ($p<0.02$); the oldest mice have the roughest cartilage (Table 4.2).

4.3.9 Elastic Modulus

Stiffness was found to decrease significantly with age ($p<0.02$, Table 4.2). Cartilage from knockout joints averaged a lower elastic modulus at all age points but no statistically significant difference was detected ($p<0.09$).

4.3.10 Diffusivity

For the first time, microscale diffusion was measured in mouse cartilage. The diffusion rate of 70kDa dextrans through the ECM of femoral condyle cartilage averaged 13 $\mu m^2/s$ and was highly variable. Relative to the other values, diffusivity in the 2-

month knockout cartilage stood out as particularly high: 17 $\mu m^2/s$ ($p<0.06$ relative to 15-month knockout data; $p<0.05$ relative to all other data) (Table 4.2).

4.4 Discussion

This study adds to the evidence of musculoskeletal abnormalities that stem from an absence of collagen VI. Within the bone, differences between the knees of *Col6a1*$^{+/+}$ and *Col6a1*$^{-/-}$ mice are particularly apparent in the trabecular bone of the proximal tibia. Surprisingly, given the expected transition to skeletal maturity, knockout mice show limited evidence of bone changes between 2 months and 9 months compared to the dramatic changes observed in wild-type mice. Within the cartilage, degradation was slower and slighter in the knockout mouse. Measures of diffusion, novel in mouse cartilage, did not point to any sustained ECM differences between genotypes. Similarly, the cartilage surface measurements performed here, which included roughness, coefficient of friction, and elastic modulus, were not affected by the lack of collagen VI.

Trabecular bone characteristics in the proximal tibia are strikingly different in the knockout knees. Relative to the wild-type trabecular bone, the knockout trabecular bone shows lower relative bone volume, bone volume, trabecular number, trabecular thickness, and connectivity density, but higher trabecular separation and SMI. Overall, these *Col6a1*$^{-/-}$ trabecular bone differences correlate with thinner, more widely spaced trabecular struts, which is an outcome not inconsistent with collagen-knockout or -

mutated mice based on the available literature. Mice with a collagen I mutation (*oim*) present with fewer and thinner trabeculae in the femoral head relative to their wild-type comparisons (Chipman *et al.* 1993). *Col10a1*$^{-/-}$ mice show an early decrease in newly formed bony trabeculae and evidence of patchy mineralization of trabeculae, but an overall greater trabecular bone content in 4-week-old femurs (Kwan *et al.* 1997). Truncation of COL2A1 in mice leads to lower trabecular relative bone volume, lower trabecular thickness, and greater trabecular separation in the 3-month-old lumbal vertebral bodies (Nieminen *et al.* 2008). Mice deficient in both COL9A1 and cartilage oligomeric matrix protein (COMP) show a non-significantly lower trabecular mineral density at 1 month of age (Blumbach *et al.* 2008). Overall, microCT has seldom been used to assess bone morphometry in mice with collagen mutations or ablations; further data in this field would enable more-quantitative comparisons among studies of these animals.

Given the muscle myopathy of *Col6a1*$^{-/-}$ mice (Bonaldo *et al.* 1998), abnormal loading may be present at the knee and could influence trabecular bone characteristics. Overall, the *Col6a1*$^{-/-}$ trabecular bone differences closely match the pattern of changes seen in studies of constrained locomotor modes (Carlson *et al.* 2008), mechanically-altered loading (e.g., (Giesen *et al.* 2004)), or disuse (e.g., (Damrongrungruang *et al.* 2004)). Nonetheless, *Col6a1*$^{-/-}$ mice do not show altered activity levels (C57BL/6 background, (Bonaldo *et al.* 1998)), nor do they lose proteoglycans from the cartilage

matrix or undergo bone loss. However, the microCT data suggest that careful study of the mechanical loads at the knee might reveal further differences between the *Col6a1*$^{-/-}$ and *Col6a1*$^{+/+}$ mice.

Mineral deposition in the tibial metaphysis happens earlier but fails to progress in the knockout mouse. The mineral content of the tibial metaphysis 25-slice region was constant (~0.75 μg HA) at all ages in the knockout mouse. That value was intermediate to the wild-type mineral content, which was a low 0.31 μg at 2 months yet quadrupled with skeletal maturity to 1.15 μg at 9 and 15 months. To the best of the authors' knowledge, this knockout mouse pattern of mineral deposition has not previously been described. The implications are unknown. Given previous evidence of skeletal changes during maturation in young *Col6a1*$^{-/-}$ mice, including whole-body bone mineral density (DXA) abrupt increases from 1-month old to 3-months old (Alexopoulos *et al.* 2009), it is surprising to see no indication of additional mineral deposition in the proximal tibial metaphysis as these mice age. However, abnormalities in collagen VI, a protein widespread in the bone growth plate, have been linked to a variety of ossification abnormalities including reduced bone mineral density (Alexopoulos *et al.* 2009), ligament ossification disorders (Tanaka *et al.* 2003; Tsukahara *et al.* 2005; Kong *et al.* 2007), and delayed skeletal development (Alexopoulos *et al.* 2009). These studies, together with the mineral deposition pattern observed, imply an important role for collagen VI in timely and proper bone development.

Knee cartilage of the *Col6a1*-knockout mouse, in contrast to hip cartilage, shows evidence of a protective effect of COL6A1 absence. The modified Mankin grading of these histology sections shows clear progression of osteoarthritic degradation the wild-type knees, whereas the 9-month-old knockout cartilage is still as intact as 2-month-old wild-type cartilage and the 15-month-old knockout cartilage as intact as the 9-month-old wild-type cartilage. Beneath the cartilage, the knockout subchondral bone never thickens; however, the wild-type subchondral bone thickens more than 4-fold. In contrast to this slower degradation pattern in knockout knees, previous study of the hip joint identified accelerated and more extreme osteoarthritic progression for knockout mice (Alexopoulos *et al.* 2009). This disparity between joints may be attributable to the effects of collagen VI mutations on muscle physiology: reduced collagen VI in Bethlem myopathy leads to proximal hypotonia and distal joint contractures (Pepe *et al.* 2002; Lampe and Bushby 2005), and joint laxity has been found to be involved in the development of osteoarthritis (e.g., (Gillquisl 1990; van Osch *et al.* 1995)). Although the hip is not commonly more susceptible than the knee to osteoarthritis, hip (but not knee) dislocations are considered a diagnostic criterion for Ullrich congenital muscular dystrophy (Pepe *et al.* 2002), suggesting that laxity at the hip joint may be a particular problem in *Col6a1*-knockout mice.

The novel measurement of microscale diffusion through mouse cartilage revealed limited matrix changes. Diffusive transport of 70kDa dextran, which not only

reflects nutrient transport but also probes the structure of the cartilage matrix, was fairly consistent at the older ages (9 and 15 months: 13 $\mu m^2/s$) but showed a surprising difference at the 2-month time point. At 2 months, the knockout mouse femoral condyle cartilage had a diffusivity 55% higher than that of the wild-type (11 $\mu m^2/s$ versus 17 $\mu m^2/s$). This points to a difference in ECM microstructure that may correspond to a developmental delay (Alexopoulos *et al.* 2009) or an improper ratio or assembly of the matrix components in the knockouts, later corrected via remodeling. The coefficients of diffusion measured in the mouse cartilage are somewhat lower those obtained for diffusion of 70kDa dextran through cartilage of other species: 23 $\mu m^2/s$ in the ECM of porcine cartilage using SCAMP (Leddy/Christensen *et al.* 2008); 31 $\mu m^2/s$ in pig cartilage using fluorescence recovery after photobleaching (FRAP) (Leddy and Guilak 2003); and 40 $\mu m^2/s$ in bovine cartilage using radiotracer tracking (Torzilli *et al.* 1997). The lower rate of diffusion seen in the murine cartilage may be due to species-to-species variation in assembly of or proportions of matrix components.

Mechanical properties of the cartilage surface failed to reveal differences between the knockout and wild-type cartilage. The measures of boundary friction coefficients were highly variable; on average, they showed no statistically significant change with age or genotype. The coefficients (0.21 ± 0.14) corresponded well to previous friction data collected via this technique for 10-week-old (0.42 ± 0.19) and 20-week-old (0.25 ± 0.11) C57BL/6J mice (Coles *et al.* 2008; Coles *et al.* 2009). Elastic

modulus values also varied widely, although wild-type mice generally had a higher modulus than knockouts. Overall, values were markedly lower than previously published values (10-week and 20-week C57BL/6J mice: ~260 kPa and 354 ± 158 kPa, respectively) (Coles *et al.* 2008; Coles *et al.* 2009). Finally, first-order roughness increased with age, with a trend toward rougher cartilage surface in the oldest mice. This trend is consistent with the progression of cartilage degradation with age, seen by histology.

Overall, cartilage studies suggest that collagen VI, despite its prominent role in the PCM of cartilage, plays a low-profile role in matrix production and maintenance. Measures ranging from degradation to diffusivity to friction to roughness to elastic modulus have collectively shown that mouse knee cartilage properties are largely maintained in the absence of collagen VI. This evidence implies that the role of collagen VI in the PCM is either non-critical at the tissue level or, alternatively, may be satisfied via compensatory mechanisms.

In conclusion, this study of *Col6a1*$^{-/-}$ mice provides evidence of musculoskeletal abnormalities at the knee as a consequence of collagen VI absence. The trabecular bone characteristics reveal distinct structural differences between the knockout and wild-type bones. The proximal metaphysis mineral content does not increase with skeletal maturity in the knockout; the implications of this trend are unclear, but the cause may be unusual mechanical loads or dysregulation of bone development in the absence of collagen VI. Knockout knee cartilage degrades much

more slowly, even though its physical properties are very similar to those of wild-type cartilage. To further elucidate the unusual knockout knee patterns seen here, future studies should test the knockout mouse knees for joint laxity and range of motion. Additionally, computed tomography (CT) data from knees of humans diagnosed with Bethlem myopathy or Ullrich congenital muscular dystrophy would provide valuable insight into the sensitivity of the mechanism by which collagen VI influences bone development. Finally, given that human ligament ossification disorders have been linked to collagen VI mutations, the role of collagen VI in ligaments at the knockout mouse knee should be thoroughly investigated beyond the simple quantification in this study of the premature thickening of the knockout mouse medial collateral ligament. Overall, this *Col6a1*$^{-/-}$ mouse presents an effective tool to explore the role of collagen VI throughout the musculoskeletal tissues and to improve our understanding of how reduction in or mutation of collagen VI can lead to so wide a variety of human musculoskeletal disorders.

Chapter 5.

Summary and Conclusions

5.1 Summary

Although collagen VI has only a minor presence in the body, it nonetheless plays an important role. Much of the research on collagen VI has related to its function in skeletal muscles, since its mutation can result in Bethlem myopathy or Ullrich congenital muscular dystrophy. However, its roles in other tissues of the body are poorly understood. The objective of this research has been to elucidate the role of collagen VI in the structure and properties of the knee.

In articular cartilage, the pericellular matrix (PCM) is defined by the presence of collagen VI, which localizes exclusively to this region. Therefore, the PCM warrants careful attention in this study of collagen VI of the joint. The PCM has been shown to play an important mechanical function in cartilage, with possible biochemical and biophysical roles, as well. By its enveloping presence around each chondrocyte, the PCM serves as a gateway through which any signal to or from the cell must pass, whether that signal be mechanical or biochemical.

Because the PCM is structurally and compositionally distinct from the extracellular matrix (ECM) of cartilage, the PCM may be more restrictive (or more permissive) to the passage of molecules. This possibility was first examined in Chapter 2, which sought to compare diffusion in the PCM to diffusion in the ECM. The PCM, with its higher proteoglycan content, was expected to have a lower diffusivity than the ECM.

In order to test this hypothesis, an appropriate method for measuring diffusion within the PCM was necessary. Scanning microphotolysis (SCAMP) (Kubitscheck *et al.* 1998) was selected as the photobleaching model for this purpose, but considerable revisions were first necessary. For use with a commercial microscope, the model was modified to incorporate time spent not bleaching, with an asymmetrical time step; to accommodate real-world asymmetries in the point-spread function; and to disambiguate the bleached state of the first recorded line. Additionally, the experimental setup was changed by speeding up the scans in order to accommodate faster diffusion coefficients. After these changes, the implemented model fit the experimental SCAMP data well. Furthermore, the bleached region of tissue was sufficiently constrained that SCAMP testing could adequately fit inside the confines of the PCM.

This SCAMP technique was applied to measure diffusion of FITC-dextrans within the ECM and PCM of porcine cartilage (Leddy/Christensen *et al.* 2008). As expected, the PCM diffusivity was lower. These differences (70kDa: 19<23 $\mu m^2/s$; 500kDa: 14<17 $\mu m^2/s$) were statistically significant; however, the biological significance is unclear. In this case, the closeness of the results does not strongly indicate that signaling molecules would be hindered from reaching or departing the cell via diffusion, but they nonetheless indicate a measurable difference in the underlying structure of the two matrices — additional evidence of the distinction between the PCM and ECM.

Given that the PCM is adjacent to the cell, catabolic cytokines such as interleukin-1 (IL-1), a player in osteoarthritis of the knee, were expected to first drive degradation in this matrix. To probe these degradative changes, the SCAMP technique was again employed in Chapter 3, this time with the globular protein ovalbumin as the diffusing molecule. Effects of time, matrix, and zone were examined. Although the PCM diffusivity was significantly different from that of the ECM, this manifested as a universal difference of ~2 $\mu m^2/s$ — with no evidence of a PCM-specific increase in diffusivity. Thus, it was not possible to conclude that the PCM degrades first in IL-1-treated articular cartilage. However, another diffusing molecule might have been more sensitive to any such PCM-first degradation, suggesting that expanding this study to include a range of molecular weights or molecular shapes could be a valuable follow-up to this initial experiment.

Evaluating the collagen VI-rich PCM in contrast to the collagen VI-null ECM of cartilage provided important information – by association – on the role of this protein, but only partially addressed the role of collagen VI in the knee. To complement those studies, Chapter 4 focused upon a knockout mouse that entirely lacks collagen VI. In this way, the specific effects of collagen VI absence were observed and quantified.

The *Col6a1*-knockout mice appeared as healthy and active as their wild-type peers. The knees of the mice were evaluated at 2, 9, and 15 months and showed substantial differences.

Despite severely reduced cartilage PCM stiffness in the knockout mice (as measured at the hip (Alexopoulos *et al.* 2009)), the physical properties of the knee cartilage were hardly affected. In fact, instead of compromising the integrity of the cartilage tissue and yielding earlier degradation, the lack of collagen VI at the knee protected the cartilage and delayed its degradation. Such an effect should not be attributed to improvements in the cartilage tissue in the absence of collagen VI; rather, it is more likely to be the result of changed joint articulation with a concomitant reduction in forces through and wear of the knee cartilage.

The subchondral bone thickness measures in the knockout knee told a similar tale. Although this region usually thickens as the joint begins to degrade, the knockout bone subchondral thickness never increased, not even at 15 months when the cartilage finally showed signs of slight degradation.

In fact, the knockout bone properties were quite different from those of the wild-type. In the region of tibial metaphysis examined, all mineral bone deposition had occurred by 2 months in the knockout. This does not correspond to the expected mineral increase with mouse skeletal maturity, which is estimated to happen around 4 months in wild-type mice.

Examination of the tibial epiphysis trabecular bone provided further evidence of altered bone properties. In comparison to the wild-type trabecular bone, the knockouts present trabecular bone with lower bone volume, relative bone volume, trabecular

number, trabecular thickness, and connectivity density, but higher trabecular spacing and structure model index (more rod-like). Altogether, this pattern of trabecular properties in the *Col6a1*-knockout mouse knees is consistent with patterns recorded in reduced or altered mechanical loading. Notably, though, this pattern is not inconsistent with the limited data available on trabecular changes observed in other collagen-knockout or collagen-mutated mice.

5.2 Future Directions

Is the *Col6a1*-knockout mouse knee subjected to different loads than the wild-type knee? Although the knockout mice are smaller at 1 month (Alexopoulos *et al.* 2009), they have matched the body mass of the wild-type mice by the ages examined in this study. Thus, the knees of the knockout mice are not supporting a different body weight. In past research on *Col6a1*-knockout mice from a C57BL/6 background, the knockouts ran on their wheels marginally less than the wild-types, but the difference was not significant (Bonaldo *et al.* 1998). Thus, the knees are not exposed to significantly different levels of activity. However, research has shown that bone morphometry can be altered by style of locomotion (Carlson *et al.* 2008). It is quite possible that these *Col6a1*-knockout mice have altered their locomotion as a result of their muscle myopathy or ligament ossification (e.g., in the medial collateral ligament). This hypothesis should be evaluated by gait analysis and joint laxity testing.

Why does reduced PCM stiffness fail to affect the cartilage surface physical properties in the *Col6a1*-knockout knees? In view of the hypothesized role of the PCM, this less-stiff, collagen VI-free PCM should have affected the mechanical signals received by the chondrocyte and thereby influenced the ECM produced by the cells. It is possible that although the cartilage ECM and surface are initially of poor quality, by 2 months of age sufficient cartilage matrix remodeling has occurred to repair any hypothesized deficit. In this case, testing younger mice might reveal cartilage surface abnormalities that are no longer present at 2 months.

What additional applications might call for the new SCAMP technique? This SCAMP method was developed to measure diffusivity in the tiny, confined volume of the cartilage PCM. However, it could easily be used to measure diffusion in other regions of similar sizes, as evidenced by its use in the ECM of mouse cartilage, whose diffusivity had not previously been evaluated. SCAMP is particularly well suited for diffusion measurements in the nucleus. SCAMP may also be appropriate for characterizing diffusional release of drugs from micro-scale biomaterials.

Although the first focus of this dissertation was on the role of collagen VI within the pericellular matrix, the study of knockout mouse knees suggests that human mutations in collagen VI are unlikely to symptomatically manifest in the knee cartilage (e.g., by early or accelerated osteoarthritis). However, diseases known to be linked to collagen VI mutations could possibly be diagnosed at a young age by CT scan of the

proximal tibial trabeculae. (Of course, the availability of genetic testing reduces the need for such a diagnostic tool.) Nonetheless, in patients with collagen VI mutations, CT scans of the tibial trabeculae might be used to assess physical therapy progress if the patients were working toward achieving a normal structure and function of the knee.

What is the next step in evaluating the role of collagen VI in the knee? The challenge of interpreting the effects of collagen VI absence on different tissues in the knee points to a role for a conditional knockout mouse. Using the *Col6a1*-knockout mouse currently available, it is unclear whether the knockout cartilage is inherently more resistant to degradation, or whether the knockout cartilage is subjected to less wear. In a mouse whose collagen VI was absent only from cartilage tissue, interpretation of the cartilage degradation results would be far more straightforward. Similarly, a conditional knockout mouse whose collagen VI production was eliminated at a particular age would clarify whether differences observed in the knee were strictly developmental versus ongoing in nature.

5.3 Conclusions

Overall, then, the work presented in this dissertation conclusively shows that collagen VI does have an important role in the structure and properties of the knee joint. In cartilage, diffusivity is slower in the collagen VI-delimited PCM as compared to the remainder of the cartilage matrix. This remains true even as cartilage degrades in the

presence of IL-1, as it might in arthritis. During this process, diffusivity in both the ECM and PCM increase simultaneously, a change attributable to proteoglycan breakdown in both of these matrices. Finally, mice lacking collagen VI developed knees with abnormal trabeculae, unusual ligamentous ossifications, atypical bone mineral deposition, and uncommon lack of cartilage degradation.

Appendix A. SCAMP Diffusion-Reaction Equations

The SCAMP diffusion-reaction equations (Eqs. 2.1-2.2) were solved as follows (Eqs. A1-A6). The short time step includes both bleaching and diffusion components.

Step 1, x implicit:

$$\begin{aligned} & C_{i,j,k}^{t+1/3} - \frac{D\Delta t}{2\Delta x^2}\left(C_{i-1,j,k}^{t+1/3} - 2C_{i,j,k}^{t+1/3} + C_{i+1,j,k}^{t+1/3}\right) + \frac{k_{ijk}\Delta t}{2}\left(C_{i,j,k}^{t+1/3}\right) \\ & = C_{i,j,k}^{t} + \frac{D\Delta t}{2\Delta x^2}\left(C_{i-1,j,k}^{t} - 2C_{i,j,k}^{t} + C_{i+1,j,k}^{t}\right) + \frac{D\Delta t}{\Delta y^2}\left(C_{i,j-1,k}^{t} - 2C_{i,j,k}^{t} + C_{i,j+1,k}^{t}\right) \\ & + \frac{D\Delta t}{\Delta z^2}\left(C_{i,j,k-1}^{t} - 2C_{i,j,k}^{t} + C_{i,j,k-1}^{t}\right) - \frac{k_{ijk}\Delta t}{2}\left(C_{i,j,k}^{t}\right) \end{aligned} \qquad \text{(Eq. A1)}$$

Step 2, *y* implicit:

$$\begin{aligned} & C_{i,j,k}^{t+2/3} - \frac{D\Delta t}{2\Delta y^2}\left(C_{i,j-1,k}^{t+2/3} - 2C_{i,j,k}^{t+2/3} + C_{i,j+1,k}^{t+2/3}\right) + \frac{k_{ijk}\Delta t}{2}\left(C_{i,j,k}^{t+2/3}\right) \\ & = C_{i,j,k}^{t} + \frac{D\Delta t}{2\Delta x^2}\left(C_{i-1,j,k}^{t} - 2C_{i,j,k}^{t} + C_{i+1,j,k}^{t}\right) + \frac{D\Delta t}{2\Delta y^2}\left(C_{i,j-1,k}^{t} - 2C_{i,j,k}^{t} + C_{i,j+1,k}^{t}\right) \\ & + \frac{D\Delta t}{\Delta z^2}\left(C_{i,j,k-1}^{t} - 2C_{i,j,k}^{t} + C_{i,j,k-1}^{t}\right) + \frac{D\Delta t}{2\Delta x^2}\left(C_{i-1,j,k}^{t+1/3} - 2C_{i,j,k}^{t+1/3} + C_{i+1,j,k}^{t+1/3}\right) \\ & - \frac{k_{ijk}\Delta t}{2}\left(C_{i,j,k}^{t+1/3}\right) \end{aligned} \qquad \text{(Eq. A2)}$$

Step 3, *z* implicit:

$$\begin{aligned} & C_{i,j,k}^{t+1} - \frac{D\Delta t}{2\Delta z^2}\left(C_{i,j,k-1}^{t+1} - 2C_{i,j,k}^{t+1} + C_{i,j,k+1}^{t+1}\right) + \frac{k_{ijk}\Delta t}{2}\left(C_{i,j,k}^{t+1}\right) \\ & = C_{i,j,k}^{t} + \frac{D\Delta t}{2\Delta x^2}\left(C_{i-1,j,k}^{t} - 2C_{i,j,k}^{t} + C_{i+1,j,k}^{t}\right) + \frac{D\Delta t}{2\Delta y^2}\left(C_{i,j-1,k}^{t} - 2C_{i,j,k}^{t} + C_{i,j+1,k}^{t}\right) \\ & + \frac{D\Delta t}{2\Delta z^2}\left(C_{i,j,k-1}^{t} - 2C_{i,j,k}^{t} + C_{i,j,k-1}^{t}\right) + \frac{D\Delta t}{2\Delta x^2}\left(C_{i-1,j,k}^{t+1/3} - 2C_{i,j,k}^{t+1/3} + C_{i+1,j,k}^{t+1/3}\right) \\ & + \frac{D\Delta t}{2\Delta y^2}\left(C_{i,j-1,k}^{t+2/3} - 2C_{i,j,k}^{t+2/3} + C_{i,j+1,k}^{t+2/3}\right) - \frac{k_{ijk}\Delta t}{2}\left(C_{i,j,k}^{t+2/3}\right) \end{aligned} \qquad \text{(Eq. A3)}$$

The long time step, during which the laser is off, includes only the diffusion component.

Step 1, x implicit:

$$\begin{aligned} & C_{i,j,k}^{t+1/3} - \frac{D\Delta t}{2\Delta x^2}\left(C_{i-1,j,k}^{t+1/3} - 2C_{i,j,k}^{t+1/3} + C_{i+1,j,k}^{t+1/3}\right) \\ & = C_{i,j,k}^{t} + \frac{D\Delta t}{2\Delta x^2}\left(C_{i-1,j,k}^{t} - 2C_{i,j,k}^{t} + C_{i+1,j,k}^{t}\right) + \frac{D\Delta t}{\Delta y^2}\left(C_{i,j-1,k}^{t} - 2C_{i,j,k}^{t} + C_{i,j+1,k}^{t}\right) \\ & + \frac{D\Delta t}{\Delta z^2}\left(C_{i,j,k-1}^{t} - 2C_{i,j,k}^{t} + C_{i,j,k-1}^{t}\right) \end{aligned} \quad \text{(Eq. A4)}$$

Step 2, y implicit:

$$\begin{aligned} & C_{i,j,k}^{t+2/3} - \frac{D\Delta t}{2\Delta y^2}\left(C_{i,j-1,k}^{t+2/3} - 2C_{i,j,k}^{t+2/3} + C_{i,j+1,k}^{t+2/3}\right) \\ & = C_{i,j,k}^{t} + \frac{D\Delta t}{2\Delta x^2}\left(C_{i-1,j,k}^{t} - 2C_{i,j,k}^{t} + C_{i+1,j,k}^{t}\right) + \frac{D\Delta t}{2\Delta y^2}\left(C_{i,j-1,k}^{t} - 2C_{i,j,k}^{t} + C_{i,j+1,k}^{t}\right) \\ & + \frac{D\Delta t}{\Delta z^2}\left(C_{i,j,k-1}^{t} - 2C_{i,j,k}^{t} + C_{i,j,k-1}^{t}\right) + \frac{D\Delta t}{2\Delta x^2}\left(C_{i-1,j,k}^{t+1/3} - 2C_{i,j,k}^{t+1/3} + C_{i+1,j,k}^{t+1/3}\right) \end{aligned} \quad \text{(Eq. A5)}$$

Step 3, z implicit:

$$\begin{aligned} & C_{i,j,k}^{t+1} - \frac{D\Delta t}{2\Delta z^2}\left(C_{i,j,k-1}^{t+1} - 2C_{i,j,k}^{t+1} + C_{i,j,k+1}^{t+1}\right) \\ & = C_{i,j,k}^{t} + \frac{D\Delta t}{2\Delta x^2}\left(C_{i-1,j,k}^{t} - 2C_{i,j,k}^{t} + C_{i+1,j,k}^{t}\right) + \frac{D\Delta t}{2\Delta y^2}\left(C_{i,j-1,k}^{t} - 2C_{i,j,k}^{t} + C_{i,j+1,k}^{t}\right) \\ & + \frac{D\Delta t}{2\Delta z^2}\left(C_{i,j,k-1}^{t} - 2C_{i,j,k}^{t} + C_{i,j,k-1}^{t}\right) + \frac{D\Delta t}{2\Delta x^2}\left(C_{i-1,j,k}^{t+1/3} - 2C_{i,j,k}^{t+1/3} + C_{i+1,j,k}^{t+1/3}\right) \\ & + \frac{D\Delta t}{2\Delta y^2}\left(C_{i,j-1,k}^{t+2/3} - 2C_{i,j,k}^{t+2/3} + C_{i,j+1,k}^{t+2/3}\right) \end{aligned} \quad \text{(Eq. A6)}$$

(From original article co-authored with HA Leddy and F Guilak, reprinted with permission of ASME: "Microscale Diffusion Properties of the Cartilage Pericellular Matrix Measured Using 3D Scanning Microphotolysis." Journal of Biomechanical Engineering 130(6): 061002, 2008.)

Appendix B. Modified Mankin Grading Rubric

Parameter	Grade	Description
Cartilage structure	0	Normal
	1	Undulating articular surface, but no fibrillation
	2	Mild superficial fibrillation involving < half of plateau/condyle
	3	Mild superficial fibrillation involving ≥ half of plateau/condyle
	4	Mild fibrillation/clefts/loss involving ≤ 1/3 depth of noncalcified articular cartilage thickness in < half of plateau/condyle
	5	Mild fibrillation/clefts/loss involving ≤ 1/3 depth of noncalcified articular cartilage thickness in ≥ half of plateau/condyle
	6	Moderate fibrillation/clefts/loss involving ≤ 2/3 depth of noncalcified articular cartilage thickness in < half of plateau/condyle
	7	Moderate fibrillation/clefts/loss involving ≤ 2/3 depth of noncalcified articular cartilage thickness in ≥ half of plateau/condyle
	8	Severe fibrillation/clefts/loss involving ≤ 2/3 depth of noncalcified articular cartilage thickness in < half of plateau/condyle
	9	Severe fibrillation/clefts/loss involving > 2/3 depth of noncalcified articular cartilage thickness in ≥ half of plateau/condyle
	10	Clefts/loss of articular cartilage through tidemark
	11	Clefts/loss of articular cartilage through to subchondral bone
Tidemark duplication	0	None (only one tidemark)
	1	2 tidemarks
	2	>2 tidemarks
	3	No visible tidemark remaining
Safranin-O staining	0	Normal (no loss of staining in non-calcified cartilage)
	1	Moderate loss of staining in ≤ 1/2 depth of noncalcified cartilage thickness and involving < half of plateau/condyle
	2	Moderate loss of staining in ≤ 1/2 depth of noncalcified cartilage thickness and involving ≥ half of plateau/condyle
	3	Moderate loss of staining in > 1/2 depth of noncalcified cartilage thickness and involving < half of plateau/condyle
	4	Moderate loss of staining in > 1/2 depth of noncalcified cartilage thickness and involving ≥ half of plateau/condyle
	5	Severe loss of staining ≤ 1/2 depth of noncalcified cartilage thickness and involving < half of plateau/condyle
	6	Severe loss of staining ≤ 1/2 depth of noncalcified cartilage thickness and involving ≥ half of plateau/condyle
	7	Severe loss of staining in > 1/2 depth of noncalcified cartilage thickness and involving < half of plateau/condyle
	8	Severe loss of staining in > 1/2 depth of noncalcified cartilage thickness and involving ≥ half of plateau/condyle
Fibrocartilage	0	None
	1	Fibrous tissue/fibrocartilage covers < 1/3 of plateau/condyle
	2	Fibrous tissue/fibrocartilage covers > 1/3 of plateau/condyle
Hypertrophic chondrocytes in calcified cartilage	0	0-5 hypertrophic chondrocytes
	1	6-10 hypertrophic chondrocytes
	2	>10 hypertrophic chondrocytes
Subchondral bone	0	Subchondral bone thickness is primarily < articular cartilage thickness in the load-bearing region
	1	Subchondral bone thickness is primarily = articular cartilage thickness in the load-bearing region
	2	Subchondral bone thickness is primarily > articular cartilage thickness in the load-bearing region

References

Alexopoulos LG, Bonaldo P, and Guilak F (2005a). The biomechanical role of type VI collagen in the chondrocyte pericellular matrix: Accelerated development of osteoarthritis in col6a1 deficient mice. Orthopaedic Research Society.

Alexopoulos LG, Haider MA, Vail TP, and Guilak F (2003). "Alterations in the mechanical properties of the human chondrocyte pericellular matrix with osteoarthritis." Journal of Biomechanical Engineering **125**(3): 323-33.

Alexopoulos LG, Setton LA, and Guilak F (2005b). The biomechanical role of the chondrocyte pericellular matrix in articular cartilage. Acta Biomaterialia, Elsevier Sci Ltd. **1(3):** 317-325.

Alexopoulos LG, Williams GM, Upton ML, Setton LA, and Guilak F (2005c). "Osteoarthritic changes in the biphasic mechanical properties of the chondrocyte pericellular matrix in articular cartilage." Journal of Biomechanics **38**(3): 509-17.

Alexopoulos LG, Youn I, Bonaldo P, and Guilak F (2009). "Developmental and osteoarthritic changes in Col6a1-knockout mice: Biomechanics of type VI collagen in the cartilage pericellular matrix." Arthritis & Rheumatism **60**(3): 771-779.

Amblard D, Lafage-Proust M-H, Laib A, Thomas T, Rüegsegger P, Alexandre C, and Vico L (2003). "Tail Suspension Induces Bone Loss in Skeletally Mature Mice in the C57BL/6J Strain but Not in the C3H/HeJ Strain." Journal of Bone and Mineral Research **18**(3): 561-569.

Ameye LG and Young MF (2006). "Animal models of osteoarthritis: lessons learned while seeking the "Holy Grail"." Current Opinion in Rheumatology **18**(5): 537-47.

Axelrod D, Koppel DE, Schlessinger J, Elson E, and Webb WW (1976). "Mobility Measurement by Analysis of Fluorescence Photobleaching Recovery Kinetics." Biophysical Journal **16**(9): 1055-1069.

Ballock RT and O'Keefe RJ (2003). "Physiology and pathophysiology of the growth plate." Birth Defects Research Part C: Embryo Today: Reviews **69**(2): 123-143.

Beamer WG, Donahue LR, Rosen CJ, and Baylink DJ (1996). "Genetic variability in adult bone density among inbred strains of mice." Bone **18**(5): 397-403.

Bertini E and Pepe G (2002). "Collagen type VI and related disorders: Bethlem myopathy and Ullrich scleroatonic muscular dystrophy." European Journal of Paediatric Neurology **6**(4): 193-8.

Betz P, Nerlich A, Wilske J, Tubel J, Penning R, and Eisenmenger W (1993). "Immunohistochemical localization of collagen types I and VI in human skin wounds." International Journal of Legal Medicine **106**(1): 31-4.

Bidanset DJ, Guidry C, Rosenberg LC, Choi HU, Timpl R, and Hook M (1992). "Binding of the proteoglycan decorin to collagen type VI." J. Biol. Chem. **267**(8): 5250-5256.

Biewener AA and Bertram JE (1994). "Structural response of growing bone to exercise and disuse." J Appl Physiol **76**(2): 946-955.

Blumbach K, Niehoff A, Paulsson M, and Zaucke F (2008). "Ablation of collagen IX and COMP disrupts epiphyseal cartilage architecture." Matrix Biology **27**(4): 306-318.

Bonaldo P, Braghetta P, Zanetti M, Piccolo S, Volpin D, and Bressan GM (1998). "Collagen VI deficiency induces early onset myopathy in the mouse: an animal model for Bethlem myopathy." Human Molecular Genetics **7**(13): 2135-40.

Bonaldo P, Russo V, Bucciotti F, Doliana R, and Colombatti A (1990). "Structural and functional features of the alpha 3 chain indicate a bridging role for chicken collagen VI in connective tissues." Biochemistry **29**(5): 1245-54.

Bornstein P (2002). "Cell-matrix interactions: the view from the outside." Methods in Cell Biology **69**: 7-11.

Boudreau N, Myers C, and Bissell MJ (1995). "From laminin to lamin: regulation of tissue-specific gene expression by the ECM." Trends in Cell Biology **5**(1): 1-4.

Bray DF, Bray RC, and Frank CB (1993). "Ultrastructural immunolocalization of type-VI collagen and chondroitin sulphate in ligament." Journal of Orthopaedic Research **11**(5): 677-685.

Bruns RR, Press W, Engvall E, Timpl R, and Gross J (1986). "Type VI collagen in extracellular, 100-nm periodic filaments and fibrils: identification by immunoelectron microscopy." J. Cell Biol. **103**(2): 393-404.

Buckwalter JA and Mankin HJ (1997). "Instructional Course Lectures, The American Academy of Orthopaedic Surgeons - Articular Cartilage. Part II: Degeneration and Osteoarthrosis, Repair, Regeneration, and Transplantation." J Bone Joint Surg Am **79**(4): 612-32.

Burg MA, Tillet E, Timpl R, and Stallcup WB (1996). "Binding of the NG2 Proteoglycan to Type VI Collagen and Other Extracellular Matrix Molecules." J. Biol. Chem. **271**(42): 26110-26116.

Buschmann MD, Gluzband YA, Grodzinsky AJ, and Hunziker EB (1995). "Mechanical Compression Modulates Matrix Biosynthesis in Chondrocyte Agarose Culture." Journal of Cell Science **108**: 1497-1508.

Cao L, Youn I, Guilak F, and Setton LA (2006). "Compressive Properties of Mouse Articular Cartilage Determined in a Novel Micro-Indentation Test Method and Biphasic Finite Element Model." Journal of Biomechanical Engineering **128**(5): 766-771.

Carlson KJ, Lublinsky S, and Judex S (2008). "Do different locomotor modes during growth modulate trabecular architecture in the murine hind limb?" Integr. Comp. Biol.: icn066.

CDC. (2008). "Arthritis: The Nation's Leading Cause of Disability." Retrieved August 31, 2008, from http://www.cdc.gov/nccdphp/publications/AAG/arthritis.htm.

Chang J, Nakajima H, and Poole CA (1997). "Structural colocalisation of type VI collagen and fibronectin in agarose cultured chondrocytes and isolated chondrons extracted from adult canine tibial cartilage." Journal of Anatomy **190**(04): 523-532.

Chevrier A, Monica Nelea, Mark B. Hurtig, Caroline D. Hoemann, Michael D. Buschmann (2009). "Meniscus structure in human, sheep, and rabbit for animal models of meniscus repair." Journal of Orthopaedic Research **9999**(9999): n/a.

Chipman SD, Sweet HO, McBride DJ, Davisson MT, Marks SC, Shuldiner AR, Wenstrup RJ, Rowe DW, and Shapiro JR (1993). "Defective Pro-alpha-2(I) Collagen-synthesis in a Recessive Mutation in Mice - A Model of Human Osteogenesis Imperfecta." Proceedings of the National Academy of Sciences of the United States of America **90**(5): 1701-1705.

Chiravarambath S, Simha NK, Namani R, and Lewis JL (2009). "Poroviscoelastic Cartilage Properties in the Mouse From Indentation." Journal of Biomechanical Engineering **131**(1): 011004-9.

Choi JB, Youn I, Cao L, Leddy HA, Gilchrist CL, Setton LA, and Guilak F (2007). "Zonal changes in the three-dimensional morphology of the chondron under compression: the relationship among cellular, pericellular, and extracellular deformation in articular cartilage." Journal of Biomechanics **40**(12): 2596-603.

Chu ML, Pan TC, Conway D, Saitta B, Stokes D, Kuo HJ, Glanville RW, Timpl R, Mann K, and Deutzmann R (1990). "The structure of type VI collagen." Annals of the New York Academy of Sciences **580**: 55-63.

Cole BJ and Harner CD (1999). "Degenerative arthritis of the knee in active patients: evaluation and management." J Am Acad Orthop Surg **7**(6): 389-402.

Coles J, Cha C-J, Blum J, Cheng A, Warman M, Jay G, Guilak F, and Zauscher S (2009). Microscale Surface Properties of Prg4 Knockout Joints Measured as a Function of Age. Orthopaedic Research Society Transactions. Las Vegas, NV, Orthopaedic Research Society. **34**.

Coles JM, Blum JJ, Jay GD, Darling EM, Guilak F, and Zauscher S (2008). "In situ friction measurement on murine cartilage by atomic force microscopy." Journal of Biomechanics **41**(3): 541-8.

Collins DH and McElligott TF (1960). "Sulphate (35SO4) Uptake by Chondrocytes in Relation to Histological Changes in Osteo-Arthritic Human Articular Cartilage." Ann Rheum Dis **19**(4): 318-330.

Colombatti A and Bonaldo P (1987). "Biosynthesis of chick type VI collagen. II. Processing and secretion in fibroblasts and smooth muscle cells." Journal of Biological Chemistry **262**(30): 14461-6.

Colombatti A, Bonaldo P, Ainger K, Bressan GM, and Volpin D (1987). "Biosynthesis of chick type VI collagen. I. Intracellular assembly and molecular structure." Journal of Biological Chemistry **262**(30): 14454-60.

Colombatti A, Mucignat MT, and Bonaldo P (1995). "Secretion and matrix assembly of recombinant type VI collagen." Journal of Biological Chemistry **270**(22): 13105-11.

Conchello J-A (1995). Fluorescence Photobleaching Correction for Expectation-Maximization Algorithm. Proceedings of SPIE. **2412(21):** 138-146.

Conchello JA (1998). "Superresolution and convergence properties of the expectation-maximization algorithm for maximum-likelihood deconvolution of incoherent images." Journal of the Optical Society of America a-Optics Image Science and Vision **15**(10): 2609-2619.

Conchello JA, Kim JJ, and Hansen EW (1994). "Enhanced 3-dimensional reconstruction from confocal scanning microscope images. II. Depth discrimination versus signal-to-noise ratio in partially confocal images." Applied Optics **33**(17): 3740-3750.

Costouros JG, Dang AC, and Kim HT (2004). "Comparison of chondrocyte apoptosis in vivo and in vitro following acute osteochondral injury." Journal of Orthopaedic Research **22**(3): 678-683.

Damrongrungruang T, Kuroda S, Kondo H, Aoki K, Ohya K, and Kasugai S (2004). "A Simple Murine Model for Immobilization Osteopenia." Clinical Orthopaedics and Related Research **425**: 244-251.

Darling EM, Topel M, Zauscher S, Vail TP, and Guilak F (2008). "Viscoelastic properties of human mesenchymally-derived stem cells and primary osteoblasts, chondrocytes, and adipocytes." Journal of Biomechanics **41**(2): 454-464.

Darling EM, Zauscher S, Block JA, and Guilak F (2007). "A Thin-Layer Model for Viscoelastic, Stress-Relaxation Testing of Cells Using Atomic Force Microscopy: Do Cell Properties Reflect Metastatic Potential?" Biophysical Journal **92**(5): 1784-1791.

Darling EM, Zauscher S, and Guilak F (2006). "Viscoelastic properties of zonal articular chondrocytes measured by atomic force microscopy." Osteoarthritis and Cartilage **14**(6): 571-579.

David-Vaudey E, Ghosh S, Ries M, and Majumdar S (2004). "T2 relaxation time measurements in osteoarthritis." Magnetic Resonance Imaging **22**(5): 673-82.

Derjaguin B (1934). "Molekulartheorie der äußeren Reibung." Zeitschrift für Physik A Hadrons and Nuclei **88**: 661-675.

Doane KJ, Howell SJ, and Birk DE (1998). "Identification and functional characterization of two type VI collagen receptors, alpha 3 beta 1 integrin and NG2, during avian corneal stromal development." Investigative Ophthalmology & Visual Science **39**(2): 263-75.

Doane KJ, Yang G, and Birk DE (1992). "Corneal cell-matrix interactions: type VI collagen promotes adhesion and spreading of corneal fibroblasts." Experimental Cell Research **200**(2): 490-9.

Douglas JJ and Gunn JE (1964). "A general formulation of alternating direction methods. I. Parabolic and hyperbolic problems." Numer. Math. **6**: 428-453.

Dziadek M, Darling P, Bakker M, Overall M, Zhang RZ, Pan TC, Tillet E, Timpl R, and Chu ML (1996). "Deposition of collagen VI in the extracellular matrix during mouse embryogenesis correlates with expression of the alpha 3(VI) subunit gene." Experimental Cell Research **226**(2): 302-15.

Engvall E, Hessle H, and Klier G (1986). "Molecular assembly, secretion, and matrix deposition of type VI collagen." Journal of Cell Biology **102**(3): 703-10.

Evans RC and Quinn TM (2005). "Solute diffusivity correlates with mechanical properties and matrix density of compressed articular cartilage." Archives of Biochemistry and Biophysics **442**(1): 1-10.

Evans RC and Quinn TM (2006a). "Dynamic compression augments interstitial transport of a glucose-like solute in articular cartilage." Biophysical Journal **91**(4): 1541-1547.

Evans RC and Quinn TM (2006b). "Solute convection in dynamically compressed cartilage." Journal of Biomechanics **39**(6): 1048-1055.

Fan Z, Soder S, Oehler S, Fundel K, and Aigner T (2007). "Activation of Interleukin-1 Signaling Cascades in Normal and Osteoarthritic Articular Cartilage." Am J Pathol **171**(3): 938-946.

Fischer AE, Carpenter TA, Tyler JA, and Hall LD (1995). "Visualisation of mass transport of small organic molecules and metal ions through articular cartilage by magnetic resonance imaging." Magnetic Resonance Imaging **13**(6): 819-26.

Fitzgerald J, Rich C, Zhou FH, and Hansen U (2008). "Three Novel Collagen VI Chains, {alpha}4(VI), {alpha}5(VI), and {alpha}6(VI)." J. Biol. Chem. **283**(29): 20170-20180.

Flahiff CM, Alexopoulos LG, Bonaldo P, Guilak F, and Setton LA (unpublished data). "Mechanical properties of articular cartilage in the col6a1 mouse model of osteoarthritis."

Fritton JC (2006). Mechanical loading induced adaptation of the mouse tibia. Ithaca, New York, Cornell University. **Doctor of Philosophy**.

Fritton JC, Myers ER, Wright TM, and van der Meulen MCH (2005). "Loading induces site-specific increases in mineral content assessed by microcomputed tomography of the mouse tibia." Bone **36**(6): 1030-1038.

Furman BD, Strand J, Hembree WC, Ward BD, Guilak F, and Olson SA (2007). "Joint degeneration following closed intraarticular fracture in the mouse knee: a model of posttraumatic arthritis." Journal of Orthopaedic Research **25**(5): 578-92.

Gara SK, Grumati P, Urciuolo A, Bonaldo P, Kobbe B, Koch M, Paulsson M, and Wagener R (2008). "Three Novel Collagen VI Chains with High Homology to the {alpha}3 Chain." J. Biol. Chem. **283**(16): 10658-10670.

Gennerich A and Schild D (2002). "Anisotropic diffusion in mitral cell dendrites revealed by fluorescence correlation spectroscopy." Biophysical Journal **83**(1): 510-522.

Giesen EBW, Ding M, Dalstra M, and van Eijden TMGJ (2004). "Changed Morphology and Mechanical Properties of Cancellous Bone in the Mandibular Condyles of Edentate People." Journal of Dental Research **83**(3): 255-259.

Gillquisl J (1990). Knee stability: its effect on articular cartilage. Articular Cartilage and Knee Joint Function: Basic Science and Arthroscopy. J Ewing. New York, Raven Press**:** 267-271.

Goldring MB (2000). "Osteoarthritis and cartilage: the role of cytokines." Current Rheumatology Reports **2**(6): 459-65.

Gouze JN, Bordji K, Gulberti S, Terlain B, Netter P, Magdalou J, Fournel-Gigleux S, and Ouzzine M (2001). "Interleukin-1beta down-regulates the expression of glucuronosyltransferase I, a key enzyme priming glycosaminoglycan

biosynthesis: influence of glucosamine on interleukin-1beta-mediated effects in rat chondrocytes." Arthritis & Rheumatism **44**(2): 351-60.

Griffiths MR, Shepherd M, Ferrier R, Schuppan D, James OFW, and Burt AD (1992). "Light microscopic and ultrastructural distribution of type VI collagen in human liver: alterations in chronic biliary disease." Histopathology **21**(4): 335-344.

Groma V (1998). "Demonstration of collagen type VI and alpha-smooth muscle actin in renal fibrotic injury in man." Nephrol. Dial. Transplant. **13**(2): 303-310.

Guilak F, Alexopoulos LG, Upton ML, Youn I, Choi JB, Cao L, Setton LA, and Haider MA (2006). "The pericellular matrix as a transducer of biomechanical and biochemical signals in articular cartilage." Annals of the New York Academy of Sciences **1068**: 498-512.

Guilak F and Mow VC (2000). "The mechanical environment of the chondrocyte: a biphasic finite element model of cell-matrix interactions in articular cartilage." Journal of Biomechanics **33**(12): 1663-1673.

Guilak F, Sah R, and Setton LA (1997). Physical Regulation of Cartilage Metabolism. Basic Orthopaedic Biomechanics. VC Mow and WC Hayes. Philadelphia, Lippencott-Raven Publishers**:** 179-207.

Guilak F, Setton LA, and Kraus VB (2000). Structure and Function of Articular Cartilage. Textbook of Sports Medicine. WE Garrett, KP Speer, and DT Kirkendall. Baltimore, Lippincott William & Wilkins.

Haider MA, Schugart RC, Setton LA, and Guilak F (2006). "A mechano-chemical model for the passive swelling response of an isolated chondron under osmotic loading." Biomechanics and Modeling in Mechanobiology **5**(2-3): 160-171.

Han JN and Herzfeld J (1993). "Macromolecular Diffusion in Crowded Solutions." Biophysical Journal **65**(3): 1155-1161.

Han L, Dean D, Ortiz C, and Grodzinsky AJ (2007). "Lateral nanomechanics of cartilage aggrecan macromolecules." Biophysical Journal **92**(4): 1384-1398.

Harding JW and Sneddon IN (1945). "The Elastic Stresses Produced by the Indentation of the Plane Surface of a Semi-Infinite Elastic Solid by a Rigid Punch." Proceedings of the Cambridge Philosophical Society **41**(1): 16-26.

Harumiya S, Gibson MA, and Koshihara Y (2002). "Antisense suppression of collagen VI synthesis results in reduced expression of collagen I in normal human osteoblast-like cells." Bioscience, Biotechnology & Biochemistry **66**(12): 2743-7.

Hauselmann HJ, Flechtenmacher J, Michal L, Thonar EJ, Shinmei M, Kuettner KE, and Aydelotte MB (1996). "The superficial layer of human articular cartilage is more susceptible to interleukin-1-induced damage than the deeper layers." Arthritis & Rheumatism **39**(3): 478-88.

Hayes WC and Mockros LF (1971). "Viscoelastic properties of human articular cartilage." J Appl Physiol **31**(4): 562-568.

Heinegard D and Oldberg A (1989). "Structure and biology of cartilage and bone matrix noncollagenous macromolecules." FASEB J. **3**(9): 2042-2051.

Henkelman RM, Stanisz GJ, Menezes N, and Burstein D (2002). "Can MTR be used to assess cartilage in the presence of Gd-DTPA2-?" Magnetic Resonance in Medicine **48**(6): 1081-4.

Higashi K, Higuchi I, Niiyama T, Uchida Y, Shiraishi T, Hashiguchi A, Saito A, Horikiri T, Suehara M, Arimura K, and Osame M (2006). "Abnormal expression of proteoglycans in Ullrich's disease with collagen VI deficiency." Muscle & Nerve **33**(1): 120-6.

Hildebrand T and Ruegsigger P (1997). "Quantification of Bone Microarchitecture with the Structure Model Index." Computer Methods in Biomechanics and Biomedical Engineering **1**(1): 15 - 23.

Hootman J, Bolen J, Helmick C, and Langmaid G (2006). Prevalence of Doctor-Diagnosed Arthritis and Arthritis-Attributable Activity Limitation --- United States, 2003-2005. Morbidity & Mortality Weekly Report, Centers for Disease Control and Prevention. **55:** 1089-1092.

Howell SJ and Doane KJ (1998). "Type VI collagen increases cell survival and prevents anti-beta 1 integrin-mediated apoptosis." Experimental Cell Research **241**(1): 230-41.

Hulth A, Lindberg L, and Telhag H (1970). "Experimental Osteoarthritis in Rabbits." Acta Orthopaedica Scandinavica **41**(5): 522-530.

Hunziker EB, Quinn TM, and Häuselmann HJ (2002). "Quantitative structural organization of normal adult human articular cartilage." Osteoarthritis and Cartilage **10**(7): 564-572.

Hwang WS, Li B, Jin LH, Ngo K, Schachar NS, and Hughes GNF (1992). "Collagen fibril structure of normal, aging, and osteoarthritic cartilage." The Journal of Pathology **167**(4): 425-433.

Irwin WA, Bergamin N, Sabatelli P, Reggiani C, Megighian A, Merlini L, Braghetta P, Columbaro M, Volpin D, Bressan GM, Bernardi P, and Bonaldo P (2003). "Mitochondrial dysfunction and apoptosis in myopathic mice with collagen VI deficiency." Nature Genetics **35**(4): 367-71.

Jacques C, Gosset M, Berenbaum F, and Gabay C (2006). "The role of IL-1 and IL-1Ra in joint inflammation and cartilage degradation." Vitamins & Hormones **74**: 371-403.

Keene DR, Engvall E, and Glanville RW (1988). "Ultrastructure of type VI collagen in human skin and cartilage suggests an anchoring function for this filamentous network." Journal of Cell Biology **107**(5): 1995-2006.

Keene DR, Ridgway CC, and Iozzo RV (1998). "Type VI Microfilaments Interact with a Specific Region of Banded Collagen Fibrils in Skin." J. Histochem. Cytochem. **46**(2): 215-220.

Keene DR, Sakai LY, and Burgeson RE (1991). "Human bone contains type III collagen, type VI collagen, and fibrillin: type III collagen is present on specific fibers that may mediate attachment of tendons, ligaments, and periosteum to calcified bone cortex." J. Histochem. Cytochem. **39**(1): 59-69.

Kielty CM, Lees M, Shuttleworth CA, and Woolley D (1993). "Catabolism of intact type VI collagen microfibrils: susceptibility to degradation by serine proteinases." Biochemical & Biophysical Research Communications **191**(3): 1230-6.

Kinsey ST, Locke BR, Penke B, and Moerland TS (1999). "Diffusional anisotropy is induced by subcellular barriers in skeletal muscle." Nmr in Biomedicine **12**(1): 1-7.

Klein G, Muller CA, Tillet E, Chu ML, and Timpl R (1995). "Collagen type VI in the human bone marrow microenvironment: a strong cytoadhesive component." Blood **86**(5): 1740-8.

Kong Q, Ma X, Li F, Guo Z, Qi Q, Li W, Yuan H, Wang Z, and Chen Z (2007). "COL6A1 polymorphisms associated with ossification of the ligamentum flavum and ossification of the posterior longitudinal ligament." Spine **32**(25): 2834-8.

Krishnan R, Kopacz M, and Ateshian GA (2004). "Experimental verification of the role of interstitial fluid pressurization in cartilage lubrication." Journal of Orthopaedic Research **22**(3): 565-70.

Kubitscheck U, Wedekind P, and Peters R (1998). "Three-dimensional diffusion measurements by scanning microscophotolysis." Journal of Microscopy **192**(2): 126.

Kuo HJ, Maslen CL, Keene DR, and Glanville RW (1997). "Type VI collagen anchors endothelial basement membranes by interacting with type IV collagen." Journal of Biological Chemistry **272**(42): 26522-9.

Kvist AJ, Nyström A, Hultenby K, Sasaki T, Talts JF, and Aspberg A (2008). "The major basement membrane components localize to the chondrocyte pericellular matrix -- A cartilage basement membrane equivalent?" Matrix Biology **27**(1): 22-33.

Kwan KM, Pang MKM, Zhou S, Cowan SK, Kong RYC, Pfordte T, Olsen BR, Sillence DO, Tam PPL, and Cheah KSE (1997). "Abnormal Compartmentalization of Cartilage Matrix Components in Mice Lacking Collagen X: Implications for Function." J. Cell Biol. **136**(2): 459-471.

Lai WM, Hou JS, and Mow VC (1991). "A triphasic theory for the swelling and deformation behaviors of articular cartilage." Journal of Biomechanical Engineering **113**(3): 245-58.

Laib A, Barou O, Vico L, Lafage-Proust M, Alexandre C, and Rügsegger P (2000). "3D micro-computed tomography of trabecular and cortical bone architecture with application to a rat model of immobilisation osteoporosis." Medical and Biological Engineering and Computing **38**(3): 326-332.

Lamande SR, Bateman JF, Hutchison W, McKinlay Gardner RJ, Bower SP, Byrne E, and Dahl HH (1998a). "Reduced collagen VI causes Bethlem myopathy: a

heterozygous COL6A1 nonsense mutation results in mRNA decay and functional haploinsufficiency." Human Molecular Genetics **7**(6): 981-9.

Lamande SR, Shields KA, Kornberg AJ, Shield LK, and Bateman JF (1999). "Bethlem Myopathy and Engineered Collagen VI Triple Helical Deletions Prevent Intracellular Multimer Assembly and Protein Secretion." J. Biol. Chem. **274**(31): 21817-21822.

Lamande SR, Sigalas E, Pan TC, Chu ML, Dziadek M, Timpl R, and Bateman JF (1998b). "The role of the alpha3(VI) chain in collagen VI assembly. Expression of an alpha3(VI) chain lacking N-terminal modules N10-N7 restores collagen VI assembly, secretion, and matrix deposition in an alpha3(VI)-deficient cell line." Journal of Biological Chemistry **273**(13): 7423-30.

Lampe AK and Bushby KMD (2005). "Collagen VI related muscle disorders." Journal of Medical Genetics **42**(9): 673-85.

Lampe AK, Zou Y, Sudano D, O'Brien KK, Hicks D, Laval SH, Charlton R, Jimenez-Mallebrera C, Zhang RZ, Finkel RS, Tennekoon G, Schreiber G, van der Knaap MS, Marks H, Straub V, Flanigan KM, Chu ML, Muntoni F, Bushby KMD, and Bonnemann CG (2008). "Exon skipping mutations in collagen VI are common and are predictive for severity and inheritance." Human Mutation **29**(6): 809-22.

Leddy HA (2007). Diffusional Properties of Articular Cartilage. Biomedical Engineering. Durham, North Carolina, Duke University. **Doctor of Philosophy**.

Leddy HA, Awad HA, and Guilak F (2004). "Molecular diffusion in tissue-engineered cartilage constructs: Effects of scaffold material, time, and culture conditions." Journal of Biomedical Materials Research, Part B: Applied Biomaterials **70B**(2): 397-406.

Leddy HA and Guilak F (2003). "Site-specific molecular diffusion in articular cartilage measured using fluorescence recovery after photobleaching." Annals of Biomedical Engineering **31**(7): 753-60.

Leddy HA, Haider MA, and Guilak F (2006). "Diffusional anisotropy in collagenous tissues: fluorescence imaging of continuous point photobleaching." Biophysical Journal **91**(1): 311-6.

Leddy HA/Christensen SE, and Guilak F (2008). "Microscale diffusion properties of the cartilage pericellular matrix measured using 3D scanning microphotolysis." Journal of Biomechanical Engineering **130**(6): 061002.

Lee GM, Paul TA, Slabaugh M, and Kelley SS (2000). "The incidence of enlarged chondrons in normal and osteoarthritic human cartilage and their relative matrix density." Osteoarthritis and Cartilage **8**(1): 44-52.

Lee GM, Zhang F, Ishihara A, McNeil CL, and Jacobson KA (1993). "Unconfined lateral diffusion and an estimate of pericellular matrix viscosity revealed by measuring the mobility of gold-tagged lipids." Journal of Cell Biology **120**(1): 25-35.

Li XJ, Jee WSS, Chow S-Y, and Woodbury DM (1990). "Adaptation of cancellous bone to aging and immobilization in the rat: A single photon absorptiometry and histomorphometry study." The Anatomical Record **227**(1): 12-24.

Lima EG, Tan AR, Tai T, Bian L, Stoker AM, Ateshian GA, Cook JL, and Hung CT (2008). "Differences in Interleukin-1 Response Between Engineered and Native Cartilage." Tissue Engineering Part A **14**(10): 1721-1730.

Lin S-P, Petty EM, Gibson LH, Inserra J, Seashore MR, and Yang-Feng TL (1992). "Smallest terminal deletion of the long arm of chromosome 2 in a mildly affected boy." American Journal of Medical Genetics **44**(4): 500-502.

Linn FC and Sokoloff L (1965). "Movement and Composition of Interstitial Fluid of Cartilage." Arthritis & Rheumatism **8**: 481-94.

Loeser RF (1997). "Growth factor regulation of chondrocyte integrins. Differential effects of insulin-like growth factor 1 and transforming growth factor beta on alpha1beta1 integrin expression and chondrocyte adhesion to type VI collagen." Arthritis & Rheumatism **40**(2): 270-276.

Lubkin SR and Wan X (2006). "Optimizing detection of tissue anisotropy by fluorescence recovery after photobleaching." Bulletin of Mathematical Biology **68**(8): 1873-1891.

Luby-Phelps K, Taylor DL, and Lanni F (1986). "Probing the Structure of Cytoplasm." Journal of Cell Biology **102**(6): 2015-2022.

Mankin HJ, Dorfman H, Lippiello L, and Zarins A (1971). "Biochemical and Metabolic Abnormalities in Articular Cartilage from Osteo-Arthritic Human Hips: II. Correlation of Morphology with Biochemical and Metabolic Data." J Bone Joint Surg Am **53**(3): 523-537.

Marcelino J and McDevitt CA (1995). "Attachment of articular cartilage chondrocytes to the tissue form of type VI collagen." Biochimica et Biophysica Acta (BBA) - Protein Structure and Molecular Enzymology **1249**(2): 180-188.

Maroudas A (1970). "Distribution and Diffusion of Solutes in Articular Cartilage." Biophys. J. **10**(5): 365-379.

Maroudas A (1975). "Biophysical chemistry of cartilaginous tissues with special reference to solute and fluid transport." Biorheology **12**(3-4): 233-48.

Maroudas A (1976). "Transport of solutes through cartilage: permeability to large molecules." J Anatomy **122**(Pt 2): 335-347.

Maroudas A (1979). Physicochemical properties of articular cartilage. Adult Articular Cartilage. MAR Freeman. Bath, England, Pitman Medical.

Maroudas A, Ziv I, Weisman N, and Venn M (1985). "Studies of hydration and swelling pressure in normal and osteoarthritic cartilage." Biorheology **22**(2): 159-69.

Matsumoto T, Nakayama K, Kodama Y, Fuse H, Nakamura T, and Fukumoto S (1998). "Effect of Mechanical Unloading and Reloading on Periosteal Bone Formation and Gene Expression in Tail-Suspended Rapidly Growing Rats." Bone **22**(5, Supplement 1): 89S-93S.

Mauck RL, Hung CT, and Ateshian GA (2003). "Modeling of neutral solute transport in a dynamically loaded porous permeable gel: Implications for articular cartilage biosynthesis and tissue engineering." Journal of Biomechanical Engineering-Transactions of the Asme **125**(5): 602-614.

McDevitt CA, Marcelino J, and Tucker L (1991). "Interaction of intact type VI collagen with hyaluronan." FEBS letters **294**(3): 167-170.

Menezes NM, Gray ML, Hartke JR, and Burstein D (2004). "T2 and T1rho MRI in articular cartilage systems." Magnetic Resonance in Medicine **51**(3): 503-9.

Miyamoto Y, Shi D, Nakajima M, Ozaki K, Sudo A, Kotani A, Uchida A, Tanaka T, Fukui N, Tsunoda T, Takahashi A, Nakamura Y, Jiang Q, and Ikegawa S (2008). "Common variants in DVWA on chromosome 3p24.3 are associated with susceptibility to knee osteoarthritis." Nature Genetics **40**(8): 994-998.

Mollnau H, Munkel B, and Schaper J (1995). "Collagen VI in the extracellular matrix of normal and failing human myocardium." Herz **20**(2): 89-94.

Moskowitz RW, Davis W, Sammarco J, Martens M, Baker J, Mayor M, Burstein AH, and Frankel VH (1973). "Experimentally Induced Degenerative Joint Lesions Following Partial Meniscectomy in the Rabbit." Arthritis & Rheumatism **16**(3): 397-405.

Mow VC, Holmes MH, and Lai WM (1984). "Fluid transport and mechanical properties of articular cartilage: a review." Journal of Biomechanics **17**(5): 377-94.

Mow VC, Kuei SC, Lai WM, and Armstrong CG (1980). "Biphasic creep and stress relaxation of articular cartilage in compression? Theory and experiments." Journal of Biomechanical Engineering **102**(1): 73-84.

Mow VC, Proctor CS, and Kelly MA (1989). Biomechanics of articular cartilage. Cartilage: Biomechanics of the Musculoskeletal System. M Nordin and VH Frankel. Philadelphia, Lea and Febiger**:** 31-58.

Mow VC and Ratcliffe A (1997). Basic Orthopaedic Biomechanics. Philadelphia, Lippincott-Raven.

Mow VC, Ratcliffe A, and Poole AR (1992). "Cartilage and diarthrodial joints as paradigms for hierarchical materials and structures." Biomaterials **13**(2): 67-97.

Muehleman C, Bareither D, Huch K, Cole AA, and Kuettner KE (1997). "Prevalence of degenerative morphological changes in the joints of the lower extremity." Osteoarthritis & Cartilage **5**(1): 23-37.

Muir H, Bullough P, and Maroudas A (1970). "The distribution of collagen in human articular cartilage with some of its physiological implications." Journal of Bone & Joint Surgery - British Volume **52-B**(3): 554-563.

Neidel J and Zeidler U (1993). "Independent effects of interleukin 1 on proteoglycan synthesis and proteoglycan breakdown of bovine articular cartilage in vitro." Agents & Actions **39**(1-2): 82-90.

Nieminen J, Sahlman J, Hirvonen T, Lapvetelainen T, Miettinen M, Arnala I, Malluche HH, and Helminen HJ (2008). "Disturbed synthesis of type II collagen interferes with rate of bone formation and growth and increases bone resorption in transgenic mice." Calcified Tissue International **82**(3): 229-237.

O'Hara BP, Urban JPG, and Maroudas A (1990). "Influence of cyclic loading on the nutrition of articular cartilage." Annals of the Rheumatic Diseases **49**(7): 536-539.

Ogletree DF, Carpick RW, and Salmeron M (1996). "Calibration of frictional forces in atomic force microscopy." Review of Scientific Instruments **67**(9): 3298-3306.

Oono T, Specks U, Eckes B, Majewski S, Hunzelmann N, Timpl R, and Krieg T (1993). "Expression of type VI collagen mRNA during wound healing." Journal of Investigative Dermatology **100**(3): 329-34.

Pan T-C, Zhang R-Z, Sudano DG, Marie SK, Bönnemann CG, and Chu M-L (2003). "New Molecular Mechanism for Ullrich Congenital Muscular Dystrophy: A Heterozygous In-Frame Deletion in the COL6A1 Gene Causes a Severe Phenotype." The American Journal of Human Genetics **73**(2): 355-369.

Park S, Costa KD, and Ateshian GA (2004). "Microscale frictional response of bovine articular cartilage from atomic force microscopy." Journal of Biomechanics **37**(11): 1679-87.

Pepe G, Bertini E, Bonaldo P, Bushby K, Giusti B, de Visser M, Guicheney P, Lattanzi G, Merlini L, Muntoni F, Nishino I, Nonaka I, Yaou RB, Sabatelli P, Sewry C, Topaloglu H, and van der Kooi A (2002). "Bethlem myopathy (BETHLEM) and Ullrich scleroatonic muscular dystrophy: 100th ENMC International Workshop, 23-24 November 2001, Naarden, The Netherlands." Neuromuscular disorders : NMD **12**(10): 984-993.

Pepe G, Giusti B, Bertini E, Brunelli T, Saitta B, Comeglio P, Bolognese A, Merlini L, Federici G, Abbate R, and Chu M-L (1999). "A Heterozygous Splice Site Mutation in COL6A1 Leading to an In-Frame Deletion of the [alpha]1(VI) Collagen Chain in an Italian Family Affected by Bethlem Myopathy." Biochemical and Biophysical Research Communications **258**(3): 802-807.

Peters R, Brunger A, and Wedekind P (1981). "Continuous fluorescence microphotolysis: A sensitive method for study of diffusion processes in single cells." Proceedings of the National Academy of Sciences of the United States of America **78**(2): 962-966.

Petreaca M and Martins-Green M (2008). Cell-ECM Interactions in Repair and Regeneration. Principles of Regenerative Medicine. A Atala, R Lanza, R Nerem, and JA Thomson. San Diego, Academic Press**:** 66-99.

Petrini S, Tessa A, Stallcup WB, Sabatelli P, Pescatori M, Giusti B, Carrozzo R, Verardo M, Bergamin N, Columbaro M, Bernardini C, Merlini L, Pepe G, Bonaldo P, and Bertini E (2005). "Altered expression of the MCSP/NG2 chondroitin sulfate proteoglycan in collagen VI deficiency." Molecular & Cellular Neurosciences **30**(3): 408-17.

Pfaff M, Aumailley M, Specks U, Knolle J, Zerwes HG, and Timpl R (1993). "Integrin and Arg-Gly-Asp Dependence of Cell Adhesion to the Native and Unfolded Triple Helix of Collagen Type VI." Experimental Cell Research **206**(1): 167-176.

Poole AR, Rosenberg LC, Reiner A, Ionescu M, Bogoch E, and Roughley PJ (1996). "Contents and distributions of the proteoglycans decorin and biglycan in normal and osteoarthritic human articular cartilage." Journal of Orthopaedic Research **14**(5): 681-9.

Poole CA (1992). Chondrons: The chondrocyte and its pericellular microenvironment. Articular Cartilage and Osteoarthritis. KE Kuettner, R Schleyerbach, JG Peyron, and VC Hascall. New York, Academic Press**:** 201-220.

Poole CA (1997). "Articular cartilage chondrons: form, function and failure." Journal of Anatomy **191**(Pt 1): 1-13.

Poole CA, Ayad S, and Gilbert RT (1992). "Chondrons from articular cartilage. V. Immunohistochemical evaluation of type VI collagen organisation in isolated chondrons by light, confocal and electron microscopy." Journal of Cell Science **103**(Pt 4): 1101-10.

Poole CA, Ayad S, and Schofield JR (1988). "Chondrons from articular cartilage: I. Immunolocalization of type VI collagen in the pericellular capsule of isolated canine tibial chondrons." Journal of Cell Science **90**(Pt 4): 635-43.

Poole CA, Honda T, Skinner SJ, Schofield JR, Hyde KF, and Shinkai H (1990). "Chondrons from articular cartilage (II): Analysis of the glycosaminoglycans in the cellular microenvironment of isolated canine chondrons." Connective Tissue Research **24**(3-4): 319-30.

Poole CA, Matsuoka A, and Schofield JR (1991). "Chondrons from articular cartilage. III. Morphologic changes in the cellular microenvironment of chondrons isolated from osteoarthritic cartilage." Arthritis & Rheumatism **34**(1): 22-35.

Quinn TM, Kocian P, and Meister JJ (2000). "Static compression is associated with decreased diffusivity of dextrans in cartilage explants." Archives of Biochemistry & Biophysics **384**(2): 327-34.

Rantakokko J, Uusitalo H, Jamsa T, Tuukkanen J, Aro HT, and Vuorio E (1999). "Expression Profiles of mRNAs for Osteoblast and Osteoclast Proteins as Indicators of Bone Loss in Mouse Immobilization Osteopenia Model." Journal of Bone and Mineral Research **14**(11): 1934-1942.

Rauch A, Pfeiffer RA, and Trautmann U (1996). "Deletion or triplication of the alpha 3(VI) collagen gene in three patients with 2q37 chromosome aberrations and symptoms of collagen-related disorders." Clinical Genetics **49**(6): 279-285.

Recker RR, Ed. (1983). Bone histomorphometry: techniques and interpretation. Boca Raton, FL, CRC.

Regatte RR, Akella SVS, Borthakur A, Kneeland JB, and Reddy R (2002). "Proteoglycan depletion-induced changes in transverse relaxation maps of cartilage: comparison of T2 and T1rho." Academic Radiology **9**(12): 1388-94.

Regatte RR, Akella SVS, Lonner JH, Kneeland JB, and Reddy R (2006). "T1rho relaxation mapping in human osteoarthritis (OA) cartilage: comparison of T1rho with T2." Journal of Magnetic Resonance Imaging **23**(4): 547-53.

Ruoslahti E and Yamaguchi Y (1991). "Proteoglycans as Modulators of Growth Factor Activities." Cell **64**(5): 867-869.

Saha N, Moldovan F, Tardif G, Pelletier J-P, Cloutier J-M, and Martel-Pelletier J (1999). "Interleukin-1beta-converting enzyme/caspase-1 in human osteoarthritic tissues:

Localization and role in the maturation of interleukin-1beta and interleukin-18." Arthritis & Rheumatism **42**(8): 1577-1587.

Sakata T, Sakai A, Tsurukami H, Okimoto N, Okazaki Y, Ikeda S, Norimura T, and Nakamura T (1999). "Trabecular Bone Turnover and Bone Marrow Cell Development in Tail-Suspended Mice." Journal of Bone and Mineral Research **14**(9): 1596-1604.

Salter DM, Hughes DE, Simpson R, and Gardner DL (1992). "Integrin expression by human articular chondrocytes." Rheumatology **31**(4): 231-234.

Sandy JD, Oneill JR, and Ratzlaff LC (1989). "Acquisition of hyaluronate-binding affinity in vivo by newly synthesized cartilage proteoglycans." Biochemical Journal **258**(3): 875-880.

Shaw PJ and Rawlins DJ (1991). "The Point-Spread Function of a Confocal Microscope: Its Measurement and Use in Deconvolution of 3D Data." Journal of Microscopy-Oxford **163**: 151-165.

Smit TH, Muller R, van Dijk M, and Wuisman PIJM (2003). "Changes in bone architecture during spinal fusion: three years follow-up and the role of cage stiffness." Spine **28**(16): 1802-8; discussion 1809.

Sniekers YH and van Donkelaar CC (2005). "Determining diffusion coefficients in inhomogeneous tissues using fluorescence recovery after photobleaching." Biophysical Journal **89**(2): 1302-1307.

Söder S, Hambach L, Lissner R, Kirchner T, and Aigner T (2002). "Ultrastructural localization of type VI collagen in normal adult and osteoarthritic human articular cartilage." Osteoarthritis and Cartilage **10**(6): 464-470.

Söderhäll C, Marenholz I, Kerscher T, Rüschendorf F, Esparza-Gordillo J, Worm M, Gruber C, Mayr G, Albrecht M, Rohde K, Schulz H, Wahn U, Hubner N, and Lee Y-A (2007). "Variants in a Novel Epidermal Collagen Gene (*COL29A1*) Are Associated with Atopic Dermatitis." PLoS Biol **5**(9): e242.

Specks U, Mayer U, Nischt R, Spissinger T, Mann K, Timpl R, Engel J, and Chu ML (1992). "Structure of recombinant N-terminal globule of type VI collagen alpha 3 chain and its binding to heparin and hyaluronan." EMBO Journal **11**(12): 4281-90.

Specks U, Nerlich A, Colby TV, Wiest I, and Timpl R (1995). "Increased expression of type VI collagen in lung fibrosis." Am. J. Respir. Crit. Care Med. **151**(6): 1956-1964.

Stockwell RA (1971). "The interrelationship of cell density and cartilage thickness in mammalian articular cartilage." Journal of Anatomy **109**(Pt 3): 411-21.

Stockwell RA (1979). Biology of Cartilage Cells. Cambridge, Cambridge University Press.

Tadashi H, Maureen P, Ya Z, Gregg AW, Gideon AR, and Le TD (2006). "Characterization of articular cartilage and subchondral bone changes in the rat anterior cruciate ligament transection and meniscectomized models of osteoarthritis." Bone **38**(2): 234-243.

Takahashi T, Cho HI, Kublin CL, and Cintron C (1993). "Keratan sulfate and dermatan sulfate proteoglycans associate with type VI collagen in fetal rabbit cornea." J. Histochem. Cytochem. **41**(10): 1447-1457.

Tanaka T, Ikari K, Furushima K, Okada A, Tanaka H, Furukawa K-I, Yoshida K, Ikeda T, Ikegawa S, Hunt SC, Takeda J, Toh S, Harata S, Nakajima T, and Inoue I (2003). "Genomewide linkage and linkage disequilibrium analyses identify COL6A1, on chromosome 21, as the locus for ossification of the posterior longitudinal ligament of the spine." American Journal of Human Genetics **73**(4): 812-22.

Temple MM, Xue Y, Chen MQ, and Sah RL (2006). "Interleukin-1 alpha induction of tensile weakening associated with collagen degradation in bovine articular cartilage." Arthritis and Rheumatism **54**(10): 3267-3276.

Torzilli PA (1993). "Effects of temperature, concentration and articular surface removal on transient solute diffusion in articular cartilage." Medical & Biological Engineering & Computing **31 Suppl**: S93-8.

Torzilli PA, Adams TC, and Mis RJ (1987). "Transient solute diffusion in articular cartilage." Journal of Biomechanics **20**(2): 203-14.

Torzilli PA, Arduino JM, Gregory JD, and Bansal M (1997). "Effect of proteoglycan removal on solute mobility in articular cartilage." Journal of Biomechanics **30**(9): 895-902.

Torzilli PA, Rose DE, and Dethmers DA (1982). "Equilibrium water partition in articular cartilage." Biorheology **19**(4): 519-37.

Trier U, Olah Z, Kleuser B, and Schafer-Korting M (1999). "Fusion of the binding domain of Raf-1 kinase with green fluorescent protein for activated Ras detection by fluorescence correlation spectroscopy." Pharmazie **54**(4): 263-8.

Tsay TT and Jacobson KA (1991). "Spatial Fourier Analysis of Video Photobleaching Measurements. Principles and Optimization." Biophysical Journal **60**(2): 360-368.

Tsukahara S, Miyazawa N, Akagawa H, Forejtova S, Pavelka K, Tanaka T, Toh S, Tajima A, Akiyama I, and Inoue I (2005). "COL6A1, the candidate gene for ossification of the posterior longitudinal ligament, is associated with diffuse idiopathic skeletal hyperostosis in Japanese." Spine **30**(20): 2321-4.

Urban JP, Maroudas A, Bayliss MT, and Dillon J (1979). "Swelling pressures of proteoglycans at the concentrations found in cartilaginous tissues." Biorheology **16**(6): 447-64.

van den Berg WB, Joosten LA, Kollias G, and van De Loo FA (1999). "Role of tumour necrosis factor alpha in experimental arthritis: separate activity of interleukin 1beta in chronicity and cartilage destruction." Annals of the Rheumatic Diseases **58 Suppl 1**: I40-8.

van der Kraan PM, Vitters EL, van Beuningen HM, van de Putte LB, and van den Berg WB (1990). "Degenerative knee joint lesions in mice after a single intra-articular collagenase injection. A new model of osteoarthritis." Journal of Experimental Pathology **71**(1): 19-31.

van der Sluijs JA, Geesink RGT, van der Linden AJ, Bulstra SK, Kuyer R, and Drukker J (1992). "The reliability of the mankin score for osteoarthritis." Journal of Orthopaedic Research **10**(1): 58-61.

van Osch GJ, Blankevoort L, van der Kraan PM, Janssen B, Hekman E, Huiskes R, and van den Berg WB (1995). "Laxity characteristics of normal and pathological murine knee joints in vitro." Journal of Orthopaedic Research **13**(5): 783-91.

Vico L, Novikov VE, Very JM, and Alexandre C (1991). "Bone histomorphometric comparison of rat tibial metaphysis after 7-day tail suspension vs. 7-day spaceflight." Aviation Space & Environmental Medicine **62**(1): 26-31.

von der Mark H, Aumailley M, Wick G, Fleischmajer R, and Timpl R (1984). "Immunochemistry, genuine size and tissue localization of collagen VI." European Journal of Biochemistry **142**(3): 493-502.

Wachsmuth M, Weidemann T, Muller G, Hoffmann-Rohrer UW, Knoch TA, Waldeck W, and Langowski J (2003). "Analyzing intracellular binding and diffusion with continuous fluorescence photobleaching." Biophysical Journal **84**(5): 3353-63.

Wagener R, Gara SK, Kobbe B, Paulsson M, and Zaucke F (2009). "The knee osteoarthritis susceptibility locus DVWA on chromosome 3p24.3 is the 5' part of the split COL6A4 gene." Matrix Biology **In Press, Accepted Manuscript**.

Walters DA, Cleveland JP, Thomson NH, Hansma PK, Wendman MA, Gurley G, and Elings V (1996). "Short cantilevers for atomic force microscopy." Review of Scientific Instruments **67**(10): 3583-3590.

Watrin-Pinzano A, Ruaud J-P, Olivier P, Grossin L, Gonord P, Blum A, Netter P, Guillot G, Gillet P, and Loeuille D (2005). "Effect of proteoglycan depletion on T2 mapping in rat patellar cartilage." Radiology **234**(1): 162-70.

Wedekind P, Kubitscheck U, and Peters R (1994). "Scanning microphotolysis: a new photobleaching technique based on fast intensity modulation of a scanned laser beam and confocal imaging." Journal of Microscopy **176**(Pt 1): 23-33.

Weiss C, Rosenberg L, and Helfet AJ (1968). "An ultrastructural study of normal young adult human articular cartilage." Journal of Bone & Joint Surgery - American Volume **50**(4): 663-74.

Wiberg C, Hedbom E, Khairullina A, Lamande SR, Oldberg A, Timpl R, Morgelin M, and Heinegard D (2001). "Biglycan and Decorin Bind Close to the N-terminal Region of the Collagen VI Triple Helix." J. Biol. Chem. **276**(22): 18947-18952.

Wiberg C, Heinegard D, Wenglen C, Timpl R, and Morgelin M (2002). "Biglycan Organizes Collagen VI into Hexagonal-like Networks Resembling Tissue Structures." J. Biol. Chem. **277**(51): 49120-49126.

Woo SL, Kuei SC, Amiel D, Gomez MA, Hayes WC, White FC, and Akeson WH (1981). "The effect of prolonged physical training on the properties of long bone: a study of Wolff's Law." J Bone Joint Surg Am **63**(5): 780-787.

Woods VL, Jr., Schreck PJ, Gesink DS, Pacheco HO, Amiel D, Akeson WH, and Lotz M (1994). "Integrin expression by human articular chondrocytes." Arthritis & Rheumatism **37**(4): 537-44.

Youn I, Choi JB, Cao L, Setton LA, and Guilak F (2006). "Zonal variations in the three-dimensional morphology of the chondron measured in situ using confocal microscopy." Osteoarthritis & Cartilage **14**(9): 889-97.

Zeichen J, van Griensven M, Albers I, Lobenhoffer P, and Bosch U (1999). "Immunohistochemical localization of collagen VI in arthrofibrosis." Archives of Orthopaedic & Trauma Surgery **119**(5-6): 315-8.

Zhang R-Z, Sabatelli P, Pan T-C, Squarzoni S, Mattioli E, Bertini E, Pepe G, and Chu M-L (2002). "Effects on Collagen VI mRNA Stability and Microfibrillar Assembly of Three COL6A2 Mutations in Two Families with Ullrich Congenital Muscular Dystrophy." J. Biol. Chem. **277**(46): 43557-43564.

Biography

SUSAN ELIZABETH CHRISTENSEN

Born November 19, 1981 in Lexington, Kentucky

EDUCATION

Duke University, Durham, North Carolina
Doctor of Philosophy, Biomedical Engineering, September 2009
Master of Science, Biomedical Engineering, December 2008

Swarthmore College, Swarthmore, Pennsylvania
Bachelor of Science, Engineering, June 2003
Bachelor of Arts, Linguistics, June 2003

PEER-REVIEWED PUBLICATIONS

Leddy HA* / **Christensen SE***, Guilak F. Microscale diffusion properties of the cartilage pericellular matrix measured using 3D scanning microphotolysis. Journal of Biomechanical Engineering. 130(6):061002, 2008 Dec. (*Co-First Authors)

Fermor B, **Christensen SE**, Youn I, Cernanec J, Davies CM, Weinberg JB. Oxygen, nitric oxide and articular cartilage. European Cells & Materials. 13:56-65, 2007 Apr.

Tognana E, Chen F, Padera RF, Leddy HA, **Christensen SE**, Guilak F, Vunjak-Novakovic G, Freed LE. Adjacent tissues (cartilage, bone) affect the functional integration of engineered calf cartilage in vitro. Osteoarthritis & Cartilage. 13(2):129-38, 2005 Feb.

PRESENTATIONS

Christensen SE, Bonaldo P, Guilak F. Absence of type VI collagen alters mouse knee morphology. Gordon Research Conference on Musculoskeletal Biology & Bioengineering. Poster presentation, Andover, New Hampshire, 2008.

Leddy HA, **Christensen SE**, Guilak F. Differences in molecular diffusivity between the pericellular and extracellular matrices of articular cartilage. 52nd Annual Meeting of the Orthopaedic Research Society, Vol.31, Poster/Podium #0367, Chicago, Illinois, 2006.

Christensen SE, Leddy HA, Guilak F. Modeling scanning microphotolysis to measure molecular diffusion in articular cartilage. Joint SIAM-SMB (Society for Industrial and Applied Mathematics; Society for Mathematical Biology) Conference on Life Sciences. Podium presentation, Raleigh, North Carolina, 2006.

Fermor B, Youn I, **Christensen SE**, Guilak F. The influence of oxygen tension on matrix turnover and physical properties of articular cartilage. 51st Annual Meeting of the Orthopaedic Research Society, Vol.30, Poster/Podium #0299, Washington, D.C., 2005.

OTHER PUBLICATIONS

Christensen EB, **Christensen SE**. *Algebra Antics*.
Roseville, Minnesota: MindWare, 2009.

Christensen EB, **Christensen SE**. *Spellbinders Level A*.
Fort Atkinson, Wisconsin: Nasco, 2007.

Christensen EB, **Christensen SE**. *Spellbinders Level B*.
Fort Atkinson, Wisconsin: Nasco, 2007.

Christensen EB, **Christensen SE**. *Tactic Twisters Level A*.
Roseville, Minnesota: MindWare, 2006.

Christensen EB, **Christensen SE**. *Tactic Twisters Level B*.
Roseville, Minnesota: MindWare, 2006.

Christensen EB, **Christensen SE**. *Venn Perplexors Level D*.
Roseville, Minnesota: MindWare, 2004.

Christensen EB, **Christensen SE**. *Rod-Clue Puzzles*.
Vernon Hills, Illinois: ETA/Cuisenaire, 2001.

HONORS AND AWARDS

2006	Grosswirth-Salny Scholarship (Mensa Education & Research Foundation)
2003-2007	James B. Duke Fellowship
2003-2006	National Defense Science and Engineering Graduate Fellowship
2003	Oak Leaf Award (Swarthmore College)
2003	Phi Beta Kappa Membership
2003	Sigma Xi Membership
2002	Sarah Kaighn Cooper Scholarship (Swarthmore College)
2001	Tau Beta Pi Membership

ADDITIONAL EXPERIENCE

2007-2009	President, Society of Duke Fellows
2007, 2008	Coordinator, Great Day of Service
2006-2008	Chair, Community Outreach Committee
2004-2005	Teaching Assistant, Duke University
	Electrobiology
	Introduction to Biomechanics
	Models of Cellular and Molecular Systems
2002-2003	Member, Swarthmore College Judiciary Committee